MICRONEEDLE BASED DEVICE TO SAMPLE INTERSTITIAL FLUID THROUGH SKIN

A Dissertation
Presented to
The Academic Faculty

by

Pradnya P. Samant

In Partial Fulfillment
of the Requirements for the Degree
Ph.D. in the
School of Chemical and Biomolecular Engineering

Georgia Institute of Technology
May 2018

MICRONEEDLE BASED DEVICE TO SAMPLE INTERSTITIAL FLUID THROUGH SKIN

Approved by:

Dr. Mark R. Prausnitz, Advisor
School of Chemical and Biomolecular Engineering
Georgia Institute of Technology

Dr. Hang Lu
School of Chemical and Biomolecular Engineering
Georgia Institute of Technology

Dr. Julie Champion
School of Chemical and Biomolecular Engineering
Georgia Institute of Technology

Dr. Paul Yager
Department of Bioengineering
University of Washington

Dr. David Ku
School of Mechanical Engineering
Georgia Institute of Technology

Date Approved:30 November, 2017

To my father

ACKNOWLEDGEMENTS

Although it is my name on the degree, it is supported by the valuable support and contributions of many others. First and foremost, I would like to thank my advisor Dr. Mark Prausnitz. Throughout the duration of my PhD he has been a solid source of strength. I have learnt from him essential skills in sound scientific practice, creative problem solving, and the importance of discipline and organization in research. His expertise in oral and written communication has sharpened my soft skills and enabled me to become a better communicator. Working with him and observing him closely over the years, I have admired his intelligence and learnt to stay grounded and humble while being successful. It is no exaggeration to say that he has made me a better scientist and an even better person. I would also like to acknowledge my committee members Dr. Julie Champion, Dr. David Ku, Dr. Hang Lu, and Dr. Paul Yager. Their insightful comments and continued support have greatly shaped this work.

This work was a collaborative effort between Georgia Tech and Emory University. I have been fortunate to work alongside some great collaborators. Dr. Megan Niedzwiecki and Dr. Gary Miller at the Rollins School of Public Health at Emory University are a vital part of this project and their contribution has greatly helped in fully realizing the utility of this technology. Megan has worked with me on this project for many years and has often walked the extra mile to ensure that data analysis was done in the manner and within the timeframe desired. The members of the Clinical Biomarkers Laboratory at Emory University School of Medicine – Dr. Vilinh Tran, Dr. Douglas Walker, Dr. Dean Jones - were a great help in the analysis of all samples. Lastly, Dr. Felner, our collaborator at the Department of Endocrinology, Emory University School of Medicine, has been very helpful in establishing

the clinical utility of this method. Dr. Felner, an established pediatric endocrinologist, has contributed great ideas to the project, helped me understand the impact of this work on real patients, and motivated me always. Nicholas Raviele and the staff at Stamps Health Services have helped tremendously in organizing and conducting human studies.

Much of this work would have been impossible without the fantastic team in the Laboratory for Drug Delivery at Georgia Tech. I cannot thank enough Donna Bondy, our administrative coordinator. She always kept things running smoothly behind the scenes, was two steps ahead of me always in keeping up with deadlines, and was always willing to be a shoulder to lean on during tough times. Her presence in the lab lightens everybody up and nothing could be the same without her – she is the lifeline of the lab. I was also extremely privileged to work with the best minds in the country right beside me. I would like to thank all my colleagues including but not limited to – Dr. Jaya Arya, Dr. Bryce Chiang, Brandon Gerberich, Dr. Yasmine Gomaa, Sebastien Henry, Dr. Stefany Holguin, Dr. Jessica Joyce, Dr. Haripriya Kalluri, Dr. Yoo Chun Kim, Chandana Kolluru, Dr. Jae Hwan Jung, Simple Kumar, Juan Mena-Lapaix, Dr. Jeong Woo Lee, Dr. Song Li, Dr. Wei Li, Dr. Devin McAllister, Dr. Wilmarie Medina-Ramos, Dr. Matthew Mistilis, Dr. Mohammad Mofidfar, Dr. James Norman, Joshua Palacios, Monica Perez, Winston Pewin, Dr. Aritra Sengupta, Richard Shafer, Dr. Andrey Romanyuk, Andrew Tadros, and Richard Terry. Although we all have out separate projects, we all helped and learned from each other, bouncing ideas and creatively trying to solve each other's problems. The lab environment was always open and collaborative that greatly helped the quality of work. Devin and Sebastien taught me the intricacies of developing protocols and conducting clinical studies ethically and safely. I have really enjoyed all my interactions with the diagnostics team – Chandana and Juan- coming

up with some crazy ideas and some good ones. Late night dinners with Matt and Jessica have always been a source of great joy (and great food) and I consider teaching them how to cook good Indian food to be one of my better achievements at Georgia Tech. All graduate students (plus Priya) would often get together over lunch, dinner, or a movie. It helped take the edge off work and made the lab a happier place. Lastly, a huge thank you to my quad – Bryce, Stefany, Monica, and Simple- without whom I couldn't have willingly survived grad school. Our numerous antics and pranks (some of which remain undiscovered) have been a source of great entertainment. Bryce, your cats will live on forever in the quad and in our memories. Stef, I will miss all our political discussions, our 'deep' conversations, and all your office pranks. Monica has been a beacon of light for our quad and a great organizer of all of our lab's social events. I would like to thank my undergraduate researchers Caroline Massaro, Katie Neuberger, Ant Yuescuoy, Zack Schneidermann They did a lot of the legwork in fabrication, analyzing data, and helped things progress at a much faster pace.

I came to Atlanta in 2011 to a new country and my friends here have become my Atlanta family, making this city my home away from home. My friends outside of work, especially my girls gang – Grace and Suja – have made life in Atlanta delightful. We have shared ups and downs, laughter and tears, and make lifelong friendships along the way. The ChBE Indian gang was always a source of great strength and dinners, movies, board game nights have made many evenings and weekends enjoyable. I would especially like to thank Lalit Darunte who stood by me always, supported my every endeavor, provided much needed intellectual inputs, and emotional stability.

Last, but certainly not least, I must thank my family who have been my support system throughout it all. My father, Prakash Samant, passed away before he could see me get this

degree, but his teachings, his principles, and his aspirations for me have motivated me long after he is gone. My mother, Medha Samant, my aunt, Minal Damle, and my uncle, Mahesh Damle, have stood firmly behind me supporting my pursuit of higher education even though it meant living in diametrically opposite corners of the world all these years. They have sacrificed their own happiness to create opportunities for me, for which I am eternally grateful.

Finally, having lived all my childhood and some of my adulthood in a developing country like India, I have been guilty of sometimes becoming immune to the poverty around me. There are millions of children in India who are bright, capable but lack resources to get an education and remain in low skilled jobs. I feel very lucky to be part of the elite few in India who could readily access education and opportunities to get to where I am. I do hope somewhere in my lifetime, I get to do some bit of work and return this favor to my people and my country.

TABLE OF CONTENTS

LIST OF TABLES

LIST OF FIGURES

SUMMARY

Diagnosis of diseased state and regular monitoring during treatment is essential to effective management of diseases. Detection of biomarkers in body fluids such as blood, urine, saliva, and sweat is the basis for diagnosis. In addition to these body fluids, interstitial fluid (ISF) is a major body fluid that surrounds the cells and tissues in the body and connects blood vessels with cellular matter. ISF is currently used for a few diagnostic applications such as continuous glucose monitoring and to monitoring local drug concentrations in skin. However, even though ISF is a valuable source of biomarkers, its use in diagnostic research and clinical applications is limited because the current methods to sample ISF are cumbersome, time-consuming, invasive, and can cause discomfort to the patient.

In this study, we have developed a simple, reliable method that can sample multiple microliters of ISF through skin using a microneedle (MN) based system. MNs are microscopic needles that can penetrate past the upper skin layers and reach the lower dermis and access the ISF in the lower skin layer. Since MNs are small and easy to handle, they are ideal as a minimally-invasive device to sample ISF.

We designed four MN systems that utilize different mechanisms and driving forces to push the ISF from the dermis into the MNs and eventually towards the skin surface. Hydrogel MNs, porous MNs, and hollow MNs absorb surrounding ISF, creating a concentration gradient for ISF. An osmosis based MN system and a direct pressure based MN system created a pressure gradient in the dermis for ISF flow. Experimentally, it was observed that the highest ISF sampling rate was obtained with a pressure induced gradient. To evaluate the transport of ISF through skin, a theoretical model was developed exploring ISF flow with

various driving forces and the rate limiting steps. The major resistance to ISF flow is flow through dermis and hence a pressure gradient in the dermis greatly enhances flow rates compared to a concentration gradient. We translated these experimental and theoretical findings in human volunteers. MNs were used to create micropores in the skin surface with suction applied over these micropores to drive the ISF from the dermis towards the skin surface. This method sampled multiple microliters of ISF from human participants within minutes.

To evaluate the composition of ISF, we investigated the metabolomic profile of suction blister ISF and compared it with plasma in 10 human participants. Common biomarkers such as glucose, creatinine, and urea were detected in both fluids, indicating the possible utility of ISF as a surrogate for blood. Several metabolites were also found uniquely in ISF or elevated in ISF indicating it may offer additional value compared to blood for detection of certain metabolites. Several amino acids, creatinine, cartinine and betaine metabolites correlated well between ISF and blood, indicating that ISF can reliably detect biomarkers with similar accuracy as in blood.

To evaluate the performance of MNs in-vivo in human volunteers, we first optimized the MN system to reliably sample multiple microliters of clear ISF from the forearm. A metabolomics analysis of ISF vs. blood from 20 participants revealed that almost 2/3rd of the features found were common between all fluids. Similar to the previous study, several important clinical markers were detected in ISF and plasma, which indicated the possible utility of this method for detection of these markers in the clinic. Many clinically relevant metabolites were found uniquely in ISF compared to plasma. This indicated that MNs could be used to research metabolic processes and dermatological markers that are otherwise

difficult or impossible to find in blood. The concentration of biomarkers in ISF correlated well with the concentration in blood in dynamic situations suggesting that the MN system can capture variations in biomarker concentrations over time with similar accuracy as blood. The MN treatment was generally well tolerated, with the pain not significantly different from pain of venipuncture or fingerstick. Mild erythema was observed at the site of MN treatment that resolved within a few days.

This MN-based technique is a significant improvement over other ISF sampling techniques because of its minimally-invasive nature and ease of use. We believe that this MN system can become a platform technology that can be used by researchers and clinicians to access ISF for diagnostic purposes in the future. Initially, this technique may be limited to research on ISF and the biomarkers or metabolic processes within ISF. Eventually, we hope that this technology gets translated into clinical use to sample ISF in a simple reliable manner and use it for disease diagnosis, population screening, or regular biomarker monitoring.

1 CHAPTER 1. INTRODUCTION

Detection of biomarkers in various body fluids is essential for effective diagnosis, monitoring, and treatment of diseases. Common body fluids used for detection are blood, urine, saliva, and sweat. However, another major body fluid and a source of valuable markers, the ISF, is largely unexplored in major part due to lack of simple, reliable techniques to sample this fluid. MNs are a promising device to sample this fluid as they can access the ISF through skin in a minimally-invasive and simple manner. Our goal is to develop a MN based system to sample clinically relevant volumes of ISF (1-10 µL) through skin within a practical time frame of 20 min. By showing clinical utility of this device and establishing the value of ISF as a source of valuable biomarkers, we hope to develop this platform technology that can be used by researchers and clinicians for diagnostic research and applications.

2 CHAPTER 2. BACKGROUND

2.1 Diagnosis and monitoring of disease

Detection and regular monitoring of disease states is essential to prevention, diagnosis, prognosis, and treatment of the disease. Detection of various physiological and molecular markers in the body, also called biomarkers, are key elements for diagnosis [1] [2]. WHO has stated that a true definition of biomarkers includes "almost any measurement reflecting an interaction between a biological system and a potential hazard, which may be chemical, physical, or biological. The measured response may be functional and physiological, biochemical at the cellular level, or a molecular interaction" [3].

Several biomarkers are currently validated for monitoring the onset, progression and treatment of many diseases. The discovery of new biomarkers and methods to detect these has changed the landscape for how various conditions are diagnosed and monitored. Early disease diagnosis has great potential to reduce the rising healthcare costs [4-6]. Infectious diseases such as tuberculosis, malaria, dengue can be diagnosed easily with a blood test, ensuring timely treatment. Regular monitoring in chronic diseases is key to their effective management [7, 8].

Diabetics test their blood sugar multiple times a day, patients with high cholesterol have their cholesterol and blood pressure tested regularly and those on blood thinning medicines have their clotting time routinely monitored. There is growing research interest in identifying novel biomarkers that help in diagnosing disease, predicting therapeutic response, or improving clinical practice [9, 10]. Research and clinical use of biomarkers

has evolved over the years from simple physiological characteristics such as blood pressure or heart rate, laboratory blood tests such as blood glucose, complete blood count to now cutting-edge predictive DNA microarray [11, 12], personalized testing such as mammaPrint for predicting breast cancer recurrence [13, 14], and monitoring local drug concentrations to determine drug bioavailability and pharmacokinetics [15].

2.1.1 Source of biochemical biomarkers

Molecular biomarkers are detected most commonly in body fluids such as blood [16], urine [17, 18] sweat [19], or saliva [20, 21]. Blood is the gold standard for most diagnostic tests because it is systemic and has well established protocols for sampling in the clinic. The ability to draw blood by fingersticks has further enabled the acceptance of blood for diagnostics in the clinic and the emergence of new point-of-care diagnostics [22]. Fingersticks are routinely done by the patients themselves to collect capillary blood. Common fingerstick tests that can be done at home include glucose testing for diabetics, cholesterol testing for people with high cholesterol, prothrombin testing or patients on drug-thinning medicines. Although blood tests are commonplace, the inability to draw blood by the patients themselves, the clinical expertise required, and the pain and apprehension felt by patients, limits the use of blood tests. The blood volume with capillary fingersticks is small and variable and there is possibility of contamination with ISF and substances on skin surface that can introduce errors in the measurement of biomarkers [23, 24].

Urine, sweat, and saliva are more easily accessible for sampling and hence have generated more interest in diagnosis. Urine-based tests are routinely used for determination of ovulation, pregnancy, or menopause by measuring the concentrations of specific hormones present in the urine [25, 26]. However, circadian rhythm and water intake can have a significant effect on the concentration of biomarkers in urine, thus impacting the accuracy of the tests [27, 28].

Saliva is a source of biochemical information available in a minimally-invasive manner. Monitoring saliva is useful for determination of drug concentrations and biomarkers of diseases of the oral cavity and GI tract [29]. Saliva-based HIV [30] tests are also now regularly used in the field. However, there are many elements that can interfere with the accuracy of saliva-based assays such as presence of different food substances in the mouth.

There has been a significant increase in sweat analysis in recent years due to its potential for non-invasive monitoring of fluid, hydration, and electrolyte loss by elite athletes [31]. Diagnosis of cystic fibrosis is made by determination of chloride levels in sweat [32]. Current methods to sample sweat require techniques such as pilocarpine induced sweat collection and are not optimized for at-home detection. Also, since sweat, and saliva have limited fluid volumes, the biomarkers found in these body fluids is limited.

2.1.2 Recent trends in diagnostics

A recent trend dominating diagnostics is the emergence of point-of-care technologies. Decentralization of healthcare is an intrinsically powerful concept that can lay the foundation for a more affordable, accountable and flexible healthcare system.

Decentralization mainly involves movement of acute services from centralized institutes such as hospitals and clinics to home. Aging population, huge discrepancy between healthcare in the developing and the developed world and the increasing burden of healthcare costs on the economy make this shift welcome and essential.

The emergence of point-of-care devices marks this quiet revolution happening in the healthcare industry. Point-of-care diagnostics enables rapid diagnosis, early detection and management of a variety of conditions and diseases under various settings, such as at home, in an ambulance, in a clinic or out on the field [33]. The glucose self-monitoring system and the home pregnancy test kits are textbook examples of high impact point-of-care diagnostic systems that have revolutionized management of diabetes and onset of pregnancy. The global point-of-care diagnostics market was valued at $13.8 billion in 2011 [34] and is estimated to grow rapidly. It has huge implications in global health where such devices can play important role in detection of infectious diseases, STDs, malnutrition in low-resource settings, provide critical surveillance data and help manage long-term health strategies [35]. Portable blood chemistry analyzers, triage for cardiovascular markers, continuous glucose monitors have been commercialized and well accepted in developed countries [1, 2, 33, 36, 37].

A subset of point-of-care diagnostics marker is smart wearable devices. Smart wearable systems market shows big potential and profit [38-40]. There are countless variations of these systems in the form of sensors, smart fabrics, wireless communicators, cellphone apps, etc. This includes physical as well as chemical sensing. Monitoring physical parameters such as heart rate, pulse, temperature, body motion, sleep patterns is well

established through devices such as wrist bands, chest electrodes, and cellphones [41]. However, for complete information about the overall health of a user, it is critical to monitor essential biomarkers along with physical parameters. These biomarkers include electrolytes, glucose, dissolved gases, heavy metals, environmental pollutants, etc. The most common currently used wearable chemical sensors include continuous glucose monitors. These sensors need to be inserted and removed from the body on a weekly basis.

There are several limitations in monitoring chemicals within the body. Chemical sensors are usually bulky, making them unviable to be adapted towards wearable technology. Implantable chemical sensors require surgery to insert and remove. A majority of wearable chemical sensors like the continuous glucose monitors needs frequent calibration. Their response may not be stable over time requiring frequent sensor change. Current chemical sensor designs do not lend themselves well to multiple analytes being tracked simultaneously to get comprehensive data on the wearer and surroundings. Thus, there is a growing demand to develop multifunctional wearable devices that can monitor analytes continuously with a low turnaround time and communicate the data effectively to the user/healthcare practitioner [42]. Towards that end, devices under development like the Biostamp involve a thin skin-like sensor that has the capability to monitor multiple analytes and physiological parameters simultaneously [19]. There are numerous challenges towards development of fully-integrated chemical sensors such as sensor stability, portable power sources as well as data integration and privacy. Development of such devices will require collaborative efforts between researchers, engineers, and physicians and will enable users to access more comprehensive information about themselves in a continuous manner.

2.2 Interstitial fluid

ISF bathes and surrounds the cells and tissues of the body. It makes up a large fraction of the body – around 20-25% of body weight [43]. About 60-70% of body fluid content is constituted by ISF. ISF is formed as plasma traverses blood vessels and equilibrates with the cell and tissue environment. It provides a means of delivering materials to the cells, enables intercellular communication and removes metabolic waste. ISF transports nutrients from the blood vessels to the cells and waste products from the cells to the blood stream. The driving force for flow of fluid from plasma to ISF is generated by the pressure difference arising from hydrostatic pressure generated by blood vessels and osmotic pressure of ISF (Figure 2.1) [44, 45]. Water and dissolved solutes, other than large proteins, exit capillaries near the arteriolar end because the capillary pressure is much greater than that of the ISF. As the volume of the water in the capillary decreases, the pressure within the capillary also decreases but remains greater than ISF.

Proteins remaining in the capillary contribute an osmotic force that tends to draw water back into the capillary. The combination of decreased pressure within the capillary and the osmotic force caused by proteins leads to the recapture of much of the water that left the capillary. Lymph vessels drain any excess fluid from the interstitial space. The schematic below shows the flow of fluid from blood vessels into the interstitium and to the lymphatic system [46].

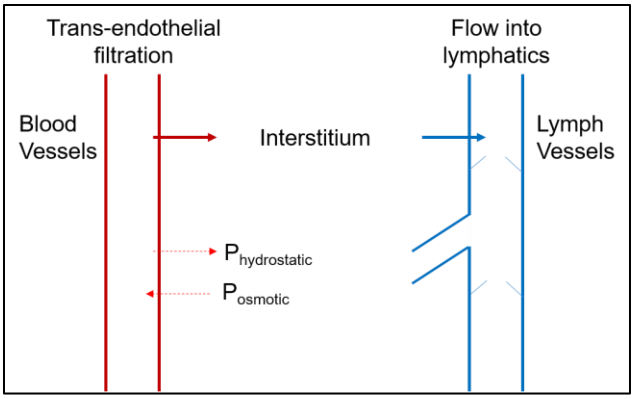

Figure 2.1: Schematic of flow of ISF from blood vessels to the interstitium under osmotic pressure and eventual uptake by the lymphatic system.

The endothelium of capillaries separates plasma from ISF. Red blood cells, large plasma proteins and platelets cannot pass through this endothelium. However, most hydrophilic small molecules freely equilibrate between plasma and ISF, for example electrolytes such as sodium, chloride and small molecules such as glucose and uric acid. Thus, the composition of ISF is similar to plasma without the plasma proteins. In addition, the ISF contains metabolites generated from local cell processes and other cellular components such as nucleosides and lipids. This constitutes mainly amino acids, sugars, salts, fatty acids, coenzymes, hormones, neurotransmitters, waste products from cells as well as cell debris resulting from cell necrosis [47-49].

ISF is an attractive body fluid to screen for biomarkers. Previous studies have shown that it contains various biomarkers that are uniquely found in ISF and also many that are elevated in the ISF compared to plasma [50, 51]. These include systemic as well as local biomarkers. Unlike plasma that acts at a systemic level, ISF operates at a local level. Cell necrosis or cell apoptosis lead to formation of cell debris which releases unique biomarkers into the ISF. Hence, ISF is capable of reflecting changes in the local environment.

Biomarkers related to tumors are found in tumor ISF [52-54]. Similarly, bronchoalveolar lavage fluid [55, 56] and cerebrospinal fluid [57-59] contain important local biomarkers. Drug concentrations in the skin are monitored by measuring the concentrations of these drugs in the skin ISF [60, 61].

ISF does not clot and is hence useful for continuous monitoring of biomarkers unlike blood that requires discrete measurements [62, 63]. Continuous monitoring of glucose in ISF in the subcutaneous space is widespread with commercial devices by Dexcom, Abbott, and Medtronic [64-66]. There is growing interest in other non-invasive means to monitor glucose [67].

Proteins in plasma are present in wide dynamic concentrations from very high levels for albumin to very low levels for regulatory proteins/hormones. Since disease-specific biomarkers are typically present at low concentrations, they are consequently masked by the high abundant proteins and can remain undetected. Depletion of high-abundance proteins from the serum is challenging as it causes some of the low-abundance proteins to be lost due to non-specific binding. Even after depletion, low-abundance protein concentrations are about 2-3 orders of magnitude lower than high-abundance proteins. ISF has much lower concentrations (about an order of magnitude) of high-abundance proteins like albumin and globulin [68]. Thus, biomarkers which cannot be detected in plasma may be detected in ISF.

2.3 Skin anatomy and skin as a source of interstitial fluid

The skin is the largest and most accessible organ of the body and that makes it attractive for minimally-invasive sampling techniques. It acts as a protective shield, regulates body temperature, functions as a sensory organ, and prevents loss of water from the body or entry of pathogens into the body and stores water and fat [69]

2.3.1 Skin anatomy

Although, skin characteristics vary throughout the body, skin is essentially constituted of three layers – the epidermis, the dermis and the subcutaneous fat layer.

The stratum corneum is outermost layer of the epidermis. It ranges in thickness from 8-20 um. It is made of 10-30 layers of flat dead corneocytes arranged in a brick and mortar type of model tightly joined by lipidic intercellular glue. Although it is a dead tissue, it plays an important role in skin physiology. It is responsible for the barrier properties of skin against loss of body fluids and penetration of chemicals into the body [70, 71].

The viable epidermis lies below the stratum corneum. It consists of ten layers of randomly oriented living cells like keratinocytes and basal cells. It is devoid of blood vessels. The thickness of viable epidermis typically is 50-100 μm. The most important role of the viable epidermis is to renew the stratum corneum. It does this by continuous division and keratinization of keratinocytes in the upper layers of the viable epidermis. The deeper layers of epidermis provide cells that mature and form new stratum corneum. The total turnover time is about 15 days. Besides, the epidermis also provides an immune barrier, generates cytokines, provides protection against UV and secretes hormones [71].

The epidermis is separated from the dermis by a basement membrane. The dermis is the thickest layer of skin with thickness ranging from 1-2 mm. The backbone of the dermis is an interconnected network of collagen and elastin fibers. This network is embedded in an interstitial ground substance made of nonfibrillar collagen, proteoglycans and glycoproteins. The hygroscopic nature of glycoproteins attracts water which makes up almost 70% of dermis volume. The dermis contains nerve endings, lymphatics, vasculature, hair follicles, sebaceous glands and sweat glands. The dermis can be separated into two layers – the papillary and adventitial dermis (20-100 um) and the reticular dermis (over 500 um). The papillary dermis plays a role in immune response, provides nutrition to the epidermis and plays an important role in inflammatory response. The reticular dermis plays a mechanical role, holding the structure of the tissue in place protecting against mechanical aggressions [71].

The subcutaneous tissue lies between the dermis and underlying muscle. It consists of interstitial tissue and adipose tissue. The thickness of the subcutis depends on body sites and varies between individuals. The interstitial tissue is similar to dermis with more fluid content. The adipose tissue constitutes a major component of body fat mass. The subcutis preserves body heat and prevents injury by acting as a shock absorber [71, 72].

2.3.2 Current methods sampling interstitial fluid via skin

The barriers of stratum corneum and viable epidermis prevent easy access to the underlying dermal ISF. Overcoming these barriers, various methods have been developed to sample

ISF through the skin. These include suction blisters, suction effusion, microdialysis/microperfusion, reverse iontophoresis and use of ultrasound.

2.3.2.1 Suction Blister method:

Suction blisters are a widely used technique to sample ISF from skin. Negative pressure is applied to the skin for up to 2 hours sometimes at elevated temperatures of up to 40^0C. This causes the dermis and epidermis to separate. Dermal ISF is drawn into this gap by suction, forming a blister. The ISF in the blister can be sampled with a conventional needle and syringe [73]. This technique has been used widely in literature to study wound healing properties of the epidermis [74, 75], to study diseased skin [76] and also for treatment of skin diseases such as psoriasis and vitiligo [77]. Major drawback of this method is the requirement for specialized equipment for generating vacuum over long periods of time, trained personnel to perform the procedure, and injury at the site of treatment that can take weeks to heal. There are various risks involved in the procedure such as increased chances of infection, bleeding. There is also the possibility of a discoloration left at the skin site where the suction blister was applied. All these factors make suction blisters unattractive as a clinical method to sample ISF. It however remains the only technique to sample a large volume of ISF (e.g., > 10 µL) from skin.

Suction effusion: This method involves tape stripping a small part of the skin to remove the stratum corneum followed by application of negative pressure. The absence of stratum corneum allows ISF to come up to the surface [78]. However, similar to suction blister method, this technique requires use of specialized equipment over long period of time.

There is discomfort associated with tape stripping as well as application of suction for prolonged times that may lead to skin damage.

2.3.2.2 Microdialysis and microperfusion

Microdialysis is a sampling technique that is used for continuous measurement of free, unbound analyte concentrations in the extracellular fluid of virtually any tissue. For the skin, this involves implantation of a probe with a semipermeable hollow fiber into skin. A physiological solution also known as the perfusate, is flown through the probe at very low flow rates (0.5-5 µL/min). Because of the concentration gradient, solutes passively diffuse into the tube and equilibrate with the perfusate. The perfusate at the outlet contains components of ISF [79]. This is a useful technique to measure concentration of low molecular weight analytes without interference from proteins owing to the semi-permeable membrane. Microdialysis has been used for continuous monitoring of analytes like glucose, various metabolites in tissues such as the brain, skin and subcutaneous space [80-82]. Microdialysis is routinely used to gather information about local drug concentrations in skin. However, it is unsuitable for measurement of proteins because of MN cut off and low rates of diffusion. Frequent calibrations and fine-tuning is required to maintain sensitivity and the measured concentration is not the true concentration of the analyte in ISF.

Open flow microperfusion requires implantation of a stainless-steel mesh instead of a semipermeable membrane into the skin. The direct liquid pathway between the probe's perfusate and the surrounding ISF provides a diluted but otherwise unchanged ISF sample, since no dialysis or filtering occurs. Compared to microdialysis, there is no upper bound

on the molecular weight of analytes that can be sampled using this method. This results in a complete representation of the ISF for relative and absolute quantification in the target tissue [83]. This technique has been used to monitor drug concentrations in skin and evaluate its bioavailability as well as pharmacokinetics [84, 85].

2.3.2.3 Reverse Iontophoresis

A small electric current applied across the skin can be used to non-invasively extract small analytes such as glucose and electrolytes. The skin is negatively charged at physiological pH, and acts therefore as a permeselective membrane to cations. This preferential passage of counterions induces an electroosmotic solvent flow that carries neutral molecules in the anode-to-cathode direction. The flux of analytes across the skin depends on charge applied, permeability of the analyte and concentration of the analyte. The non-invasive nature of this technique makes it an attractive candidate for potential point-of-care applications[86, 87]. Glucowatch is one such device that measures glucose concentration in ISF of the skin by electro-osmosis that results from reverse iontophoresis [88]. However, since this is an indirect measurement of concentration that is influenced by a variety of parameters, frequent calibration is required to maintain the accuracy of this device [89]. Continuous wear and application of current across the skin sometimes resulted in skin irritation. Hence, the device eventually turned commercially unviable.

2.3.2.4 Low frequency ultrasound

Low frequency ultrasound (frequency in the range 1–3 MHz, and intensity <0–2 W/cm^2) is capable of increasing permeability of the skin due to disruption in the barrier properties

of stratum corneum. This can thus be exploited to sample dermal analytes in a non-invasive manner [90].

Use of implantable sensor: Implantation of a small, wearable sensor inside the body is commonly used for detection of analyte concentrations in the subcutaneous space. Such sensors are commonly used to monitor the glucose levels in the body continuously. The sensor inserted into the subcutaneous space detects the concentration of glucose in the subcutaneous space [91].

The techniques mentioned above have limitations and so far, have been unsuccessful in being widely adopted for minimally-invasive, cost-effective diagnostic technologies. Thus, there is a need to develop a simple, reliable and low-cost method to sample ISF through skin.

2.3.3 Metabolomics of interstitial fluid

The field of metabolomics is a key discipline in the study of the metabolism of living organisms in a wide range of conditions, including health and disease. Metabolites are the downstream products of cellular function and represent a sensitive measure of the actions of upstream molecular species such as genes, transcripts, and enzymes, including the effects of disease, drugs, toxicity, and the environment. Hence, identification and quantitative analysis of metabolites in humans and animal and cell models of numerous human diseases offer avenues for understanding, diagnosing, and managing human diseases; assessing disease risk factors associated with drugs, toxins, and the environment; and ultimately developing personalized treatment options [92].

Metabolomic analysis of body fluids has seen considerable research interest due to the development of highly sensitive, high throughput techniques such as mass spectrometry [93]. Mass spectrometry is a powerful analytical technique that can detect analytes in the picomolar to attomolar range. This can be used to identify and analyze hundreds of compounds in a single sample. Mass spectrometry measures the mass-to-charge ratio (m/z) of ions to identify and quantify molecules in simple and complex mixtures. Mass spectrometry is widely used tool in research to identify biomarkers, study drug mechanisms [94].

Since ISF contacts tissue, it transports analytes of various metabolic processes between cells and blood vessels. Thus, metabolomics of ISF presents a useful tool to study different metabolic processes and identify new biomarkers that are not otherwise found in blood, urine or saliva [50, 51, 54, 95, 96]

2.4 **Microneedles for biosensing**

2.4.1 Introduction to microneedles

MNs are microscopic needles with length varying from 100-1500 µm. Several MNs are typically incorporated onto a single backing layer to form a MN patch [97]. They are around 50-500 µm at base and taper to a sharp tip with tip radius of less than 1 µm up to about 20 µm. They are sharp enough to penetrate through the stratum corneum, creating micropores into the underlying epidermis and dermis. These micropores can be used to either deliver therapeutics into the skin or to sample fluid/tissue from skin. MN patches were initially developed as a tool for drug delivery applications. Being easy to use,

inexpensive, pain-free and absent of sharps waste make MNs an attractive option in a point of care setting.

There are three basic types of MNs: solid MNs, hollow MNs and dissolving MNs. A schematic of the different types of MNs and the different approaches for drug delivery are shown below in Figure 2.2. Solid MNs are made from materials such as stainless steel, glass, various polymers. They penetrate skin and leave micron sized holes on the skin. This increases permeability of skin to a drug. The drug can then be delivered using a transdermal patch [98]. Alternately the drug is coated on to the surface of the MNs and the drug load can be delivered as the MNs are inserted and the coating dissolves off [99]. Hollow MNs are usually made from metal and have a hollow bore in the center similar to a conventional hypodermic needle. This allows infusion of a larger quantity of drug into the skin [100, 101]. Dissolving MNs are made from water-soluble polymers. The drug of interest is incorporated into the MNs. The needles dissolve upon contact with ISF in the skin and incorporated drug is released [102]

MN insertion into skin is considered generally painless. It causes minimal trauma to the patient. Also, use of MNs minimizes chances of any adverse skin effects such as erythema. For these reasons, use of MNs is considered patient-friendly and user compatible [103, 104].

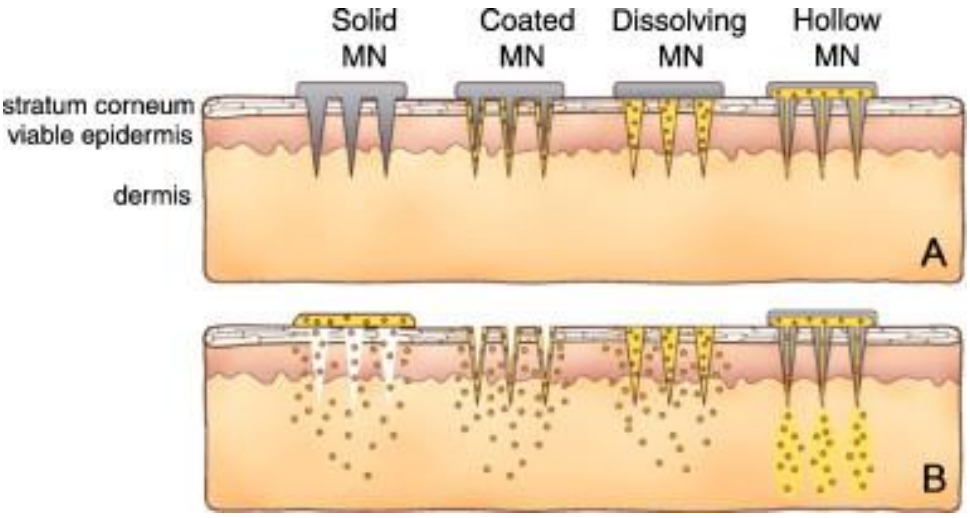

Figure 2.2: Four different types of MN patches. (A) MN patches upon initial insertion into skin. (B) Drug being delivered across the stratum corneum into the dermis and epidermis. Reproduced from [97]

2.4.2 Microneedles for sampling interstitial fluid

Research in MN array devices has progressed rapidly after microfabrication techniques made fabrication of MNs feasible in the 1990s. Although most research has focused on drug delivery applications, use of MN technology as a diagnostic tool via extraction of bodily fluids such as ISF and blood has received significant interest in recent years [105-107]. Since MNs can reach beyond the barriers of stratum corneum and viable epidermis, they can access the dermal ISF. This can enable minimally-invasive sampling of dermal ISF. MNs can be easily adapted to point-of-care devices and especially to wearable systems. MN patches can be worn as a patch/band aid and they conform well to the skin. They are lightweight making them portable and making them ideal for wear long term.

Use of MNs for diagnostics offers significant advantages over conventional techniques. Since the MN patch may be left on the skin for a prolonged time (e.g., up to one week), we

can obtain continuous or time-averaged measurements of biomarkers. Unlike traditional transdermal patches, MNs have access to a deeper body fluid source that reduces the chances of contamination occurring from environmental agents. Thus, the system can be more robust and accurate. Measurement of biomarkers in ISF is expected to be more accurate than using body fluids such as saliva, sweat or urine where concentration of biomarkers is dependent on degree of hydration, time of day, etc. Since ISF flows from the dermis into the MNs, contaminants on the skin surface may not interfere with ISF composition giving improved sensitivity and accuracy.

There are two main approaches to using MNs for diagnostics. The first approach is to have MNs/micropores as conduits to take a sample of ISF out of the body. The fluid is then analyzed for biomarkers. Sampling ISF typically yields larger volumes of ISF. This can be used for higher-order analysis of ISF like advanced testing on equipment that cannot be miniaturized. The other approach is to integrate a biosensor on the MN. This facilitates in-situ detection of biomarkers making it more suited for point-of-care. But the approach can only be used to detect a few specific biomarkers at a time using custom-designed assays.

2.4.3 Review of previous research-Microneedles for biosensing

MNs give access to ISF as they reach beyond the stratum corneum and the viable epidermis into the dermis. MNs themselves can only create pathways into the skin and other mechanisms need to be employed to extract ISF. This can be done in a variety of ways by using diffusion, hollow MNs that utilize capillary action, hydrogel MNs that swell and incorporate ISF or use of suction to draw out ISF convectively. Initial designs of MNs to

sample ISF started with a hollow MN to draw ISF through the bore utilizing capillary action or suction. Recently other approaches such as solid MNs with application of suction and hydrogel needles that swell up on contact with ISF are being explored for sampling ISF. The various approaches used to adapt MNs for biosensing applications are described below.

2.4.3.1 Approaches based on hollow microneedle designs

One of the approaches has been to design MNs to mimic blood-extraction action of a mosquito. Kobayashi [108] and Suzuki [109] described hollow MNs with a phase transition gel as an actuator. This setup was later adapted for continuous monitoring for an extended time period (10 h) by changing the gel characteristics [110]. They demonstrated proof-of-principle that glucose concentrations in a buffer solution could be measured continuously over time. Gattiker et al. described a similar system to extract ISF with microelectronics to allow in-situ detection of glucose [111]. Tsuchiya et al. also developed a MN device mimicking a mosquito with a piezoelectric actuator to extract blood via skin [112]. They showed extensive modelling to validate the feasibility of this approach [113, 114]. However, challenges in system integration, miniaturization and batch manufacturing render practical implementation of this design difficult.

Hollow MNs with capillary action: Mukhererjee et al. described a hollow MN patch with a 20x20 array of 250-350 μm long MNs. Deep Reactive Ion Etching was used to etch needles in a silicon substrate. ISF entered these needles via capillary forces and was subsequently drained into a reservoir which was connected to the needles via micro-channels. The MN patch was shown to be able to take up a variety of body fluids such as

ISF and blood. The design was also tested on one human earlobe. Glucose was detected on a colorimetric test paper after 15-20 min of extraction. However, no quantitative results were shown [115, 116]. Ebah et al. [117] extracted ISF from edematous patients. They observed that extraction of ISF was successful in subjects with increased ISF.

MNs with electrochemistry: Miller et al. [118] developed MNs that integrated carbon fibers within the MN bore for detection of hydrogen peroxide and ascorbic acid. They later modified the design to fill the MN bore space with an enzyme functionalized carbon paste. This makes the design of MNs more robust. Also, easy regeneration capacity of carbon paste electrodes facilitates re-use of the MN array. The device successfully detected hydrogen peroxide and lactate concentrations in vitro [119]. Miller et al. [120] also developed a multiplexed MN sensor that could simultaneously detect pH, lactate and glucose in one device framework. The device showed suitable performance in vitro for physiologically relevant concentration ranges. A hollow MN device with solid state ion sensitive electrodes was also developed to detect concentration of K^+ ions. The on-chip response of the electrodes to physiological concentrations of K^+ was determined [121]. Keum et al. [122] attached a MN sensor onto an endomicroscope for detection of nitric oxide during endomicroscopy. The polymer MNs were coated with PEDOT and functionalized with hemin that has high binding capacity towards nitric oxide. The MN system showed excellent sensitivity towards nitric oxide. The nitric oxide levels detected were twice as high in melanoma tissues compared to control. The sensor was also tested in vivo for mice with melanoma. The device could detect micromolar concentrations of nitric oxide in vivo in colonic tissue of mice with colon cancer. A MN based sensor array capable

of simultaneously detecting multiple analytes in physiologically relevant tissue environments was developed [120].

2.4.3.2 Use of suction

Wang et al. [123] used glass MNs that were used to make micropores into skin. Suction (200-500 mmHg) was applied for 2-10 min. Droplets of ISF, typically 1-10 µL, were drawn to the skin surface of skin in sedated rats and awake humans. Glucose concentration in the extracted ISF and plasma were shown to correlate well. The lag time between change in glucose concentration in plasma and ISF was observed to be around 10 min. Li et al. [124] described a single 1800 um long hollow MN system connected to a syringe that applies negative pressure on the system. The device could extract blood from the tail of a mouse at the rate of 0.8 uL/s on application of 100 mmHg negative pressure. However, repeated MN deformation was observed due to the high aspect ratio of the system. Recently Seventh Sense Biosystems, Inc. has developed a MN-based blood-sampling device that enables blood to be drawn through a virtually painless, one step process [125, 126].

2.4.3.3 Microneedles with in-built sensing

MNs with in-built glucose sensors: Zimmerman et al. [127, 128] first developed a MN patch with a glucose sensor built into the device. The MNs were 250 um long. ISF is extracted through the MN bore by capillary action and is pumped towards a miniature glucose sensor. The device showed a linear response to glucose concentration in the working range. However, the device response was seen to vary with flow rate which was not constant in vivo by capillary action alone. Chua et al. [129] and Jina et al. [130] describe a similar device based on glucose oxidase-based sensor along with hollow MNs for

continuous glucose monitoring. Glucose transport happened by passive diffusion through the MN bore which opens up into a central sensing chamber which is located outside the body. It was tested on 10 human subjects. Of a total 1396 paired points obtained, 75% were in region A of the Clarke Error Grid. The device was being commercialized as part of system under development by ArKal Medical, Inc. However low accuracy of the device over time rendered the venture commercially unviable. Invernale et al. [131] described a solid MN array coated with a conducting polymer PEDOT on which glucose oxidase was immobilized. This enabled faster response to changes in glucose concentration and the sensors showed a linear response over physiological glucose range. Various innovations are coming forward in this research area - such as a self-powered biofuel cell-based glucose sensor[132] and glucose responsive insulin delivery where the detection and delivery mechanisms are both integrated into a single patch system[133].

Corrie et al. [134] developed a MN array where the MNs were coated with a layer of capture protein. When inserted into the ear of a mouse immunized with flu vaccine, the capture protein on the MNs bound to the antibodies in the mouse plasma and ISF. This binding was quantified and found to be significantly different from control. Similar experiments were done by Muller et al. [135] by coating the MNs with NS1 and IgG specific capture proteins. The levels of NS1 in skin were measured by using the MNs and compared against blood and they appear to correlate well. This demonstrates the feasibility of this approach. However, there are limitations on the number of analytes that can be measured at a time and also the variety of analytes for which this technique can be developed. Lee et al. [136] showed that multiple analytes could be detected from one MN

array by measuring concentrations of pfHRP2 protein from the skin of live mice along with NS1 as a negative control and IgG as a positive control, making the device more robust.

2.4.3.4 Hydrogel based microneedle systems

MNs with external glucose detection: Sato et al. [137]developed a MN treatment system to measure interstitial glucose AUC. A study was carried out on 30 healthy human volunteers. The skin site was pre-treated with solid MNs to make micropores and a hydrogel patch with an osmolyte was placed on the pretreated site for ISF extraction. Blood glucose and interstitial glucose curves over 3h were well correlated. Further studies were done to compare glucose response in patients with and without diabetes[138]. The AUC in subjects with and without diabetes also correlated well with a lag time of ~10 min. This study demonstrated the feasibility of using MN patches for continuous glucose monitoring. Hydrogel MNs: Donnelly et al. [139-141] developed hydrogel MNs that penetrate through skin in dry state. Upon insertion, they swell on interacting with ISF of the skin. Caffarel-Salvador et al. [142] inserted MN patches in human subjects and correlated caffeine and glucose intake by the subjects over time to caffeine and glucose levels in the patch. However, the lag times in glucose detection in blood and in skin via MNs was as high as 3 hours. Also, the amount of caffeine and glucose detected in the patch over 1h was 2-3 orders of magnitude lower than the amount detected in 15 uL of blood which demonstrates the extremely low flow rates of ISF extraction into hydrogels. The low volumes of ISF absorbed create challenges in effectively analyzing fluid for a range of biomarkers. Romanyuk et al. [143] developed a method to effectively collect the ISF absorbed by hydrogel MNs by centrifuging the MN patches. Solid MNs made of carboxymethyl

cellulose (CMC) were shown to swell up on contact with hydrated rat skin in a Franz cell setup. The swelling up of CMC is presumably due to osmotic forces [144]. Chang et al. [145] showed that a MN patch made from a highly swellable hydrogel material was able to sample up to 3 µL from rats in 30 min. They showed that they could capture variations in glucose concentration and monitor glucose levels in the ISF and in the blood post-meal and post-insulin. Similarly, they were also able to show a strong correlation between cholesterol levels in blood and in ISF.

2.4.3.5 Microneedles with microdialysis functionality

Microdialysis MNs: Zahn et al. [146-148] developed a microdialysis MN that was selectively permeable to small molecular weight analytes such as glucose while excluding large molecular weight proteins. This increased the sensitivity and accuracy of detection. The MN was a hollow MN covered by a microdialysis membrane. The dialysis perfusate was flown within the MN bore which enabled diffusion of glucose into the bore due to concentration gradient.

2.4.4 Impact and possible applications

The goal of this study is to design a MN-based system that can sample ISF through skin in a minimally-invasive, reliable, and reproducible manner. Although ISF is a major body fluid, its use in research and clinic is limited because of a general lack of simple methods to sample this fluid. The development of a reliable and simple MN-based method could enable exploratory research on novel biomarkers within ISF. This could include exploring the metabolome, proteome and transcriptome of ISF as compared to plasma or other body

fluids. This could lead to discovery of unique metabolites, metabolite pathways in ISF and in the skin. Eventually this could lead to clinical utilization of ISF for diagnostics as certain analytes that are unique to or elevated in ISF are preferentially sampled in the ISF instead of blood.

Development of such a method has potential for a large impact on clinical medical diagnostics. This includes continuous monitoring of analytes in the body. MNs can be worn on the body for longer periods of time. They are also easily portable, making them ideal to be worn on the skin surface. Another critical application for such MN-based devices is lifestyle monitoring. Such devices can monitor biomarkers for everyday fitness, stress, physical activity or exercise/ overtraining. Cortisol and testosterone are markers for stress [149]. Lactate, creatine phosphor kinase, creatinine, ammonia, urea, uric acid give valuable information about quality of exercise or any overtraining/muscle fatigue that can occur during exercise [62, 150]. Such devices can be valuable for elite athletes, mountaineers and people with high stress jobs such as surgeons and military.

Chronic conditions such as diabetes, cardiovascular diseases, chronic conditions, obesity have introduced a large healthcare burden on economy especially in the developed world[151]. Continuous glucose monitoring for patients with type I/II diabetes has been receiving widespread attention. Various biomarkers are under review for understanding of Chronic kidney disease[152], monitoring of cardiovascular diseases[153], cardiometabolic diseases [154]. Having a portable MN patch that can be used for monitoring the progression of these diseases by patients at home can be hugely beneficial for effective management and planning treatment interventions for these diseases. Home-use MN patches can be

especially useful to monitor levels of biomarkers that vary daily e.g. monitoring ovulation patterns in women, daily cortisol levels for stress management, monitoring drug levels in a patient undergoing treatment. Taking frequent blood draws from infants or children can be difficult. MN-based devices could be a suitable substitute especially for newborns where continuous monitoring of critical analytes is needed.

It is also possible to get time-averaged readings of biomarkers by keeping the patch on for a longer period. In addition to regular health monitoring for known conditions and their treatment progression, such patches can also be used for preventive care. People with high cholesterol or blood pressure who are at risk for cardiac arrest can have their troponin levels monitored. A sudden increase in troponin levels can indicate heart failure. Similarly, such devices can be used for detecting and preventing stroke for people at high risk or fits in patients with multiple sclerosis.

MN patches can lend themselves well to over-the-counter patches to screen for various conditions/diseases. These tests can vary widely from screening for HIV/AIDS, STDs to looking at individual nutritional status or any nutritional deficiencies such as vitamin/micronutrient deficiency [155, 156]. They can also extend to looking at exposure to environmental pollutants [157] by measuring concentrations of these agents that may have accumulated in ISF over time. These devices can be used by people at home and can enable them to get better control over their health and health choices.

The cost and convenience of MN patches lends themselves well to their use in the field in developing nations. MN patches for diagnostics can be used by individuals or healthcare

workers to monitor for infectious diseases like malaria, HIV, tuberculosis. They can also be used for screening large populations for various conditions such as nutritional deficiencies.

There is an unmet need for development of a simple, reliable, low-cost device and method to sample useful volumes of ISF. This technology can have tremendous impact on research within drug development, diagnostics, as well as understanding cellular processes. This device can be used in the clinic to routinely monitor biomarker levels and can serve as an alternative to painful blood draws.

3 CHAPTER 3. SPECIFIC AIMS

Specific Aim 1: Evaluate mechanisms of sampling ISF by MNs through experimental studies and theoretical modeling of transport of ISF transport in skin.

Specific aim 2: Determine the composition of human suction blister ISF using high-resolution mass spectrometry.

Specific aim 3: Develop a MN system to sample ISF in human participants and identify biomarkers in the ISF compared to blood.

4 CHAPTER 4. EVALUATE MECHANISMS OF SAMPLING INTERSTITIAL FLUID BY MICRONEEDLES THROUGH EXPERIMENTAL STUDIES AND THEORETICAL MODELING OF TRANSPORT OF INTERSTITIAL FLUID TRANSPORT IN SKIN.

4.1 Introduction

Diagnosis and management of disease is increasingly facilitated by measurements of biomarkers from blood, urine, saliva and other bodily fluids. Continuing progress in biomarker discovery has enabled early diagnosis, real-time monitoring and improved disease management [158]. Blood is the most common source of biomarkers, but is limited by inability of patients to draw venous blood themselves and apprehension and sample quality of fingerstick capillary blood [159]. Urine and saliva are constrained by their limited number and variable concentration of biomarkers [21, 160]. Interstitial fluid (ISF) is another source of valuable and unique biomarkers, but is difficult to sample from the body [48]. This fluid surrounds cells and tissues throughout the body and is formed by extravasation of plasma from capillaries and modified by metabolic and other processes in the tissue [46]. ISF shuttles nutrients and waste products between blood vessels and cells and is roughly a combination of serum and cellular materials.

Previous studies showed that 83% of proteins found in serum are also in ISF, but 50% of proteins in ISF are not in serum, suggesting that ISF may be a source of unique biomarkers as well as biomarkers found in blood [50, 51]. Moreover, ISF may be suitable for continuous monitoring due to absence of clotting factors, as shown by commercial

indwelling sensors for glucose that access ISF in the subcutaneous space [91]. ISF is a better indicator of local tissue events as shown in tumor ISF collected from tissue biopsies [161].

Skin is the most accessible organ and therefore an attractive source of ISF containing systemic and dermatological biomarkers. ISF can currently be collected from skin using suction blisters by applying suction to skin at elevated temperature for up to 1 h to create blisters filled with ISF [73]. Dermal ISF can also be sampled by implantation of tubing in skin to collect ISF biomarkers by microdialysis or open flow microperfusion, which require local anesthesia and expert training [82, 85]. The time-consuming nature of these procedures, risks to patients, need for medical expertise and specialized equipment limit their use to basic research. Collection of ISF for more widespread research and possible future medical applications will benefit from a simpler, minimally invasive sampling method. This could enable further research into the nature and composition of ISF and the clinical utility of ISF as a body fluid for diagnostic applications.

We propose that microneedles (MNs) can be used to create micron-scale pathways for ISF transport out of skin across skin's outer barrier layer of stratum corneum. When coupled with a suitable driving force, a MN patch could be used to sample ISF from skin in a simple, minimally invasive manner. MNs are needle-like projections typically made from metal or polymer that measure hundreds of microns in length and thereby penetrate upper layers of skin and access skin's ISF [140, 162]. MN patches have been studied extensively for drug delivery into skin and have been safe, effective, painless and well-accepted by patients in

clinical trials and other studies. However, relatively little work has been done to develop MN patches for removal of ISF from skin.

Most of skin's ISF is in dermis [72], which comprises a network of collagen and elastin fibers surrounded by extracellular matrix that limit ISF flow due to binding and tortuosity. Hence, sampling ISF using MNs is a complex process involving three steps: (i) flow of ISF through dermis towards MNs, (ii) partition of ISF from dermis into MNs and (iii) flow of ISF through MNs to the skin surface.

Most prior efforts to collect ISF using MNs have been limited by collection of small volumes of fluid and have emphasized demonstrations of device performance rather than systematic device analysis and design [106]. Generally, diagnostic tests require at least multiple microliters of fluid for accurate measurement of analytes [163-165]. Here, we used experimental and theoretical analysis to systematically evaluate ISF collection from skin by MN patches using transport mechanisms mediated by diffusion, capillary action, osmosis, and pressure-driven convection with the goal of collecting 1-10 μL of ISF within 20 min, and then used the optimal design to sample ISF from human volunteers.

4.2 **Results**

4.2.1 ISF content in skin

To estimate the maximum amount of ISF that could be sampled from skin, we first determined that pig cadaver skin used in our studies contained 61±9 wt% fluid by fully drying skin by lyophilization. It was assumed that since the cellular epidermis constitutes

only ~10% of skin volume and there are very few cells in the dermis, this figure is representative of the amount of fluid present in the interstitium, i.e., ISF. This value is similar to reported values of ~70 wt% of human dermis comprising ISF [166]. Because pig cadaver skin mass was 0.25±0.04 g/cm^2, this corresponds to ISF content ~150 µL/cm^2 of skin. When pig skin was subjected to a large pressure (890 kPa), ISF was lost from skin through dermis at ~1 wt% per minute, such that 24±6 wt% was lost after 20 min, corresponding to ISF loss of ~60 µL/cm^2 after 20 min (Figure A. 1 in Appendix A). This value represents the volume of mobile ISF, i.e. fluid that is not otherwise bound and may provide an upper bound to the amount of ISF that could be withdrawn from skin within 20 min ex vivo, although the situation might be different in vivo due to blood flow and other effects.

4.2.2 ISF collection by diffusion into hydrogel microneedles and micropores

One mechanism of ISF collection involves diffusion of ISF into MNs, which can be accomplished by inserting dry hydrogel MNs into skin. To study this mechanism of ISF collection, we prepared patches each containing 100 pyramidal MNs composed of cross-linked polyvinyl alcohol (PVA) (**Error! Reference source not found.**). Upon insertion into skin, the MNs became swollen with ISF (**Error! Reference source not found.**b-c). After 12 h in skin, 0.0030 µL of ISF was absorbed per MN (0.30 µL/patch).

We also studied diffusion through micropores (µpores) created by puncturing and then removing metal MNs in skin (**Error! Reference source not found.**). The volume of ISF sampled through µpores was 0.0039 µL/µpore after just 20 min. The order-of-magnitude

faster ISF collection through µpores may be due to lack of transport barriers found in µpores.

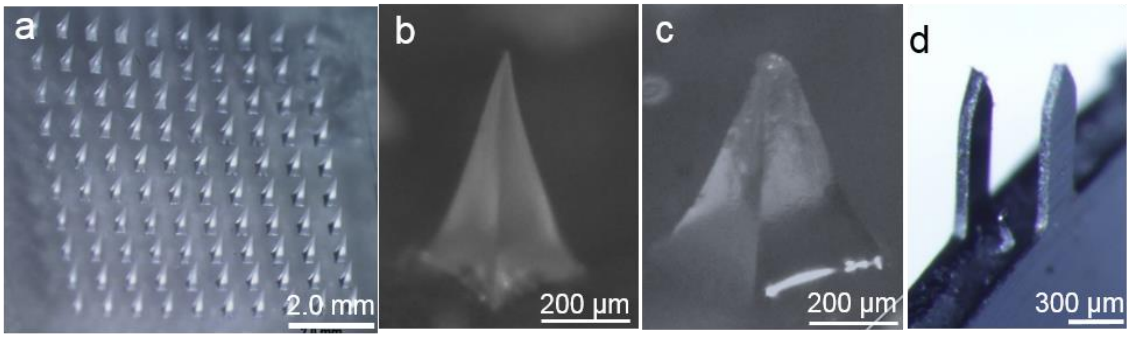

Figure 4.1: ISF collection by diffusion into hydrogel MNs and skin µpores. (a) Representative patch containing 10x10 array of dried hydrogel MNs made of polyvinyl alcohol (PVA). Magnified views of representative (b) dried hydrogel MN (520 µm tall) before insertion into skin, (c) hydrated hydrogel MN after swelling in pig skin for 12 h ex vivo and (d) two stainless steel MNs (750 µm tall)

4.2.3 Collection by capillary flow through porous and hollow microneedles

The second mechanism of ISF collection we considered involves capillaries to draw ISF from skin. This can be accomplished by flow through either a network of microcapillaries in a porous MN or a single capillary in a hollow MN.

To study porous MNs, we prepared patches each containing five MNs made from paper, which were sandwiched between two stainless steel MNs of similar dimensions for mechanical support (Figure 4.2a). Similar paper has been characterized to have porosity of 68% [167] and pore size of 2-10 µm [168]. Upon insertion into skin, microcapillaries in the porous paper matrix absorbed 0.0033 µL/MN of ISF after 20 min (Figure 4.2b,d). To study a single capillary system, we used individual hollow MNs with 108-260 µm inner

diameter (Figure 4.2c), which collected ~0.01-0.03 µL ISF after 20 min (Figure 4.2d). The greater ISF collection by hollow MNs may be explained in part because the MN orifice surface area was greater than the exposed surface area of porous MNs sandwiched between metal MNs.

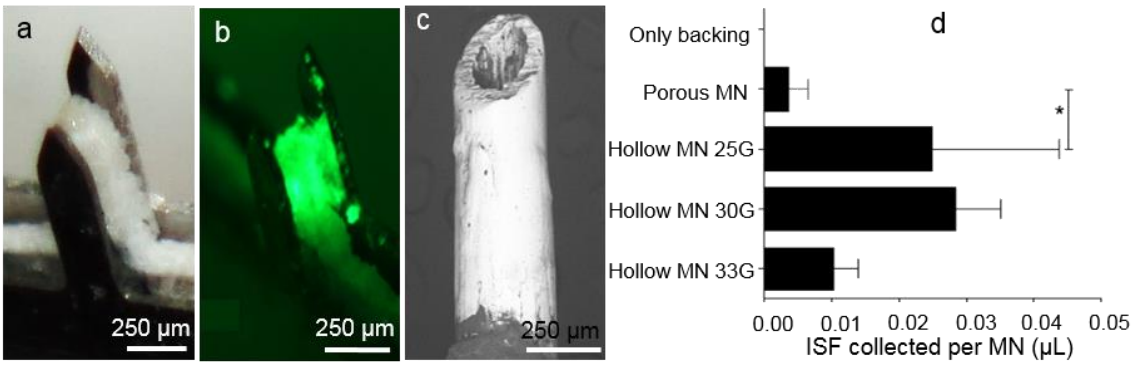

Figure 4.2: ISF collection by capillary action through porous and single-capillary MNs. (a) Representative porous paper MN sandwiched between two stainless steel MNs for mechanical support (750 µm tall). (b) Representative porous paper MN that has absorbed ISF from pig skin soaked in fluorescein to facilitate ISF imaging. (c) Representative hollow stainless steel MN (750 µm tall) with a single hollow capillary to draw fluid out of skin. (d) ISF volume sampled from pig skin after 20 min: porous paper backing with no MNs (negative control); porous paper MNs; and hollow, single-capillary MNs of 33G (108 µm inner diameter (ID)), 30G (159 µm ID) and 25G (260 µm ID). Data show mean ± SD (n = 4) *p<0.05

4.2.4 ISF collection by osmotically driven flow via micropores

The third mechanism to sample ISF from skin uses an osmotic driving force to flow ISF from skin into µpores created by MNs. To generate an osmotic pressure gradient, we filled µpores with a solution of elevated ionic strength to drive ISF from dermis into µpores.

Lacking a permselective membrane between μpores and dermis, solutes in μpores could diffuse into dermis, which accelerated the decrease of osmotic pressure gradient over time.

A 10-MN patch coated with ~20 μg of maltose per MN (Figure 4.3a) was inserted into skin for 2 min to allow maltose to dissolve, and were then removed. The maltose created an initial ionic strength of ~1.17 M in the μpore, which is much higher than surrounding ISF (0.29 M [71]) and corresponds to an osmotic pressure difference of 2.2 kPa. After 20 min, 0.0056 μL of ISF was collected at the skin surface per μpore (Figure 4.3b). In contrast, leaving MNs in skin during the 20 min ISF collection time yielded significantly less ISF (0.0006 μL/μpore), probably because MNs blocked ISF transport pathways out of skin (Figure 4.3b).

To better maintain an osmotic driving force over time, we punctured skin for 2 min with a patch containing 10 uncoated or maltose-coated MNs, and then, after removing MNs from skin, applied a 1.17 M solution of maltose to the skin surface, thereby initially filling μpores with ~1.17 M. After 20 min, treatment using uncoated or coated MNs collected 0.024 or 0.021 μL/μpore, respectively (Figure 4.3b), which were not significantly different from each other, but were greater than treatment with coated MNs without adding maltose solution. ISF collection rate during osmotically driven transport increased steadily over the course of 60 min to a total volume of 0.070 μL/μpore (Figure A. 2 in Appendix A). Varying the number of MNs from 10 to 50 increased ISF collected in rough proportion to number of MNs (Figure A. 3 in Appendix A).

As a control, we punctured skin with 10 uncoated MNs and then applied water to the skin surface, which provided no osmotic driving force. This collected 0.0039 µL ISF/µpore after 20 min (Figure 4.3b), which was significantly less than collected with an osmotic driving force and similar to ISF collection during diffusion through µpores (Figure 4.2).

To achieve still higher osmotic strength, we applied a solution of $MgCl_2$ with 12 M osmotic strength to skin punctured with a 10-MN patch. This collected 0.03 µL/µpore after 20 min (Figure 4.3b). This order-of-magnitude increase in osmotic strength increased ISF collection ~2-fold. This may be explained by a faster dissipation of osmotic driving force due to faster diffusion of $MgCl_2$ away from µpores compared to maltose.

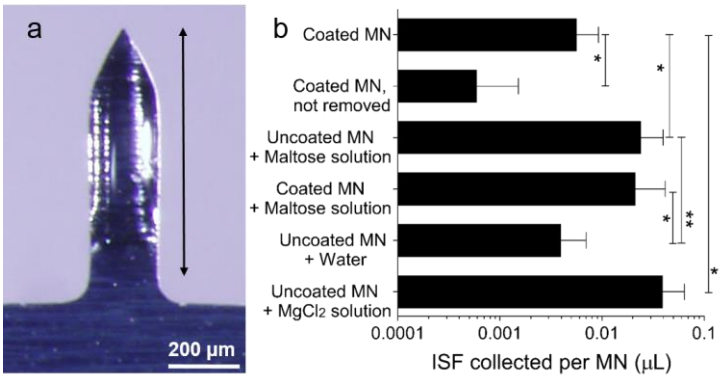

Figure 4.3: ISF collection by osmosis through µpores. (a) Representative MN coated with maltose (bar shows coated region). (b) ISF volume collected from pig skin ex vivo punctured with coated and uncoated MNs followed by application of aqueous solutions of different osmotic strength for 20 min. Data show mean ± SD (n≥4) *p<0.05 **p<0.01

4.2.5 ISF collection by pressure-driven convection via micropores

A pressure difference between the dermis and skin surface can drive ISF from dermis into and through μpores. This can be accomplished by suction to create negative pressure on the skin surface at the site of μpores or by positive pressure on the skin surface at sites distant from μpores (e.g., pinch the skin), thereby creating a positive pressure in skin near μpores (Figure A. 8 in Appendix A).

To study effects of suction on ISF collection, we punctured skin with 10-MN patches and then applied -85 kPa suction for 20 min. This produced just 0.0064 μL ISF/μpore (Figure 4.4a). We hypothesized that suction might be collapsing μpores, so we placed skin on curved surfaces (with ~5 mm or ~8 mm radius of curvature) to help spread μpores open. This increased ISF collection by two orders of magnitude to 0.30 or 0.47 μL/μpore, respectively (Figure 4.4a). Stretching skin with a strain of ~100% on a flat surface or a curved surface produced 0.84 or 0.60 μL/μpore, respectively Figure 4.4a). Altogether, these data show that suction withdrew by far the most ISF from skin, but the skin surface needed to be curved and/or stretched, apparently in order to keep μpores open.

We next placed different kinds of absorbent paper on the skin above μpores to capture ISF collected during -85 kPa suction for 20 min. Compared to ISF collected without paper (0.71 μL/μpore), placement of thin tissue paper (Kimwipe) on skin had no significant effect (0.29 μL/μpore) (Figure 4.4b). However, placement of gauze (~680 μm thick) on skin, reduced ISF collected by two orders of magnitude to 0.0035 μL/μpore. We hypothesized that gauze inhibited ISF collection because of its thickness and poor aqueous wettability. Plasma treating (to increase hydrophilicity) or pre-wetting gauze significantly increased ISF collection (0.065 or 0.12 μL/μpore, respectively, Figure 4.4b), suggesting that surface

tension played a role in ISF flow from skin to gauze. Using thinner gauze (~150 µm thick) collected 0.17 µL/µpore, which was significantly greater than when using thick gauze (Figure 4.4b). This suggests that gauze may have reduced the pressure drop within the skin and µpore, and that thinner gauze reduced it to a lesser extent.

We also studied effects of other MN parameters on ISF collection during suction. Varying number of MNs from 5 to 10 to 50 increased ISF collected in rough proportion to number of MNs (Figure A. 4 in Appendix A). Increasing MN length between 250–750 µm on 10-MN patches showed a trend of less ISF collected as MN length increased, but this was not statistically significant (Figure A. 5 in Appendix A). Use of patches with polymer MNs that tapered from a wide base (which was needed for mechanical strength of polymer MNs) was less effective compared to thin metal MNs used in the rest of this study (Figure A. 6 in Appendix A), probably because polymer MNs did not insert as deep into skin [162]. Finally, using three different MN designs, we compared curved skin to stretched skin, and found they each provided similar ISF collection under the conditions used (Figure A. 7 in Appendix A).

Finally, we generated positive pressure in skin by pinching to drive ISF out of the skin (section A1.8 in Appendix A). After applying a 10-MN patch and then administering a positive pressure (estimated to be 25 kPa inside skin below µpores) for 20 min, 0.16 µL ISF/µpore was collected (Figure 4.4c). We also found that amount of ISF collected increased linearly over time when either positive or negative pressure was applied (Figure

4.4c).

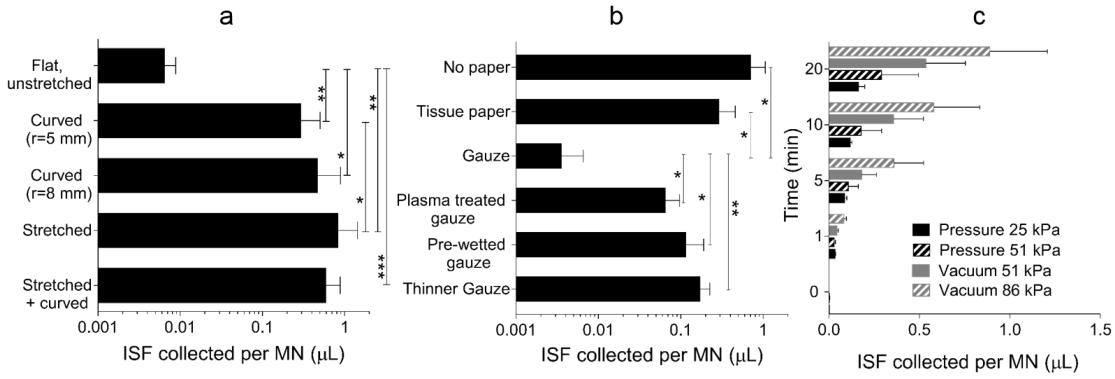

Figure 4.4: ISF collection by pressure-driven convective flow through μpores. ISF collected from MN-punctured pig skin ex vivo after 20 min of suction (-85 kPa) (a) for skin under different degrees of tension and (b) for skin covered by different absorbent papers. (c) ISF collected from pig skin ex vivo after different durations and levels of suction and positive pressure applied to skin. Data show mean±SD (n≥3) * p<0.05 ** p<0.01 *** p<0.001

4.2.6 ISF collection from the skin of human volunteers

Guided by the above findings, we used 50-MN stainless steel patches to create μpores followed by suction for 20 min (Figure A. 9). This collected 2.3±2.1 μL ISF per person based on 17 separate ISF collections from 6 different volunteers. Determination of ISF volume assumed that sodium concentration in human ISF is constant at 135 mmol/L, although this value may vary by ~10% in healthy individuals [89]. The collected fluid was clear, with little or no evidence of blood. Since ISF transport occurred through μpores and not the entire stratum corneum, ISF appeared as droplets on the skin surface (Fig. 5c). ISF flow rate was not quantified as a function of time, but our observation was that ISF first appeared on the skin surface after ~30 s of vacuum and then steadily increased over time.

There was spatial heterogeneity of ISF collection within each array of 50 μpores, where some μpores produced visible amounts of ISF and others did not. Mild erythema was observed at the skin site, which resolved completely within 24 h (Figure 4.5). In a few cases, 15-20 faint, pink, sub-millimeter spots were visible at sites where individual MNs had penetrated skin, and disappeared within 24 h. The erythema was of possible cosmetic significance, but not clinically meaningful. Volunteers generally reported little or no pain associated with the procedure. No adverse events were recorded, and overall the procedure was well tolerated.

Collected ISF from 11 subjects was analyzed for glucose and total protein content as representative biomarkers. The concentration of glucose in ISF was 91±11 mg/dL and total protein concentration was 90±21 mg/mL (Figure A. 10a). We also collected companion plasma samples from the subjects from fingerstick capillary blood. The concentration of glucose in plasma was 100±25 mg/dL and total protein concentration was 105±26 mg/mL (Figure A. 10b) which is comparable to the concentrations in ISF (Student's t-test, $p>0.05$).

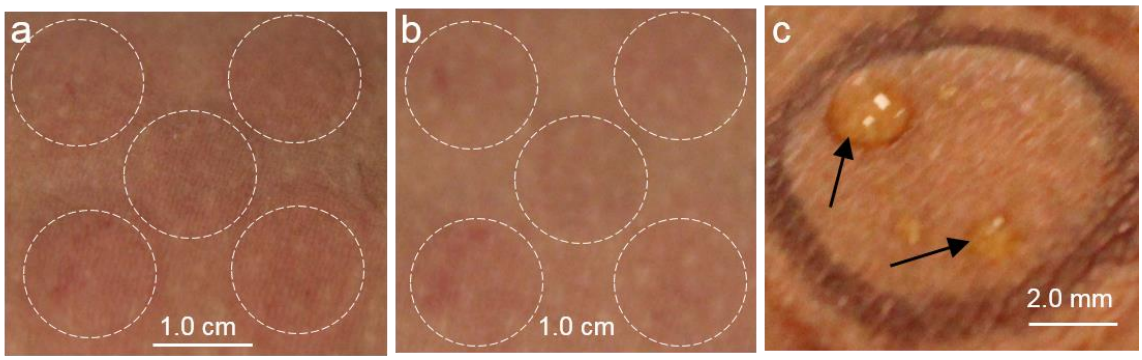

Figure 4.5: ISF collection from human volunteers by suction through μpores. Representative images of skin (a) immediately after suction show faint erythema and no evidence of edema or bleeding (dashed white circles identify sites of ISF collection

through 50 µpores) and (b) 24 h after ISF collection show resolution of erythema. (c) Representative image showing ISF droplets on skin surface after collection by suction through µpores.

4.2.7 Theoretical model to predict ISF collection rates

To better understand underlying mechanisms governing ISF transport through skin, MNs and µpores, we modeled ISF transport in the scenarios explored in this study. Our goal was to predict ISF collection rates in each scenario and identify rate-limiting steps to enable improved ISF collection. The theoretical modeling considered three steps in the transport process: transport through skin to the MN (or µpore) interface, transport/partitioning across the skin-MN interface and transport through or within MN. To provide independent predictions of ISF behavior in skin, theoretical predictions were based on first-principle models using parameter values that were measured, independently calculated or adapted from literature; there were no fitted parameters. Predicted values match experimentally observed values reasonably well, especially given the simplified theoretical analysis with no fitted parameters, and are often within the error bars of the data (see Section S2.6 in Appendix A).

ISF collection by hydrogel MNs was modeled as ISF diffusion through dermis and then, upon partitioning into the hydrogel, diffusion through the hydrogel matrix (Section S2.1 in Appendix A). As ISF diffusivity in dermis is greater than in PVA hydrogel used in this study, diffusion of ISF through hydrogel was rate-limiting and significantly constrained ISF collection rates (Figure A. 11). Using a different hydrogel with higher ISF diffusivity,

e.g., as described by Chang et. al. [169], can increase rates of ISF uptake. However, once ISF diffusivity in hydrogel approaches and exceeds that in dermis, dermis becomes a rate-limiting step and further improvements to hydrogel permeability have diminishing impact. Similarly, ISF collection through µpores is limited by low ISF diffusivity in dermis, so dermis is a rate-limiting step (Section S2.2 in Appendix A).

ISF collection by capillary flow into porous and hollow MNs involves rapid convective flow within MNs, effectively making MNs a sink, which maximizes the concentration gradient in nearby dermis (Section S2.3 in Appendix A). The rate-limiting step is exclusively in dermis, which makes ISF collection faster than in the case of hydrogel MNs or µpores where ISF diffusivity in the MN/µpore can be fast, but is still a barrier (Figure A. 13). Although changes in MN design to increase capillary forces may not increase ISF uptake further, ISF uptake scales directly with area of MN-dermis contact. This explains why ISF collected by hollow MNs was greater than porous MNs, because surface area of the hollow MN orifice was larger than of porous MNs.

ISF collection by osmotically driven flow through µpores provides a transient convective driving force in the µpore and dermis (Section S2.4 in Appendix A). As osmolyte (e.g., maltose) diffuses from the µpore, a gradient of osmolyte is formed in surrounding dermis (Figure A. 14). The resulting osmotic pressure gradient within dermis drives ISF convectively to the µpore. This driving force for ISF convection in dermis differs from ISF collection by hydrogel or capillary MNs, which rely on ISF diffusion in dermis.

However, osmotically driven convection was transient because over time osmolyte diffuses away from the μpore, such that the osmotic pressure gradient decays to zero. To increase ISF collection, osmotic driving force could be increased by increasing osmolyte concentration and could be sustained longer by decreasing diffusivity of osmolyte in dermis. Thus, high molar water solubility and high molecular weight are good, and perhaps competing, properties of optimal osmolyte.

ISF collection by pressure-driven convection through μpores creates the largest pressure drop across the rate-limiting barrier of dermis to drive ISF into μpores (Section S2.5 in Appendix A). Whether by vacuum on the skin surface or positive pressure applied by "pinching," pressure drop is inherently focused on regions with greatest flow resistance in dermis. While the initial osmotic pressure gradient was 49 kPa/mm, it dropped almost to zero after 20 min. Direct application of vacuum or pressure achieved larger pressure gradients (131 kPa/mm or 77 kPa/mm, respectively) that remained constant. ISF collection could be further increased by increasing vacuum or applied pressure, but would be limited by pain and skin damage [170].

4.3 **Discussion**

To improve on invasive and time-consuming methods to sample dermal ISF currently available [73, 82], prior studies developed hollow MNs to withdraw ISF by capillary action [116, 171], solid hydrogel MNs that swell with ISF [140, 143, 169, 172], and solid MNs to puncture μpores in skin for ISF collection under suction [123]. These prior approaches have generally been limited by small sampling volumes (e.g., <1 μl) [106]. Other MN

designs have selectively bound targeted biomarkers to MNs in skin [134, 135], which requires customized MNs and procedures to elute biomarkers off MNs for analysis.

Here, we systematically evaluated mechanisms of ISF collection from skin with the goal of a minimally invasive, simple-to-administer MN-based system to sample >1 µL ISF from skin within 20 min. This volume suffices for many assays of clinical interest like sodium, glucose, troponin and cholesterol [163-165]. A 20 min sampling-time is compatible with a typical doctor's visit and patient-administered testing at home. Theoretical modelling identified rate limiting steps to ISF flow.

4.3.1 Analysis of ISF sampling methods

Hydrogel MNs sampled the smallest ISF volume, which was limited by diffusion in dermis and MNs. As ISF diffusivity in hydrogel increases, the rate-limiting step shifts from MN to dermis. However, even when ISF diffusivity in MNs (or µpores) approaches that of free self-diffusion of water, diffusion through dermis remains rate-limiting. ISF sampling rates are constrained because of diffusion without convective forces.

Capillary action increased ISF flow rate. Due to convective transport, flow through capillaries of porous or hollow MNs was not rate-limiting, leaving diffusion through dermis as the limiting barrier. Further optimization of MN design should increase MN-dermis interfacial area, which scales directly with ISF collection rate.

ISF collection rate using osmosis increased by an order of magnitude. Diffusion of osmolyte from µpores into dermis generates an osmotic pressure gradient that drives

convective flow in the rate-limiting barrier of dermis. MNs coated with osmolyte were less effective to collect ISF probably because the small amount of osmolyte delivered into skin diffused away quickly. A reservoir of osmolyte on skin surface helped maintain high osmotic strength in µpores and dermis, even as osmolyte diffused away, thereby increasing ISF collection. Flow of ISF into µpores was governed by two transient, competing parameters: osmotic pressure generated by osmolyte diffusion into dermis near µpores (increasing osmotic pressure) and osmolyte diffusion away from µpores in dermis (decreasing osmotic pressure). ISF collection could be increased by increasing number of µpores, increasing osmotic pressure by increasing osmolyte concentration or decreasing speed of osmotic pressure gradient decay by slowing osmolyte diffusion into dermis.

While transient convection in dermis due to osmotic pressure gradients improved ISF collection, continuous application of pressure gradient across dermis via pressure or suction maximized ISF sampling. Effective ISF collection using suction required stretched/curved skin, which probably forced µpores open during vacuum application. ISF collection on the skin surface also depended on material covering the µpores to collect ISF. A thin hydrophilic cover did not interfere with pressure drop in skin and allowed ISF to readily flow out of the µpore. ISF flow varied linearly with time and pressure, and was limited by flow conductivity of dermis and applied pressure gradient. During suction, maximum possible pressure drop is 101 kPa (i.e., 1 atm), and both positive and negative pressure are further limited by sensitivity of skin tissue to pressure. Even with these constraints, ISF collection achieved the target of >1 µL within 20 min in pig skin ex vivo and human volunteers.

Future research should address limitations of the study, such as increasing ISF collection rate to produce more ISF in less time; reducing variability in amount of ISF collected probably due to interpersonal and time-dependent differences is tissue hydration and other properties; and enabling ISF collection using a smaller and simpler device compared the bulky pump used here.

4.3.2 MN treatment acceptability, safety and impact

ISF is a rich source of biomarkers that has received limited attention for lack of good collection methods. ISF can be an alternative to blood sampling; many proteins of medical interest found in blood were also in ISF from suction blisters [50, 51]. Skin proteins, like dermicidin and dermokine [173, 174], were preferentially found in ISF, suggesting that it could provide biomarkers not readily found in blood [51]. ISF is also valuable to dermatological pharmacokinetics in skin [82].

ISF sampling is currently done using suction blisters, microdialysis and microperfusion, which require expert technique, cause tissue trauma and are costly and time-consuming [73, 82, 85]. ISF collection using methods described here is minimally invasive, causes little or no pain, is simple to administer, is well tolerated by skin, and can collect useful amounts of ISF relatively quickly. Previous studies in human volunteers have shown that MNs like those used here (but without collecting ISF) create μpores that close and cause mild erythema that resolves within hours [104, 175].

Here, MNs were combined with suction to withdraw ISF from human volunteers. This combined procedure caused only mild erythema, primarily associated with suction, and

resolved within 24 h. Suction is well accepted and safely applied to skin in existing procedures such as negative-pressure wound therapy, suction electrodes for ECG recording, cupping in traditional Chinese medicine and vacuum pore suctioning for cosmetics [176-178]. Suction, although mild, may be contraindicated in certain people, such as infants or elderly who may have sensitive skin. We expect that mild, transient erythema, will be acceptable for clinical applications of MNs. Although skin infections have not been reported due to MNs in other contexts [179], formation of μpores may not be appropriate in certain populations, such as those with weak immune systems or certain skin diseases [180]. Safety of ISF collection using MNs needs additional study.

This study should motivate further investigation of ISF composition compared to other body fluids such as plasma and in different populations, and identification of clinically valuable biomarkers in ISF. We believe that MN-based ISF collection can facilitate such studies and, in the future, make ISF routinely accessible for medical research, diagnosis and monitoring. Applications could include continuous analyte measurement for monitoring concentration of glucose or drugs with narrow therapeutic index, detection and typing of local skin diseases such as skin cancer, or monitoring stress levels in susceptible populations like military. Because ISF does not clot, it might be sampled continuously by a wearable system, possibly operated by patients themsevles. A versatile method of ISF collection suitable for widespread use is required to enable these applications.

4.4 Conclusion

ISF is a unique bodily fluid of great potential interest as a source of biomarkers, but has received little prior attention due largely to lack of straightforward methods to collect ISF from skin. This study found that ISF can be collected from skin using mechanisms that provide diffusive and/or convective driving forces with effectiveness in the following rank order: diffusion < capillary action < osmosis < applied pressure/suction. As determined by theoretical modeling (with no fitted parameters), ISF transport in skin was rate-limiting, such that methods providing convective forces in dermis (i.e., osmosis and applied pressure/suction) collected the most ISF. ISF collection by MNs combined with suction was well tolerated in human volunteers and produced ISF in sufficient quantity to identify biomarkers. Mechanistic understanding, MN device prototype development and successful demonstration in human volunteers shown here may enable ISF collection by MN patch to become a platform technology for diverse applications in medical research, diagnostics and monitoring.

4.5 Materials and methods

4.5.1 Microneedle fabrication

Hydrogel MNs were prepared by casting aqueous solution of PVA onto silicone molds in the inverse shape of MN arrays, followed by PVA crosslinking at elevated temperature and drying overnight (Fig 1a,b). Metal MNs were fabricated by chemical etching stainless steel sheets. 10-MN arrays were made by adhering two planar arrays of solid metal MNs with a spacer (Fig 1d). To fabricate porous MNs, from sheets of filter paper were laser cut using

metal MNs as a protective mask. This yielded paper MNs which were sandwiched between two metal MN arrays for mechanical strength (Fig 2a). Hollow MNs were made by shortening and rebeveling hypodermic needles using a rotary tool (Fig 2c). Coated MNs were made by dipping solid metal MNs into aqueous solution of maltose (Fig 3a). See Appendix A for details.

4.5.2 Measurement of ISF content in skin

ISF content in skin was measured by weight loss of pig ear skin after lyophilization. ISF that could be removed from skin was measured by weight loss after applying pressure to pig skin over time. See Appendix A for details.

4.5.3 Measurement of ISF collected from skin during MN-based protocols

Pig ear skin was equilibrated overnight with fluorescein solution. Hydrogel MN arrays were inserted into skin for 12 h to allow MNs to extract ISF. µpores were created with a 10-MN patch inserted and removed immediately from pig skin. Fluid on skin surface was wiped off after 20 min for analysis. *P*orous MN arrays were inserted and left in skin for 20 min to collect ISF. Hollow MNs attached to a syringe were inserted and left in pig skin for 20 min to collect ISF. For osmosis, maltose from coated MN patch was allowed to dissolve to create µpores filled with maltose solution. To fill µpores with osmolyte solution, maltose solution was pipetted onto µpores created with plain/coated 10-MN arrays. The system was left for 20 min to allow micropores to take up ISF. Fluid on the skin surface was collected after 20 min with tissue paper. To evaluate ISF collected by pressure-driven convection, µpores were created in skin with a 10-MN array. Suction was applied with a vacuum pump

over µpores. To make a curvature on the skin surface, a disk was placed under the skin surface. To stretch out skin, the ends of the skin piece were stretched by hand and secured to a wooden board. Suction was applied over the micropores for designated amount of time and ISF on the surface was collected by tissue paper. For MNs utilizing pressure, µpores were created in skin. The skin piece was folded in half with the pores at the apex, and placed horizontally on the benchtop. Pressure was applied over the skin surface using iron weights for a designated amount of time. To elute all ISF solutes absorbed using MN patches, the MNs or the tissue paper or gauze used to collect ISF was soaked in DI water for 24 h. ISF collected was measured by measuring amount of fluorescein in the sample and normalizing against fluorescein concentration in skin (i.e., 1 mg/mL). All reported fluxes and flow rates were averaged over the period of ISF collection (usually 20 min).

ISF was collected from human volunteers over 20 min by applying 34-68 kPa suction over µpores created by a sterile 10-MN patch. ISF on skin surface was collected using sterile gauze pads, subsequently soaked in DI water to recover ISF. All volunteers provided informed consent. This study was approved by Georgia Tech Institutional Review Board. ISF volume was determined by sodium ion concentration normalized to its concentration in standard ISF. Glucose and protein were measured using glucose and micro-BCA assays, respectively. See Appendix A for details.

4.6 Acknowledgements

We thank D Bondy for administrative support; JC Joyce, JW Lee, W Pewin, A Romanyuk, and A Tadros for help fabricating patches; C Massaro, K Nueberger, J Palacios, Z

Schneiderman, and A Yucesoy for assistance in experiments; S Henry and DV McAllister for help developing human protocols.

5 CHAPTER 5: DETERMINE THE COMPOSITION OF HUMAN SUCTION BLISTER INTERSTITIAL FLUID USING HIGH-RESOLUTION MASS SPECTROMETRY.

5.1 Introduction

Biomarkers are a powerful tool to study the entire spectrum of disease, from the ascertainment of diagnosis, examination of disease progression, and assessment of therapeutic benefits[181]. Most commonly, biomarkers are measured in easily-accessible body fluids, such as blood, saliva, and urine. However, there are challenges associated with these fluids. Blood sampling by venipuncture is invasive, potentially painful, and requires trained personnel. Biomarker concentrations in blood samples obtained via finger pricks may be variable if not collected under properly-controlled conditions [159]. Many saliva biomarkers are detected at low concentrations, and there is potential for interference by food or drugs [21]. While urine samples are easier to obtain than blood, urinary biomarker concentrations can be highly variable due to differences in urine dilution [27].

Although ISF constitutes 60% of total body fluids in humans [45], it is greatly unexplored as a matrix for biomarker detection. ISF, which bathes and surrounds cells and tissues of the body, is formed as plasma traverses blood vessels and equilibrates with the cell and tissue environment (reviewed in [182]). ISF provides a means of delivering nutrients to cells, enables intercellular communication, and removes metabolic waste.

The detection of biomarkers in ISF has several advantages to blood, urine, and saliva. Since ISF interacts directly with intracellular fluid, it is possible that compounds that cannot be

detected in plasma may be detected in ISF. Unlike blood, ISF can be used for continuous biomarker monitoring, in part because it does not clot [62, 63]. For example, continuous glucose monitors sample ISF to measure glucose concentrations [65]. Unlike plasma, which provides an integrated measurement of biomarkers from multiple organ and metabolic systems, ISF can capture changes in the local environment [50]. For instance, ISF sampled from tumors has been studied as a source of cancer biomarkers [161, 183]. In addition, ISF has lower concentrations of high-abundance proteins like albumin and globulin compared to plasma [68], which makes it easier to screen ISF for low-abundance compounds without extensive protein depletion and sample cleanup strategies.

There are limited techniques for ISF sampling, including suction blisters [73], microdialysis [82], open flow microperfusion [85], reverse iontophoresis [87], and MN patches [106, 143]. Suction blisters are a common method to sample large volumes of ISF, which are generated by applying vacuum to a skin area. A suction application separates the dermis and epidermis, and fluid from the surrounding tissues fills the gap, creating a blister. The blister fluid is withdrawn by a conventional needle and syringe. This fluid, referred to as suction blister ISF, is largely derived from ISF, but may also contain some intracellular components and inflammatory markers that are a consequence of the collection method [78]. Compared to other ISF sampling methods—including reverse iontophoresis, wherein an electric current is applied to skin, or microdialysis, wherein a small membrane is inserted into skin—suction blister sampling is a relatively non-invasive method for ISF collection given that the method requires a single needle puncture, similar to venipuncture.

The protein composition of suction blister ISF sampled from suction blisters has been studied using mass spectrometry. From suction blisters obtained from 8 healthy individuals, Muller et. al. [51] found that the proteome of ISF from suction blisters was heterogeneous, consisting of systemic plasma components, proteins originated from cell leakage, and proteins associated with skin tissue. Comparing proteins measured in suction blister ISF and plasma from 6 individuals, Kool et. al. [50] found that 83% of proteins found in plasma were also found in suction blister ISF, whereas only half of suction blister ISF proteins were common to plasma. The authors constructed a list of 34 clinically-relevant protein biomarkers that were abundant in ISF: while 9 out of the 34 were epidermal-derived, the rest were known systemic biomarkers, suggesting the utility of ISF as a surrogate for blood-based biomarker detection, as well as a source of tissue-specific biomarkers.

While previous research has explored the protein composition of suction blister ISF, to date, no study has characterized the small-molecule composition of ISF. Metabolites provide critical information on metabolic pathway intermediates, disease states, and exposure to environmental agents. Metabolite profiling is also a key tool to study the *exposome*, an emerging research paradigm involving the investigation of complex environmental exposures, biological responses to these exposures, and their impacts on human health and disease [184].

Here, we profiled small-molecule metabolites in dermal ISF obtained from suction blisters to better understand the composition of the ISF metabolome. First, metabolites in plasma and suction blister ISF samples obtained from human volunteers were analyzed using

untargeted high-resolution metabolomics (HRM) [185]. which was used to characterize metabolites present in ISF. Second, we performed an untargeted screen for suction blister ISF metabolites that may be useful as biomarkers by identifying metabolite features that were elevated in suction blister ISF and/or strongly correlated between suction blister ISF and plasma. Collectively, the work characterizes the differences between the suction blister ISF and plasma metabolomes, as well as the potential utility of ISF for biomarker detection in clinical and exposome research.

5.2 **Results**

5.2.1 Metabolomic profiles of suction blister interstitial fluid and plasma

To examine the suction blister ISF and plasma metabolomes in volumes that can be feasibly sampled in clinical settings, we compared metabolite features detected in the volume of ISF collected *via* suction blister sampling (15 µl suction blister ISF diluted to final volume of 50 µl with LC-MS grade H_2O) against 50 µl plasma collected *via* venipuncture, which is the standard sample volume used for this metabolomics assay [186]. HRM detected 7,044 *m/z* features that were present in suction blister ISF and/or plasma (Figure 5.1). Note that *m/z* features do not necessarily correspond one-to-one with chemical compounds and may represent multiple adducts, isotopes, or fragments from the same parent ions. Comparison of suction blister ISF to plasma showed that the large majority of features were detected in both biofluids, even though suction blister ISF had been diluted to provide the minimum volume required for HRM analysis. There were 1,032 and 429 features unique to plasma and ISF, respectively, where "uniqueness" was defined as the detection

of the feature in at least one of the 10 samples in one fluid, but not in any of the 10 samples of the other biofluid.

We identified 105 metabolites (i.e., groups of adducts/isotopes derived from the same parent ions) with high confidence in the suction blister ISF samples that were matched to compounds in the Kyoto Encyclopedia of Genes and Genomes (KEGG) database [187] by accurate mass (see Appendix B). We also identified metabolites by comparing features to a library of metabolite biomarkers relevant to clinical and exposome research; compound identities were obtained by matching the accurate mass *m/z* values and retention times of the features to analytical standards in the library. The final curated list of metabolites is presented in

Table B. 1

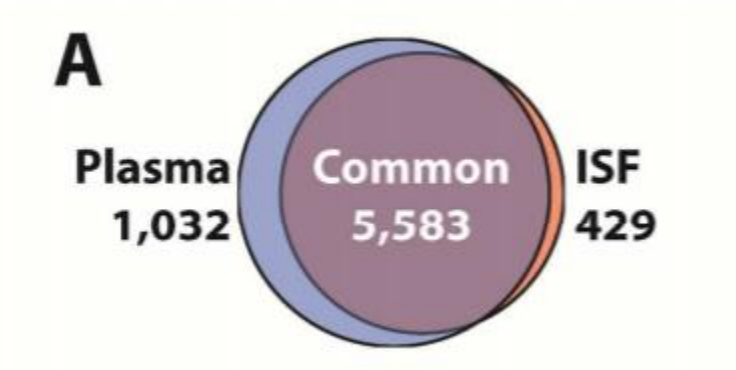

Figure 5.1: High-resolution untargeted metabolomic profiles of ISF and plasma. Venn diagram displaying the numbers of *m/z* features common and unique to ISF and plasma.

We detected a wide range of metabolites in suction blister ISF involved in amino acid metabolism, lipid metabolism, and nucleotide metabolism, as well as clinical biomarkers such as glucose, cholesterol, creatinine, and urea (Figure 5.2 and

Table B. 1 in Appendix B). Most endogenous metabolites were detected in the majority of suction blister ISF samples and were present in both ISF and plasma. We found matches for environmental toxicants, including several pesticides. Environmental compounds were generally detected in a greater number of plasma samples compared to ISF.

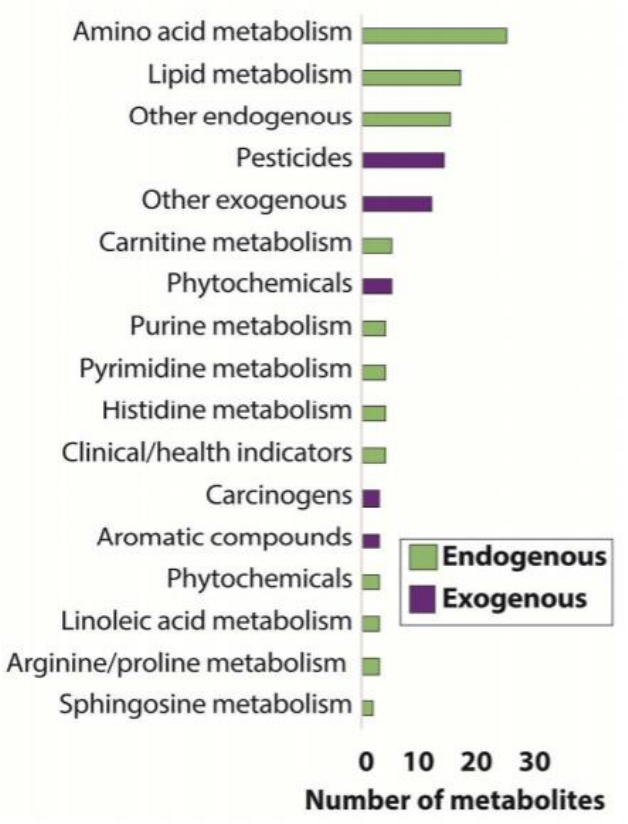

Figure 5.2: Types of metabolites detected in ISF. Figure displays the classes of metabolites identified in ISF. Bars reflect the number of metabolites detected for each class, with endogenous and environmental compounds denoted by green and purple bars, respectively. The full list of individual metabolites can be found in
.

A limited number of metabolites were unique to plasma (Table B. 2 in Appendix B). Several were environmental chemicals, including the pesticides malathion, nabam, and triadimefon; ammeline, a byproduct of the industrial compound melamine [188]; and the

mycotoxin aflatrem. Two metabolites were artifacts of the venipuncture sampling: skin disinfection was carried out with an iodine-containing compound, and ethylenediaminetetraacetic acid (EDTA) tubes were used for blood collection.

5.2.2 Metabolites markedly elevated in interstitial fluid

To identify unique characteristics of the suction blister ISF metabolome, we identified features that were elevated in ISF using a paired fold-change analysis. Since the suction blister ISF samples were diluted, these metabolites should reflect compounds that are greatly elevated in suction blister ISF relative to plasma. A curated list of all unique and elevated features with putative compound matches in the Human Metabolomics Database (HMDB) [189] is presented in Table 1.

While 316 features were unique to and elevated in suction blister ISF based on our criteria, only 23 compounds were identified by accurate mass *m/z* matching (Table 1). This may be because some of the molecules present in suction blister ISF have not yet been identified or are not included in the HMDB database. We manually classified these metabolites into several groups, including five phospholipids, three purines, two spermidines, two methionine-related compounds, six other endogenous compounds, and five dietary-derived compounds. Several of these metabolites are promising biomarkers for human health outcomes (see Discussion). Of special note was urocanic acid, a metabolite uniquely found in suction blister ISF (also found in

Table B. 1 in Appendix B**)**. Urocanic acid is produced in the stratum corneum and accumulates in the epidermis [190]. This finding is consistent with previous proteomic studies reporting an enrichment of skin-derived biomarkers in suction blister ISF [50]. Triethanolamine, another compound unique to suction blister ISF, is present in skin disinfectants used during the suction blister fluid sampling. The identification of this metabolite serves as a type of positive control, which increases the confidence in our metabolite identities.

Table 1 Metabolites markedly elevated in interstitial fluid.

Category	**Putative compound**	**Confidence score[1]**	**Log_2-fold change**
Phospholipids	Glycerophosphocholine	4	2.2
	Glycerylphosphorylethanolamine	3	1.6
	2-acetyl-1-alkyl-sn-glycero-3-phosphocholine	3	2.0
	O-Phosphoethanolamine	3	3.1
	Multiple phosphatidylinositols	1	1.8

[1] Compound identification confidence score: 4, feature was successfully grouped into a parent metabolite cluster with a unique database match; 3, feature was successfully grouped, but compound was selected from multiple database matches; 2, feature was not successfully grouped, but had a unique database match for $[M+H]^+$, $[M+Na]^+$, or $[M+K]^+$; 1, feature was not successfully grouped and compound was selected from multiple database matches for $[M+H]^+$, $[M+Na]^+$, or $[M+K]^+$.**1**

Purines	2-Deoxyinosine triphosphate	2	3.0
	Hypoxanthine	3	4.2
	Inosine	1	Unique
Table 1 continued			
Spermidine	N-Acetylspermidine	1	1.7
	Spermidine	2	Unique
Methionine	N-Formyl-L-methionine	2	2.5
	N-Acetyl-L-methionine	2	1.8
Epidermal-derived	Urocanic acid	3	Unique
Other enodgenous	Creatine	3	3.8
	4-Pyridoxic acid	2	1.8
	Glutamyl-Valine	1	2.0
	Glycylproline	1	Unique
	Phosphocreatinine	4	1.5
	Taurine	4	4.9
Food-derived	Triethanolamine	4	Unique

	3-Methylsulfinylpropyl isothiocyanate	4	Unique
	2,3,4-Trimethyltriacontane	4	Unique

Table 1 continued

	(S)-N-(45-Dihydro-1-methyl-4-oxo-1H-imidazol-2-yl)alanine	4	4.5
	Dibutyl disulfide	1	1.2

5.2.3 Metabolites strongly correlated between interstitial fluid and plasma

The identification of metabolites that are strongly correlated between plasma and suction blister ISF may provide insight into blood-based biomarkers that could be reliably monitored *via* suction blister ISF sampling. Thus, we examined the correlations between plasma and suction blister ISF intensities for 3,141 *m/z* features that were present in ≥ 4 sample pairs, of which 223 were significantly correlated ($p < 0.05$; 182 positive correlations, 41 negative correlations).

To explore the biological significance of the positively-correlated metabolites, we input the results into Mummichog [191] for pathway and module analysis (Figure 5.3). Metabolites correlated between plasma and suction blister ISF were commonly found in amino acid-related pathways (e.g., urea cycle/amino group metabolism; glycine, serine,

alanine, and threonine metabolism; aspartate and asparagine metabolism; Figure 5.3A). To explore the biological functions of the metabolites identified in the module analysis, KEGG IDs from the significant modules were input into KEGG BRITE [187], which found numerous peptides, lipids, and hormones/neurotransmitters among the correlated features (Figure 5.3B). The activity network, which contains metabolites whose identities could be predicted with high confidence, contained several amino acids (e.g., proline, glycine, homocysteine, betaine, methionine, tyrosine), nucleic acids (e.g., guanosine, guanine, uracil), and neurotransmitter-related metabolites (e.g., dopamine, methylhistamine; Figure B. 1 in Appendix B).

We compared these results against metabolites identified in a manual annotation of highly-correlated features. Here, we manually annotated 99 features with strong correlations between suction blister ISF and plasma (Spearman *rho* > 0.7) using HMDB (Table 2). Many metabolites were identified both in the activity network and Table 2, including homocysteine, betaine, methionine, proline, tyrosine, acetylcarnitine, and octenoylcarnitine, strengthening the evidence for these compound identifications. Results from pathway-associated metabolite set enrichment analysis (MSEA) [192] for metabolites in Table 2 found overrepresentation of metabolites in protein biosynthesis, betaine metabolism, methionine metabolism, and glycine, serine, and threonine metabolism ($p < 0.05$), consistent with Mummichog pathway results. Metabolites annotated manually that were not identified by Mummichog were trimethylamine N-oxide (TMAO), a microbiota-dependent compound linking carnitine and betaine metabolism [193] that has been

identified as a promising biomarker of cardiovascular disease [194], and caffeine and trigonelline, two compounds related to coffee consumption [195].

Table 2 Metabolites strongly correlated between interstitial fluid and plasma.

Category	Putative compound	Confidence score[2]	rho[3]
Betaine/methionine	Homocysteine	3	0.98
	Betaine	3	0.96
	Dimethylglycine	1	0.90
	Methionine	3	0.78
	Trimethylamine N-oxide	3	0.77

[2] Compound identification confidence score: 4, feature was successfully grouped into a parent ion cluster with a unique database match; 3, feature was successfully grouped, but compound was selected from multiple database matches; 2, feature was not successfully grouped, but had a unique database match for $[M+H]^+$, $[M+Na]^+$, or $[M+K]^+$; 1, feature was not successfully grouped and compound was selected from multiple database matches for $[M+H]^+$, $[M+Na]^+$, or $[M+K]^+$

[3] Assessed with Spearman correlation

Amino acids	Glutamine	4	0.92
	Tyrosine	3	0.88
	Proline	3	0.85
	Proline betaine	3	0.83
	Threonine	1	0.81

Table 2 continued

	Valine	3	0.76
ATP-associated	Creatinine	4	0.77
	Phosphocreatine	2	0.75
Carnitines	Acetylcarnitine	4	0.84
	trans-2-Dodecenoylcarnitine	4	0.83
	Decanoylcarnitine	4	0.81
	3,5-Tetradecadiencarnitine	4	0.80
	2-Octenoylcarnitine	4	0.71
Phospholipids	LysoPE(20:5)	4	0.89
	LysoPE(18:2)	4	0.88
Coffee-associated	Caffeine	3	0.89

	Trigonelline	3	0.87
Other endogenous	N-Butyrylglycine	1	0.81
Food-derived	Lenticin	4	0.94
	Polypropylene glycol	4	0.85
	2-(1-Propenyl)-delta 1-piperideine	2	0.80
Table 2 continued			
Other exogenous	Octadecanamide	4	0.88

A

Top metabolic pathways	*p*
Urea cycle/amino group	0.001
Glycine, serine, alanine & threonine	0.001
Aspartate and asparagine	0.002
Fatty acid	0.002
Fatty acid activation	0.003
Caffeine	0.006
Alkaloid biosynthesis II	0.008

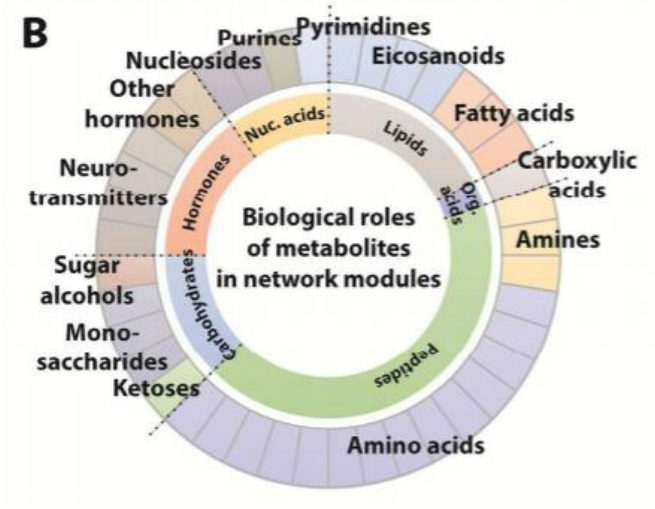

Figure 5.3 Biological roles of metabolites correlated between ISF and plasma. Results from Spearman correlations between ISF and plasma (for metabolite features present in ≥ 4 matched sample pairs) were input into Mummichog,[191] a Python program for network analysis and metabolite prediction in untargeted metabolomics datasets. Significant features ($p < 0.05$) were matched to compounds based on common adducts and isotopes, network modules (i.e., sub-communities of biologically-interconnected metabolites) were identified based on their "activity scores" (calculated from the number of significant features in the module, as well as the Newman-Girvan modularity Q), and pathway enrichment was estimated using a permutation procedure. (A) Metabolic pathways overrepresented among metabolites correlated between ISF and plasma ($p < 0.01$). (B) Radial plot of biological roles of metabolites identified in network modules, assessed using KEGG BRITE. The inner and outer rings display BRITE functional hierarchies, with the area proportionate to the number of metabolites that fall under each category. Gray boxes outlined in the outer ring show the number of metabolites that belong to each category.

5.3 Discussion

This study describes the first detailed analysis of the metabolite composition of human suction blister ISF using untargeted HRM analysis. Matched suction blister ISF and plasma samples were collected from ten human volunteers, and clinically-relevant sample volumes were analyzed by liquid chromatography with high-resolution mass spectrometry to find similarities and differences between the chemical compositions of the two biofluids. Although the majority of metabolite features were detected in both suction blister ISF and plasma, the biofluids had distinct characteristics. A diverse range of metabolites of endogenous and environmental origin were detected in suction blister ISF. Several glycerophospholipid-, purine-, and spermidine-associated metabolites were elevated in suction blister ISF, and many amino acids, nucleic acids, hormones, and exogenous compounds were well correlated between suction blister ISF and plasma. Altogether, our results suggest that metabolomic profiling of suction blister ISF has the potential to provide information about local and systemic biological activities and may be useful for monitoring established and novel biomarkers. In some cases, metabolite detection in suction blister ISF is an alternative to blood, and in other cases, suction blister ISF contains metabolites that are absent from or found in lower abundance in blood.

The large majority of endogenous metabolites in

Table B. 1 were detected in both suction blister ISF and plasma, confirming that common endogenous compounds can reliably be detected in suction blister ISF. Amino acid, lipid, and nucleotide metabolites, along with the clinical biomarkers cholesterol, glucose, creatinine, and urea, were detected in almost all of the suction blister ISF samples. Among the few metabolites that were not detected in suction blister ISF, many were environmental in origin, including several toxicants of potential relevance to environmental health. Considering the small sample volume of suction blister ISF used in the current study, it is possible that these metabolites were present in suction blister ISF but too low for reliable detection using this assay.

A primary goal of our study was to examine the usefulness of ISF sampling for metabolite biomarker detection as a substitute or companion to blood sampling via venipuncture. We identified several metabolites that were elevated in suction blister ISF compared to plasma, which reflect metabolites that may be uniquely and/or more easily assessed in ISF. Urocanic acid, an epidermal metabolite that accumulates in the stratum corneum, was unique to suction blister ISF. While it is a chromophore for ultraviolet radiation acting as a 'natural sunscreen', it has also been reported to have immunosuppressive effects and may play a detrimental role in photocarcinogenesis [196]. Spermidine, which has also been reported to be elevated in the epidermis [197], is a polyamine compound associated with anti-aging mechanisms [198]. Spermidine has promise as a biomarker for cancer aggressiveness [199], suicidal behavior in mood disorders [200], and response to breast cancer therapies [201]. Phosphocreatinine and creatine are important components of energy metabolism [202], and creatine has been identified as a potential biomarker of

mitochondrial diseases [203, 204]. Hypoxanthine and inosine, nucleotide bases formed during purine metabolism, are increased in response to injury [205] and are biomarkers for cardiac ischemia [206]; however, future work should examine the impact of the suction blister sampling protocol on the levels of these metabolites.

Several phospholipid-related compounds were elevated in suction blister ISF. Glycerophosphocholine, a building block for phospholipids in cell membranes, is a biomarker for breast cancer and myeloma, as well as Alzeimer's disease [207, 208]. Glycerophosphocholine and glycerylphosphorylethanolamine in semen have been implicated as biomarkers for infertility problems [209]. O-Phosphoethanolamine has promise as a biomarker for major depressive disorder [210] and Amyotrophic Lateral Sclerosis [211].

Exogenous food-based compounds were also elevated in suction blister ISF. One compound unique to suction blister ISF, 3-methylsulfinylpropyl isothiocyanate, is obtained through the consumption of cruciferous vegetables [212]. Isothiocyanates, which are phytochemicals with chemoprotective activities, are believed to contribute to the health benefits of vegetable-rich diets [213]. Recently, a screen for toll-like receptor (TLR) inhibitors in vegetable extracts identified 3-methylsulfinylpropyl isothiocyanate as a compound with potent anti-inflammatory effects [214]. Another food-derived compound unique to suction blister ISF, 2,3,4-trimethyltriacontane, is found in fruits [215]. While preliminary, our findings highlight the possibility for ISF as a unique source of dietary biomarkers.

We also identified metabolites that were positively correlated between suction blister ISF and plasma, which reflect metabolites whose ISF levels are informative of their blood levels. Many amino acids, neurotransmitters, and nucleic acids were strongly correlated between the fluids. Several clinically-relevant metabolites were also strongly correlated between ISF and plasma. Elevated homocysteine, a sensitive indictor of B-vitamin deficiency [216], is a biomarker for cardiovascular [217], and neurodegenerative [218] conditions. Creatinine is an important biomarker for kidney function [202]. Betaine is a metabolite that plays a role in osmoregulation [219], and TMAO is an osmolite generated by gut microbiota from betaine, choline, and carnitine [220]. Betaine and TMAO are biomarkers of cardiovascular outcomes [221, 222]. Two dietary-related compounds, caffeine and trigonelline, are found in coffee beans and are biomarkers of coffee consumption [223].

We acknowledge that our study has several limitations. The limited sample volume precluded the in-depth structural characterization of detected *m/z* features without database or library matches. The structural elucidation of these features is challenging due to the lack of reference standards, limited ISF sample volume, and low feature abundances. In addition, a limited number of the annotated metabolites were identified by comparison to authentic reference standards. The remaining metabolites were characterized using an annotation scheme that reduces false identifications through a combination of correlation, adduct and isotope clustering; while this approach has been shown to enhance annotation accuracy [224], additional laboratory analyses, such as ion dissociation and comparison to authentic reference standards, are required for absolute confirmation of identity. We cannot

disentangle the impacts of matrix effects and dilution effects under the current study design.

It is possible that the different sampling sites, i.e., blood draw from the forearm and suction blisters on the thigh, introduced variability in the composition of these fluids, although we do not expect this variability to be significant, given that plasma is part of systemic circulation. If the concentrations of metabolites at sampling sites are variable, the metabolite fold changes between suction blister ISF and plasma may have been affected. The method for suction blister generation required a 45-minute vacuum application at elevated temperatures; due to this procedure, host responses to blister generation, inflammatory reactions, and wound responses may be observed, resulting in artifacts in the suction blister ISF that would not be present in ISF from unperturbed skin. Thus, we cannot dismiss the possibility that some of our findings in suction blister ISF (e.g., metabolites elevated in suction blister ISF) might be influenced by the injury induced through the suction blister sampling method. In addition, different fluid collection protocols may introduce variability in the metabolites detected. To address this issue in part, future studies will explore the ISF and plasma metabolomes with varying sample dilutions and sampling strategies. Finally, the study had a small sample size, and we were unable to infer how sex, age, and other participant characteristics influenced our results. Nonetheless, the current study supports the use of ISF as a useful fluid for biomarker monitoring using HRM approaches and provides a framework for future clinical and exposome studies.

5.4 **Conclusions**

To our knowledge, this is the first study to compare the human suction blister ISF and plasma metabolomes with untargeted HRM profiling. We found that dermal ISF has a distinct metabolite composition that may provide value as a source of biomarkers for diagnostics and monitoring. Our findings suggest that suction blister ISF may be a unique source of several biomarkers, including several nucleotides, epidermally-derived metabolites, and dietary compounds. Additionally, many clinical biomarkers were well correlated between suction blister ISF and plasma, suggesting that ISF has the potential to serve as a surrogate source of biomarkers conventionally detected in plasma. Overall, metabolomic profiling performed in this study provides early evidence that ISF has the potential to serve as a substitute and/or complement to plasma-based biomarker detection in future clinical practice and research studies.

5.5 **Methods**

5.5.1 Obtaining plasma and interstitial fluid samples

The study was conducted using 10 healthy human volunteers and was approved by the Institutional Review Board (IRB) at the Georgia Institute of Technology. Written informed consent was obtained from all volunteers. Blood samples were taken from the forearm by venipuncture. Skin suction blister fluid was collected from suction blisters generated on the thigh by applying suction at 50 – 70 kPa below atmospheric pressure at a temperature of 40°C for ~45 min until blister formation was complete. See Appendix B for details.

5.5.2 High-resolution metabolomics

Suction blister ISF samples were diluted from 15 µL to 50 µL with water. 50 µL of biofluid (plasma or diluted suction blister ISF) was added to 100 µL of acetonitrile, vortexed and allowed to equilibrate. Proteins were precipitated by centrifuge. Aliquots were analyzed using reverse-phase C_{18} liquid chromatography (Ultimate 3000, Dionex, Sunnyvale, CA) and Fourier transform mass spectrometry (Q-Exactive, Thermo Scientific, Waltham, MA). Data was extracted using apLCMS[225] with modifications by xMSanalyzer [226]. See Appendix B for details. The metabolomics dataset is available upon request to the corresponding authors.

5.5.3 Statistical analysis and metabolite feature identification

Statistical analysis, network/pathway analysis, and metabolite set enrichment analysis were performed in RStudio v0.99.486[227] and MetaboAnalyst 3.0.[192] Metabolites were identified with analytical standards and accurate mass matching in KEGG[187] and HMDB[189] using custom dataset-wide and feature-specific deconvolution and identification algorithms. See Appendix B for details.

5.6 Acknowledgements

We wish to thank Donna Bondy for administrative support. Dr. Amit Pandya helped develop protocols and provided training for the suction blister procedure. This work was supported by grants P30 ES019776, U2C ES026560 and T32 ES012870-13 from the National Institutes of Health.

6 CHAPTER 6: DEVELOP A MICRONEEDLE SYSTEM TO SAMPLE INTERSTITIAL FLUID IN HUMAN PARTICIPANTS AND IDENTIFY BIOMARKERS IN THE INTERSTITIAL FLUID COMPARED TO BLOOD.

6.1 Introduction

Identification and measurement of biomarkers have increasing importance in advancing research and detecting and treating diseases [228]. Biomarkers are molecules found in body fluids such as blood, urine, and saliva that provide information about physiological status Diagnosis and monitoring are central to effective healthcare; e.g. diabetes management by blood glucose testing, quick detection of infectious diseases like HIV and ability to characterize cancers by blood sampling. Blood monitoring is limited by need for expert training, difficulty of continuous monitoring, and pain and apprehension associated with blood draws [229]. Urine and saliva are more accessible but have limited biomarkers and variable concentrations [230].

The most prevalent fluid in the body is interstitial fluid (ISF), constituting 75% of extracellular fluid and 15-25% of body weight. ISF surrounds cells and tissues, acting as a bridge between blood and cells [48]. It contains systemic biomarkers and can also be used for continuous monitoring. ISF contains local tissue biomarkers that can provide information about cellular and tissue physiology [51]. Previous studies have shown that ISF contains unique biomarkers not otherwise found in plasma [50].

Currently, ISF is used clinically for continuous glucose monitoring [231] and in research to determine dermatological drug bioavailability [232] or analysis of cancer tumor

microenvironment [233]. More widespread use of ISF is limited because ISF is hard to sample. In the skin, which is the most accessible organ of the body, ISF is mostly present in the lowermost skin layer of dermis, which is 70% ISF by volume [71]. Dermal ISF can be sampled by biopsy, but it is painful, requires medical expertise, can lead to scarring, and collects a mixture of extracellular ISF and intracellular material [234]. Alternatively, suction blisters, created by applying suction for an hour at elevated temperature, are filled with ISF. However, this procedure is cumbersome, feels uncomfortable, causes lasting skin damage, and provides fluid contaminated with injury markers not truly representative of ISF [73].

Microdialysis and open-flow microperfusion require implantation of a semipermeable membrane or steel-mesh tubing into skin, often under local anesthesia, which causes tissue damage, requires many hours to perform and collected analytes are limited by the permeability of the membrane [80, 85]. Reverse iontophoresis uses electric current to draw ISF components towards skin surface, but is limited to collection of small molecules, may irritate skin and requires frequent calibration because of skin permeability variation [87]. Alternatively, biosensors placed inside the body provide in situ measurement in ISF, e.g. for continuous glucose monitoring [231]. However, this requires a dedicated, implanted sensor for a given biomarker and risks infection, biofouling, and discomfort of an indwelling device.

An ideal system to sample ISF should reliably collect ≥1 μL of ISF (i.e., sufficient for many analytical assays; be minimally invasive to avoid artifacts due to tissue damage or irritation; and be simple and rapid (e.g., ≤20 min) to facilitate access and throughput. We

believe these criteria can be met using microneedles (MN), which are micron-scale needles that press into skin, penetrate past the outer skin barriers, and access dermal ISF in a minimally invasive manner. MNs have been studied clinically for drug delivery applications, where they are well tolerated and easy to use, making them well-suited for routine use in research and medicine [103]. However, previous studies of MNs for ISF sampling have been limited by sub-microliter sampling volumes.

In this study, we developed a MN-based method to sample microliter volumes of ISF from skin in a relatively simple and minimally invasive manner using relatively low-cost and commercially available equipment. We have assessed acceptability of this method by studying skin tolerability, pain and patients' opinions. The utility of this method was studied by comparing our results against ISF collection from suction blisters and plasma collection by venipuncture. We also analyzed ISF collected using MNs for biomarkers of clinical interest and/or unique to dermal ISF, and compared pharmacokinetics of a model biomarker in ISF versus plasma.

6.2 Results

6.2.1 Design of microneedle patch to sample interstitial fluid

We designed an ISF collection method that uses MNs to create pathways for ISF flow from skin using vacuum as a convective driving force. Prior approaches have employed solid, swellable MNs, which are limited in ISF collection by MN volume [142], and hollow MNs collecting biomarkers by diffusion or convection of ISF through MNs by capillary action, which are slow and/or collect small ISF volumes [235]. These prior methods provide a

driving force for ISF flow within MNs, but rely on slow diffusion of ISF through dermis to the dermis-MN interface.

In our design, vacuum application initiates a convective driving force that moves ISF through dermis to the skin surface through MN-generated pathways. These micropores are created by pressing a patch containing an array of five MNs into skin and then removing it (Fig 1a). Vacuum is applied over micropores to transport ISF through dermis and micropores to the skin surface (Figure C. 1 in Supplementary Information, Appendix C).

A challenge in method development was bleeding. Since skin is highly vascularized, vacuum application to skin punctured with MNs collected blood along with ISF. We therefore studied the effect of MN length, vacuum pressure, and timing of vacuum application in human participants. Reducing MN length from 650 to 250 μm reduced chances of blood contamination upon vacuum application (Figure C. 2 in Appendix C). We did not try shorter MN lengths due to concerns that they would not reliably insert into skin without a high-velocity applicator [162]. Delaying vacuum application for up to 10 min after MN application did not affect bleeding, but reducing vacuum pressure from -50 to -17 kPa reduced bleeding (Figure C. 3 in Appendix C). Bleeding was eliminated by slowly increasing vacuum to -50 kPa over the course of ~3 min after puncture with 250 μm MNs. This method was used in all subsequent studies.

This optimized method collected 2.3±2.6 μL clear ISF with no visual traces of blood within 20 min (See Section C.2. in Appendix C). Further optimization could increase volume and

reduce variability of ISF collection, but the current method was capable of reliably collecting useful quantities of ISF for analysis.

6.2.2 Collection of ISF from human participants

We collected ISF from 21 human participants including 10 males and 11 females aged 28±7 years (Detailed demographics in

Table C. **1**). The procedure involved covering skin with a transparent film skin dressing (Tegaderm) containing 1-cm diameter openings where MN treatment was performed (Figure 6.1). Insertion and removal of MNs was well tolerated with faint visual evidence of micropores in skin (Figure 6.1d). After administration of vacuum over the micropores for up to 20 min, skin appearance was largely unchanged (Figure 6.1c). Closer examination revealed droplets of ISF on the skin surface (Figure 6.1e). Collection and examination of ISF showed it was clear with a slight yellow tinge. One day later, there was generally no evidence of MN treatment, indicating swift recovery of skin (Figure 6.2f,g). Overall, ISF collection with MN treatment was a simple, minimally invasive, and relatively rapid method that was well tolerated by human participants.

For comparison, epidermis and dermis were separated to form ISF-filled suction blisters by applying vacuum at 40°C for up to 1 h. Draining the blister with a needle and syringe collected suction blister fluid (SBF), which was similar in appearance to ISF collected by MN (Figure 6.1b) Consistent with literature [236], suction blister treatment caused local erythema and edema, which resolved within a few days, and in some cases induced prolonged skin pigmentation. Compared to MN treatment, suction blister treatment caused significantly more severe and longer-lived tissue trauma, was more cumbersome and time-consuming to perform, and produced ISF that likely includes artifacts due to tissue injury.

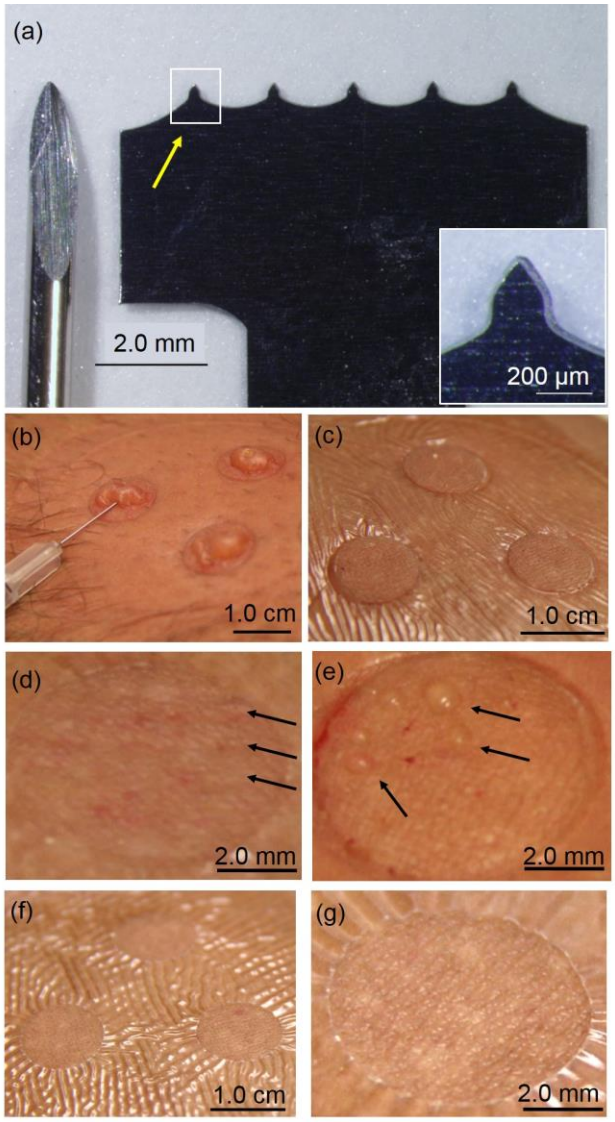

Figure 6.1: Representative images of microneedle (MN) device and interstitial fluid (ISF) collection by microneedle (MN) treatment compared to suction blister. (a) Stainless steel MN patch (right) shown next to a conventional lancet (left). Each of the five MNs (shown with arrow) is 250 µm in length, 200 µm in width at the base and tapering to 10 µm tip diameter. Inset shows a magnified view of a single MN. (b) Suction blisters formed after extended vacuum application on skin (-50 kPa to -70 kPa at 40˚C for up to 1 h) being drained with a needle and syringe to collect suction blister fluid (SBF). (c) Skin after MN application and vacuum administration (-50 kPa at room temperature for 20 min) to draw out ISF. Three treatment sites are shown, surrounded by Tegaderm skin covering, before ISF was removed from skin surface. (d) Magnified view of skin immediately after MN application. Some spots where MNs punctured skin to create micropores appear as faint red dots, which were

generally not associated with bleeding. (e) Magnified view of skin immediately after MN treatment (i.e., including vacuum administration). Droplets of ISF can be seen on the skin surface above micropores. (f) Skin shown 24 h after MN treatment. (g) Magnified view of skin 24 h after MN treatment shows no redness or erythema. Images 2b-f are all from the same subject and are representative of the study population.

Although MN treatment did not induce apparent adverse effects to skin, we carried out histopathological analysis of skin biopsies from MN-treated hairless rats to further assess safety. Visual observation of skin after MN treatment showed slight swelling and erythema that resolved within a few hours. Examination of histopathological tissue sections by a board-certified dermatopathologist revealed minor focal inflammation at 4 h after MN treatment (Figure 6.2b) that resolved within 24 h (Figure 6.2c).

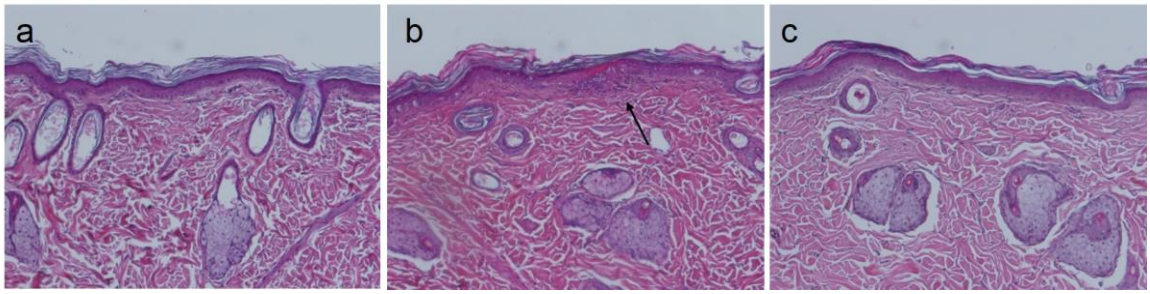

Figure 6.2: Representative images of H&E-stained sections of skin from the back of hairless rats in vivo before and after MN treatment. (a) Histology of skin section taken from the back before MN treatment. (b) Histology of skin site taken from a biopsy 4 h after MN treatment. Black arrow shows a site of minor focal inflammation. (c) Histology of skin 24 h after MN treatment did not show signs of inflammation.

6.2.3 Unique and clinically-relevant biomarkers in ISF

We collected ISF from MN treatment, SBF from suction blisters and plasma from venipuncture from the cohort of 21 participants to compare biomarker compositions of the three fluids. High-quality data were available for 20 participants from high-resolution metabolomics using liquid chromatography-mass spectrometry (LC-MS) (demographics in

Table C. 2 in Appendix C). This analysis detected 10,338 features with hydrophilic interaction chromatography (HILIC), which better detects lipophilic compounds and 7,703 features with reverse-phase C18 chromatography, which better detects polar compounds (Figure 6.3). Among features found in HILIC, 63% were common to all three body fluids; 79% were common to plasma and ISF, suggesting that these metabolite measurements in ISF may be a surrogate for plasma; and 1% were unique to ISF, suggesting that these biomarkers can be uniquely assayed in ISF. Similar data were obtained from C18 chromatography, except 14% of features were unique to ISF, indicating that polar metabolites are more likely to be specifically found in ISF compared to lipophilic metabolites.

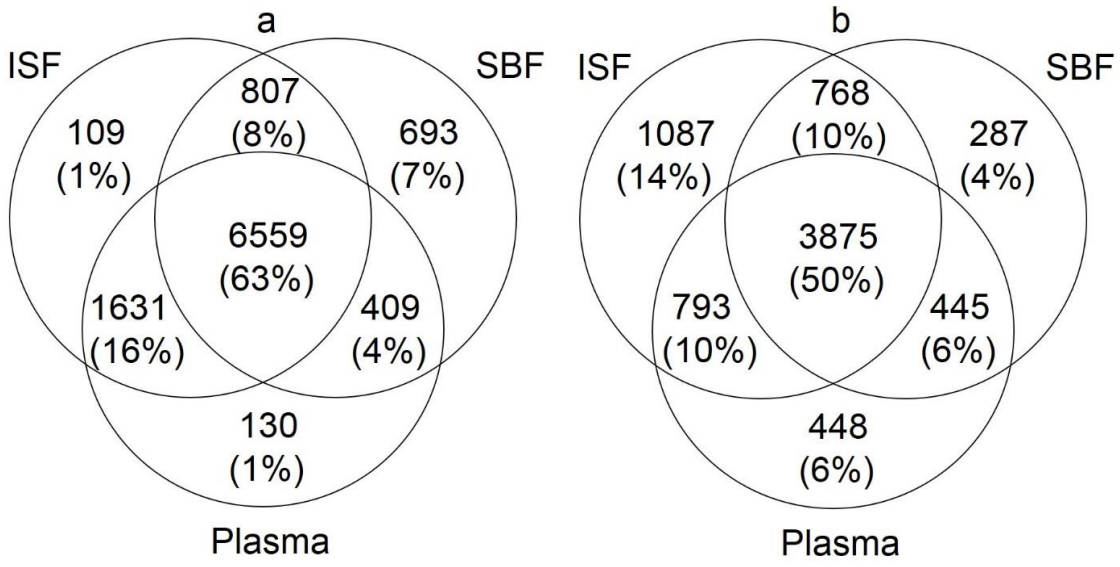

Figure 6.3: Venn diagram showing the overlap of features in ISF from MN treatment, suction blister fluid and plasma from venipuncture. Samples were analyzed using (a) hydrophilic interaction chromatography (HILIC) and (b) reverse-phase C18 liquid chromatography. After filtering, a total of 10,338 and 7,703 features were detected with HILIC and C18, respectively. A feature was considered "present" in a fluid if

the feature was detected in that fluid in more than 10% of samples (≥ 3 of 20 samples). Figures not to scale.

Comparing the 10,208 features found in ISF or SBF by HILIC, only 72% were common to both fluids, which demonstrates that ISF and SBF are not identical fluids, probably because of their different methods of sampling. To better interpret differences between ISF and SBF, a swab was wiped across intact skin and analyzed for biomarkers. Because ISF was collected from the skin surface, it may contain more epidermal and skin surface biomarkers than SBF. Consistent with this expectation, among 1,740 features detected in ISF and absent from SBF, 58% were found in the skin wipe. Among 1,102 features detected in SBF and absent from ISF, 65% were found in the skin wipe (Figure C. 4 in Appendix C). However, it should also be noted that 70% of features detected in skin swabs were also found in plasma (Figure C. 5 in Appendix C), indicating that biomarkers found on the skin surface are not necessarily contaminants. Indeed, prior studies have shown that dermal and systemic biomarkers can be collected from the skin surface [237]. Additional studies are needed to better understand differences between ISF and SBF, and the role of epidermal and skin surface biomarkers. Results from C18 chromatography were similar (Section C.3 in Appendix C).

We conducted a targeted evaluation of 90 medically-relevant biomarkers in ISF, SBF and plasma. Of these, 68 were detected in at least one fluid (Table C. 3 in Appendix C); Table 3 shows a truncated list. Most biomarkers (65%) were found with high frequency (presence in >18/20 samples) in all three fluids. Only 7% were frequently detected in plasma but not

in ISF, which further emphasizes that ISF contains many of the same biomarkers as plasma. In contrast, 11% of biomarkers were commonly found in ISF but not in plasma, which shows that ISF contains unique information.

Table 3: Prevalence of selected clinically relevant biomarkers in ISF, SBF and plasma in matched samples from 20 human participants.

Biomarker	Prevalence of biomarker[†]		
	Plasma	**ISF**	**SBF**
Clinical Markers			
Cholesterol	100%	80%	100%
Cortisol[§]	100%	30%	80%
Creatinine	100%	100%	100%
Homocysteine[*]	20%	55%	55%
Urea	100%	100%	100%
Glucose	100%	100%	100%
Lactic acid[*]	75%	100%	100%
Uric acid	100%	100%	100%
Nucleotide-related Metabolism			
Hypoxanthine[*]	0%	80%	100%
Xanthine[*]	25%	90%	100%
Uridine	100%	100%	100%
Vitamins and Cofactors			
Choline	100%	100%	100%
Pantothenic acid (Vitamin B5)	50%	60%	95%
Tetrahydrofolic acid[*]	40%	60%	30%
Fatty Acid Metabolism			
Acetyl-carnitine[§]	85%	40%	100%
Methyl-histidine[§]	80%	25%	55%

Table 3 continued

Margaric acid[*]	60%	100%	25%
Myristoleic acid	85%	100%	45%
Palmitoleic acid	90%	100%	55%
Stearic acid	75%	100%	15%
Lipid Metabolism			
Sphingosine[*]	10%	100%	50%
Leukotriene B4[*]	50%	100%	50%
Respolvin E2	100%	100%	75%
Sterol Metabolism			
Deoxycholic acid[§]	100%	55%	100%
Taurodeoxycholic acid[§]	100%	50%	100%

[†]Prevalence among 20 samples; [§]Biomarkers found with high frequency in plasma, but not in ISF; [*]Biomarkers found with high frequency in ISF, but not in plasma.

To further study biomarkers in ISF with high frequency and generally absent in plasma, we used data-driven annotation approaches to identify 116 such biomarkers. Among 24 clinically significant biomarkers, 15 were not frequently present (<50%) in SBF, possibly because they were more prevalent in epidermis or skin surface. Ten of these 15 biomarkers were also detected in the skin swab, supporting this hypothesis (

Table 4).

Table 4: Prevalence of clinically relevant biomarkers detected uniquely or predominately in ISF compared to plasma in matched samples from 20 human participants.

Biomarker	Medical significance[†]	Prevalence of biomarker[§]		
		Plasma	**ISF**	**SBF**
Urocanic acid[*]	**photocarcinogenesis,UV chromophore**	**0%**	**100 %**	**100%**
N-Acetyl-D-glucosamine	**micronutrient and drug, suppresses immune response, used to treat autoimmune diseases**	**10%**	**100 %**	**90%**
Glycogen	**energy storage**	**10%**	**100 %**	**60%**
Diethanolamine[*]	**cosmetic formulations, carcinogen**	**5%**	**100 %**	**60%**
Sphingosine[*]	**signaling molecule in skin**	**10%**	**100 %**	**50%**
Nebularine	**nucleoside**	**0%**	**100 %**	**20%**
Tributyltin chloride	**environmental pollutant used as antifouling agent, now largely banned**	**10%**	**100 %**	**10%**
Citicoline	**naturally occuring and also a nutrient supplement**	**10%**	**100 %**	**5%**
Angiotensin (5-8)	**angiotensin cascade modulates vasoconstriction**	**5%**	**100 %**	**5%**
Pentadecanoic acid	**marker for intake of milk fat**	**10%**	**100 %**	**0%**
Gamma Tocopherol	**form of vitamin E, micronutrient**	**5%**	**100 %**	**0%**
Estradiol cypionate	**natural form of estrogen - plays a role in reproduction, lactation**	**0%**	**100 %**	**0%**

Table 4 continued

Arginosuccinic acid	**biomarker for urea cycle disorder**	**0%**	**95%**	**25%**
Porphobilinogen	**biomarker for acute porphyrias, currently urine based detection**	**10%**	**95%**	**20%**
N^1,N^{12}-Diacetylspermine	**cancer biomarker**	**0%**	**95%**	**15%**
Triethanolamine*	**commonly used in skin care products**	**0%**	**90%**	**0%**
Prostanoic acid	**basic building block of prostaglandins**	**5%**	**85%**	**55%**
6-Ethylchenodeoxycholic acid	**bile acid derivative - reduces liver fat and fibrosis**	**0%**	**85%**	**0%**
Inosine	**cardiac disease biomarker**	**5%**	**80%**	**100%**
Hypoxanthine	**cardiac disease biomarker**	**0%**	**80%**	**100%**
Barbaloin	**product of aloe vera - anti-inflammatory, cathartic properties**	**0%**	**70%**	**10%**
AMPA	**neurological biomarker**	**10%**	**65%**	**90%**
Bromochloroacetic acid	**present in brominated disinfected water and may cause adverse reproductive outcomes**	**5%**	**65%**	**10%**
20-COOH-Leukotriene B4	**Involved in vasodilation**	**5%**	**55%**	**5%**

†See Figure C. 4 in Appendix C for references in support of medical significance; §Prevalence among 20 samples; *Biomarker has dermatological significance.

We also found 14 biomarkers unique to SBF and not found in ISF (

Table C. 5 in Appendix C). Of note are 2-arachidonoylglycerol, an endocannabinoid produced in the epidermis that is involved in inflammatory regulation [238], and corticosterone, which activates in the skin in response to inflammation and other stressors [239]. This indicates that SBF may contain artifacts that result from tissue trauma inherent to the suction blister sampling method.

MN treatment was well tolerated. Participants reported that pain during MN treatment was not different from suction blister or venipuncture, while suction blister sampling was significantly more painful than venipuncture (Figure C. 6a). Ongoing pain after the procedure was reported by almost half of participants with suction blisters, but only by 5% after MN treatment (Figure C. 6b). Tenderness was reported by 90% of participants at suction blister sites, but only 24% after MN treatment. Erythema was seen at 89% of suction blister sites, split between grade 1 and grade 2 in severity, whereas erythema at MN sites was less common (76%) and less severe (all grade 1). Localized swelling observed at 40% of suction blister sites and 57% of MN sites was always contained within the 1-cm^2 sites of vacuum application. Overall, MN treatment was well tolerated and generally had fewer adverse effects compared to suction blisters.

6.2.4 Monitoring systemic biomarker pharmacokinetics in ISF and plasma

Our measurements so far compare the presence of biomarkers in different body fluids, but do not address dynamic relationships as biomarkers are transported between body compartments. We therefore studied pharmacokinetics of a model biomarker (caffeine) in ISF compared to plasma over an 8 h period. Caffeine is a small, hydrophilic molecule

expected to transport and equilibrate easily between blood and ISF [240], can be safely and easily administered to human participants, and its pharmacokinetics are well known [241].

ISF and blood were sampled by MN treatment and fingerstick, respectively, in 9 healthy adult subjects (Table C. 7 in Appendix C) who had abstained from caffeine consumption for 36 h. Baseline caffeine concentrations in ISF and plasma in all participants were below 0.5 µg/mL, consistent with expected values >24 h after caffeine abstention [242]. After consuming Diet Coke containing 43 mg of caffeine, caffeine concentrations in ISF and plasma increased for ~2 h and then decayed until the end of the 8 h study (Figure 6.4a). There was a good correlation between caffeine in ISF and blood (r^2=0.73, Figure 6.4b), with a mean ISF/blood ratio of 0.95±0.52. Caffeine pharmacokinetic parameters are not significantly different from each other (r>0.05, Figure 6.4c) and are consistent with literature values [243]. Three participants later drank caffeine-free Diet Coke, which resulted in caffeine concentrations in ISF and plasma below 0.25 µg/mL at all times (Figure 6.4a).

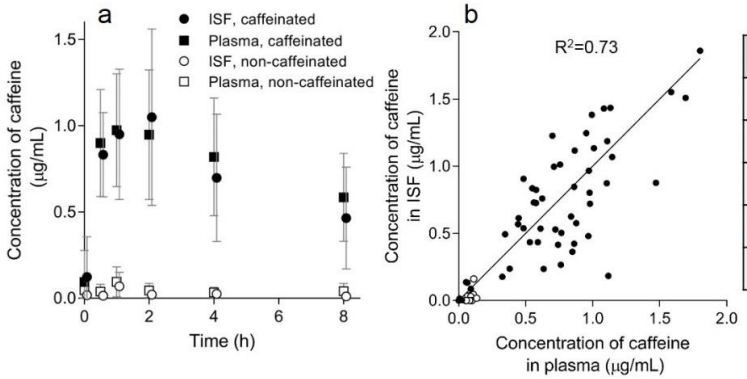

c

PK Parameter	Plasma	ISF
C_{max} (µg/mL)	1.06 (0.31)	1.03 (0.42)
t_{max} (h)	1 (0.61)	1 (0.61)
$AUC_{(0-8h)}$ (µg/mL.h)	0.084 (0.031)	0.148 (0.116)
$t_{1/2}$ (h)	9.4 (3.9)	7.5 (5.0)
CL (L/h)	4.1 (2.9)	4.7 (2.8)

Figure 6.4: Concentration of caffeine in ISF and plasma in 9 human participants. (a) Concentration of caffeine in ISF and plasma for 8 h after consumption of caffeinated

or caffeine-free Diet Coke. (b) Correlation between caffeine concentrations in ISF compared to plasma.(c) Pharmacokinetic parameters for caffeine concentrations in ISF and plasma. All data shown as mean (SD). See text for definition of symbols.

Sensations reported by participants were similar for MN and fingerstick; participants reported very slight or slight pain and stinging (Figure C. 7 in Appendix C). MN treatment induced mild erythema localized at the treatment sites that disappeared within a few days (Figure C. 10a in Appendix C). No pain or swelling was reported. In contrast, fingerstick did not cause erythema but resulted in mild, transient tenderness (Figure C. 10b in Appendix C).

6.3 Discussion

ISF is a novel body fluid of increasing interest as a source of biomarkers providing information about both dermal and systemic physiology as well as drug pharmacokinetics. ISF is also of interest for continuous monitoring of biomarkers because, unlike blood, it does not clot. However, progress in this field has been significantly limited by lack of simple, rapid, reliable and minimally invasive methods to sample ISF. Current methods include suction blisters [73], microdialysis [80, 244] and open flow microperfusion [85] which require expert training, take one or more hours to complete, cause skin injuries that require days to weeks to fully heal and often require local anesthesia due to their invasive nature.

Previous studies have demonstrated use of MNs to sample ISF. However, hollow MNs using capillary forces to draw ISF [171] and hydrogel MNs that swell with ISF upon

insertion into skin [169, 172] have generally collected sub-microliter ISF volumes, which is less than required for most diagnostic tests [235]. Here, we developed an ISF collection method using MNs to create pathways for ISF transport and using vacuum to provide a driving force that draws ISF from skin. We believe this new method will be broadly useful to the scientific and possibly future clinical communities to collect useful quantities of ISF (i.e., ≥1 μL) using a minimally invasive method that is well-tolerated and relatively rapid and simple to do. Moreover, the method uses equipment that is commercially available at relatively low cost.

In this study, we collected ISF, SBF and plasma from 20 human participants and found more than 10,000 features by LC-MS analysis, more than two-thirds of which were common to ISF and plasma. This indicates that ISF may be a surrogate for plasma in some cases. More features (14%) we detected unique to ISF using the C18 column compared to 1% using HILIC. Potssibly skin contains more lipophilic molecules that are captured better by C18 compared to HILIC. Altogether, our data indicate that biomarkers in ISF derive mostly from plasma, but there are also biomarkers specific to skin, many of which probably result from metabolic processes in the tissue.

Using a targeted approach to detect clinically valuable biomarkers, we found that most biomarkers detected in plasma were also in ISF, further supporting the idea that ISF may be a substitute for blood for diagnostic tests such as cholesterol, urea, creatinine, glucose, etc. Biomarkers found uniquely in skin include nucleosides associated with RNA like nebularine, hypoxanthine (biomarker for cardiac ischemia) and inosine (cardiac biomarker

and neuroprotective agent for possible treatment of Parkinson's disease and multiple sclerosis). We also found porphobilinogenis (currently used to detect porphyria in urine-based tests) and arginosuccinic acid (biomarker for urea cycle disorders). Several dermatologically relevant biomarkers like sphingosine (structural component of skin with signaling functionality) and diethanolamine (carcinogen found in skin products) were also detected in ISF. Additionally, exogenous molecules probably from environmental exposures were found, like bromocholoroacetic acid (possible carcinogen associated with water purification), tributylin chloride (reproductive toxin found in paint), and barbaloin (found in cosmetic formulations) (See Appendix

Table C. 4 for details).

We also compared biomarkers in ISF and SBF. Although most features found these biofluids were common to both, 21% were found only in ISF and 10% were found only in SFB, probably due to differences in sampling methods. For example, 2-arachidonoylglycerol and corticosterone (biomarkers associated with inflammation) were found only in SBF, which may represent a response to tissue damage during suction blister generation (See

Table C. 5 for details). In contrast, Leukotrine B4 (biomarker for vasodilation) was found in ISF samples, possibly because MN application can cause mild erythema.

The pharmacokinetics of caffeine (used as a safe model biomarker) in ISF closely matched plasma, probably because small, hydrophilic molecules like caffeine rapidly equilibrate between blood and ISF across capillary walls (e.g., like glucose does [245]). This indicates the possibility of using ISF to continuously monitor biomarkers currently monitored in plasma, such as glucose, lactate, and urea, without indwelling, subcutaneous probes.

Device development required optimization to prevent ISF contamination with blood from broken capillaries. We noted that blood only appeared under vacuum, perhaps because MNs make very small incisions in capillaries that can self-seal, but vacuum forces them open. We found that using very short MNs (250 μm) and slowly ramping up vacuum after MN application could avoid bleeding and collect clean ISF samples.

ISF collection using MNs was well tolerated, with mild, transient erythema and reports of brief, minor pain similar to fingerstick. We believe that most pain came from sharp edges on the MN array backing, as opposed to the MNs themselves; this problem can be fixed with minor design modification. In support of this assertion, prior studies using much larger arrays of longer MNs have been reported painless [103, 246].

Limitations of this study include need for further validation of findings in larger populations, since this study included data from only 21 human participants; careful validation of biomarker measurements using more specific assays, since this study relied

on LC-MS data only; analysis of ISF for a broader range of compounds, such as proteins; further determination of the significance of biomarkers found in ISF and their relevance to human physiology; and device improvements that minimize pain, as discussed immediately above.

6.4 Conclusions

Progress in studying ISF as a source of biomarkers for tissue physiology, dermatological drug pharmacology, novel diagnostic assays and other applications has been limited by lack of simple, minimally invasive methods to collect ISF. In this study, we developed a method to sample ISF from skin using a MN-based device that is well-tolerated, relatively rapid and simple to perform, and provides microliter quantities of ISF in a minimally invasive manner using relatively low-cost, commercially available equipment. ISF sampled from human participants and analyzed for metabolites by LC-MS was found to have most molecular features in common with plasma and/or SBF, but several of features were unique to ISF, including biomarkers of medical significance. The pharmacokinetics of a model compound, caffeine, in ISF closely matched plasma. These findings suggest that ISF can be a source of valuable biomarkers as a non-clotting alternative to blood and a source of biomarkers unique to ISF for dermal and systemic physiology. Sampling ISF from skin using a MN patch has the potential for widespread use in research for new biomarker discovery and drug development, as well as for possible future translation in the clinic for biomarker monitoring.

6.5 Acknowledgements

The authors thank Donna Bondy for administrative support; Sebastien Henry and Devin McAllister for helping design human studies; Chunyu Ma for help analyzing samples using LC-MS; and Brian Pollack for analyzing skin histopathological samples. This work was supported in part by the U.S. National Institutes of Health (U2CES026560).

6.6 Materials and methods

6.6.1 Microneedle patch fabrication and sterilization:

MN patches were designed in Solidworks 2016 software (Solidworks, Waltham, MA) and fabricated from grade 316 stainless steel as five-needle planar arrays (Tech-Etch, Plymouth, MA) by photo etching. MN length varied from 250 µm to 650 µm, with a cross-sectional area of 200 µm by 25 µm at the base and a sharp tapered tip of 10 µm diameter. MN patches were disinfected by washing with sterile 70% isopropyl alcohol (VWR, Radnor, PA) in a class II BSL hood (Thermo Fisher Scientific, Waltham, MA), packaged into self-sealing sterilization pouches (Crosstex International, Englewood, CO) and sterilized using an ethylene oxide sterilization cycle (AN74i Anprolene Gas Sterilizer, Andersen Products, Haw River, NC) that was validated using a product immersion method (WuXi AppTec, Marietta, GA).

6.6.2 ISF sampling using microneedle patches

ISF sampling through skin using MN patches was a two-step process: MN patch application to create micropores in the skin followed by application of vacuum to draw out ISF through the micropores.

6.6.2.1 Microneedle patch application

The site of MN patch application on the participant's forearm was disinfected using an alcohol swab (BD Alcohol Swab, BD, Franklin Lakes, NJ), and an area of ~50 mm2 was marked with a pen. The investigator inserted a patch comprising a five-MN planar array at the site and then removed it immediately. This process was rapidly repeated 20 times per site to create an array of 100 micropores at each site. Future studies could use a single patch comprising, for example, 100 MNs inserted simultaneously.

6.6.2.2 Vacuum application

Vacuum was applied using a Negative Pressure Cutaneous Suction System (NP-2, Electronic Divestities, Ridge Road, Finksburg, MD). The vacuum chamber was aligned with skin sites that received MN treatment. Each chamber had a bottom plate with up to five 8 mm diameter orifices through which vacuum contacted the skin. Vacuum as low as -50 kPa (gauge) was applied for up to 20 min. In the optimized protocol, vacuum was slowly ramped down to -50 kPa over the course of ~3 min. After stopping the vacuum and removing the orifice plate, clear fluid on the skin surface was collected using sterile medical gauze (Ultrapure non-woven sponges, CrossTex International, Lawrenceville, GA) and stored in a low protein-binding tube (Eppendorf North America, Westbury, NY) prior to placing in a -80°C freezer.

6.6.3 ISF sampling methods optimization

Two optimization studies were performed on a cohort of 3 male and 2 female human participants with ages of 28±4 years. All procedures were approved by the Georgia Tech Institutional Review Board (IRB) and written consent was obtained from all subjects before the study.

In the first study, patches containing MNs of 250 µm, 450 µm or 650 µm length were applied to skin as described above to create 100 micropores at each skin site. Vacuum was then applied at -17 kPa, -34 kPa or -50 kPa (gauge). The skin was observed for up to 5 min to determine if bleeding occurred.

In the second study, patches containing MNs of 250 µm length were applied to the skin to create 100 micropores at each skin site. Then, (i) vacuum of -17 kPa (gauge) was applied immediately after MN patch treatment or (ii) vacuum of -50 kPa (gauge) was applied 0, 5 or 10 min after MN patch treatment or (iii) vacuum was slowly ramped down from 0 to -50 kPa (gauge) over the course of ~3 min after MN patch treatment. If bleeding occurred, vacuum was stopped at 15 s and any fluid on skin surface was collected. In the absence of bleeding, fluid was collected after 20 min of vacuum application.

6.6.4 Blood collection by venipunture

Venipuncture samples were taken from the forearm, collected into K3 EDTA tubes (BD Vacutainer Blood Collection Tube) and spun down at 1,400 rcf for 15 min (Eppendorf centrifuge 5702 RH, Eppendorf AG, Hamburg, Germany) to separate the plasma, which was collected in Protein lo-bind tubes (Eppendorf Lo-bind). Capillary blood samples were collected by lancet puncture on the fingertip (Unistik 2 Normal, Owen Mumford, Marietta,

GA) and collected into heparin mini collection tubes (MiniCollect Lithium Heparin with Gel Separator, Gernier Bio One North America, Monroe, NC). The tubes were spun down at 1,400 rcf for 15 min (Eppendorf centrifuge 5702 RH) to separate the plasma, which was collected in Protein lo-bind tubes. All plasma samples were stored at -80°C until analysis.

6.6.5 Suction blister fluid collection from suction blisters

SBF was collected by the method developed by Kiistala [73]. Suction blisters were created on the thigh of each participant as a site easily accessible when wearing shorts and one that can be discretely covered for cosmetic reasons until suction blisters have fully healed. The skin site was first thoroughly disinfected with an alcohol swab. Suction was then applied using a Negative Pressure Cutaneous Suction System [247, 248]. Sterile orifice plates with 3 holes (8 mm diameter each) along with the suction cup were firmly attached to the skin using straps. Suction at -50 to -70 kPa (gauge) was applied at 40°C for ~45 min until blister formation was complete. Fluid from intact and hemoglobin-free blisters was collected using a Micro-Fine syringe (BD Biosciences, San Jose, CA) and stored in Protein lo-bind Eppendorf tubes at -80°C.

6.6.6 Skin surface swab

Sterile medical gauze wetted with sterile USP-grade water was rubbed against the skin for 30 s and stored in Protein lo-bind Eppendorf tubes at -80°C.

6.6.7 Histopathological analysis of skin

Six hairless rats (6 months old, female, Charles River Laboratories, Wilmington, MA) each received three treatments. MN patch plus vacuum, MN patch only, and vacuum only. For MN patch application, a patch comprising five 250 μm-long MNs was applied repeatedly on the back to create an array of 100 micropores as described above. For vacuum application, vacuum was applied at -50 kPa (gauge) for 10 min. At 4 or 24 h post-treatment, animals were euthanized by carbon dioxide gas asphyxiation and the treated skin was collected using an 6-mm biopsy punch along with untreated skin controls. After fixation in formalin, skin was prepared for histopathological analysis by sectioning and staining with hematoxylin and eosin followed by microscopic examination by a board-certified dermatopathologist at Emory University School of Medicine.

6.6.8 Pain and skin tolerability measurements

6.6.8.1 Pain

To assess pain, participants were asked if a procedures was painful. If yes, they were asked to rate the pain on a Visual Analog Scale of 1 (no pain) to 10 (worst possible pain).

6.6.8.2 Skin tolerability

Skin tolerability was measured using a quantitative skin scoring scale adapted for MN patches using established guidelines for clinical studies [104] (see Table C. 6 in Appendix C). Each skin site was scored for pain, tenderness, erythema (size and intensity) and swelling on a grading scale of 0 to 4. Pain and tenderness were scored based on the participant's response, whereas erythema and swelling were measured by the investigator. Participants were asked if they felt pain at the skin site at various times after skin treatment (e.g., MN patch administration) was complete. This pain was assessed separately from the pain associated with MN patch application, which is addressed immediately above. Tenderness was defined as any pain felt at the skin site when the investigator gently touched it. Erythema size was measured using a ruler scale and intensity was measured by visual observation of the skin site. Swelling was measured by the investigator by gently moving her thumb over the skin site to identify any raised surfaces on the skin. The investigator recorded a numerical score for each of these tests and photographically imaged the skin at each time point.

6.6.8.3 Sensory perceptions

Participants were asked if they felt the following sensory perceptions during skin treatment (e.g., MN patch administration): pain, burning, stinging, tingling, itching, warmth and tightness. If the participant replied yes to any of the above sensations, the participant was further asked to rate those sensations as very slight, slight, moderate, strong or very strong, and was also asked if those sensations felt comfortable.

6.6.9 Analytical techniques

6.6.9.1 Determination of blood volume

Collected blood volume was measured by determining hemoglobin content in blood samples using a Triton / NaOH-based method (Hemoglobin Assay Kit, Sigma-Aldrich, St. Louis, MO). Hemoglobin content in a blood sample was normalized against hemoglobin content in the capillary blood of the same participant to obtain the amount of blood in each sample.

6.6.9.2 Determination of ISF volume

Collected ISF volume was measured by determining sodium ion concentration in the collected fluid. Sodium ion concentration was determined using a sodium ion sensitive electrode (perfectION comb NA, Mettler Toledo Inc., Columbus, OH). The sodium ion content measured in the samples was normalized against a standard sodium ion concentration in ISF of 135 mmol/L to determine ISF volume. This method relies on the

expectation that sodium ion concentration is constant in the body fluids of heathy participants [89].

6.6.9.3 High-resolution metabolomics

Body fluids (ISF, SBF and plasma) were profiled using untargeted high-resolution metabolomics (HRM) with dual column/polarity liquid chromatography. Body fluid samples were diluted from 10 μL to 50 μL with distilled water, and 50 μL of diluted biofluid was added to 100 μL of acetonitrile and 2.5 μL of a mixture of 14 stable isotope standards. Samples were vortexed and allowed to equilibrate before proteins were precipitated by centrifuge. Samples were analyzed using hydrophilic interaction chromatography (HILIC; XBridge BEH Amide XP, 2.1 mm x 50 mm x 2.5 μm particle size, Waters, Milford, MA) in positive electrospray ionization mode, which better captured polar and semi-polar metabolites, and using reverse-phase C18 liquid chromatography (stainless steel column, 2.1 mm x 50 mm x 3 μm particle size, Higgins, Mountain View, CA) in negative-ion mode, which better captured fatty acids and other nonpolar metabolites. The dual chromatography setup interfaced to a high-resolution Fourier transform mass spectrometer (Q-Exactive HF, Thermo Scientific, Waltham, MA).

For each mode, analyses were performed with three technical replicates with an injection volume of 10 μL and mass-to-charge ratio (*m/z*) scan range of 85 to 1275. Body fluid types were analyzed in separate batches, with samples randomized within each fluid and distilled water blanks and pooled reference plasma (Q-Standard) samples analyzed prior to and following each batch to enable quality control, as described previously[249]. Data

extraction was performed using apLCMS[250] and xMSanalyzer[251] as *m/z* features, with an *m/z* feature defined by *m/z*, retention time, and ion abundance. Triplicates were averaged prior to data analysis. A feature was defined as "present" in a sample if the ion intensity in the sample was greater than two times the mean ion intensity of that feature in the water blank samples. Data were filtered to remove features that were not present in ≥50% of samples in at least one body fluid.

6.6.9.4 Metabolite identification:

Clinically-relevant biomarkers were identified by comparing m/z features to base peaks generated from an in-house library of authentic reference standards run under similar assay conditions[249]. Features were matched to metabolites in the library with a threshold of 10 ppm. Metabolites unique to ISF were identified with a custom dataset-wide deconvolution algorithm and Kyoto Encyclopedia of Genes and Genomes (KEGG)[187] database matching (± 10 ppm). High-confidence matches (metabolites with two or more correlated adducts and/or isotopes with similar retention times) were curated to remove unlikely peak groupings and/or biologically-implausible compounds. The presence of a metabolite was evaluated by examining the presence of the base peak in the feature grouping.

6.6.9.5 Determination of caffeine concentration

The amount of caffeine in the collected ISF and plasma was measured using ELISA (Abraxis, Warminster, PA).

6.6.9.6 Calculation of pharmacokinetic parameters

C_{max} was the highest caffeine concentration measured in ISF/plasma from each participant. t_{max} was the time at which C_{max} was measured. Area under the curve, $AUC_{(0\text{-}8h)}$, was calculated using the linear trapezoidal rule. To estimate half-life, $t_{1/2}$, an elimination rate constant (k_e) was obtained as the slope of the elimination curve on a semilog plot, and then $t_{1/2}$ was calculated as $t_{1/2} = \ln(2)/ k_e$. To estimate clearance (CL), the apparent volume of distribution (V_D) was multiplied by k_e. V_D was calculated as D/C_0 where D is the dose of caffeine (43 mg) and C_0 is the intercept of the elimination curve on the y axis.

6.6.10 Statistics

All statistical analysis was conducted using Graphpad Prism 7 Software (GraphPad Software, La Jolla, CA). Statistical differences were analyzed using Student's t-test. P-value of <0.05 was considered statistically significant.

7 CHAPTER 7: DISCUSSION

Measurement of biomarkers in body fluids is a valuable tool used to accurately diagnose and subsequently monitor diseases. Biomarker detection has enabled revolutionary technologies such as early disease diagnosis, continuous monitoring for disease management, and novel drug development. Biomarkers are detected in body fluids such as blood, urine, saliva, sweat, and tears. In addition to these body fluids, ISF is of great interest as a source of valuable biomarkers for diagnostic applications. Recent developments such as the need for regular or continuous monitoring of analytes, a need to understand metabolic processes in-depth for drug development, and the need to be able to sample biomarkers non-invasively has opened the potential for ISF as a body-fluid of interest.

A major limitation of clinically used techniques to sample ISF is the invasiveness of techniques such as sensor implantation, biopsy, microdialysis, or open-flow microperfusion. Other techniques such as reverse iontophoresis are limited by the inability to sample large molecules, and suction blisters cause discomfort and skin pigmentation that can take weeks to heal. MNs have shown promise as a technology to sample ISF through skin in a non-invasive manner. Previous studies to sample ISF using MNs have been limited by the small sample volumes of ISF which are not sufficient for multiple analyte measurement. This study developed a MN-based device that samples multiple microliters of ISF within a clinically relevant time frame of 20 min and translated this technology to collect ISF in humans and evaluate the potential for clinical use.

The first aim of this study was to build a broad understanding of transport of ISF through skin to enable an optimized MN design. In this aim, we evaluated different mechanisms to sample ISF from skin using different MN-based devices. Using this knowledge, we developed a MN-based system that could sample multiple microliters of ISF from human skin within 20 min.

MNs give access to the dermal ISF but cannot collect or pool the ISF on the skin surface on their own. There is a need for a driving force that drives ISF through the MNs or micropores onto the skin surface. This driving force can come from a concentration gradient, applied pressure gradient or osmotic pressure gradient. To generate these driving forces, various MN systems were designed.

Hydrogel MNs provided a ISF concentration gradient to drive ISF flow into the MNs. Hollow and porous MNs provided capillary forces to absorb the fluid and in turn provided a concentration gradient for ISF in the dermis. Osmotic MNs relied on a solution of higher osmotic strength than the ISF to provide a pressure gradient to drive ISF towards the micropore. Finally, MN systems that generated a pressure gradient in the dermis were designed to drive convective flow in the dermis – either by direct pressure application or application of vacuum to the skin surface. It was observed that the flow rate increased by orders of magnitude in the following order: hydrogel MNs<porous/hollow MNs<osmotic MNs<pressure-driven MNs.

To further understand the transport phenomenon in skin, we modelled the flow of ISF in skin and into the MN or micropore. There are three major steps associates with the

sampling of ISF by MNs – transport of ISF through the dermis to the MN surface, partitioning of ISF across the dermis-MN interface into the MNs, transport of ISF through the MN/micropore on the skin surface. Determination of the rate limiting step is key to developing a system that maximizes ISF flow rate.

It was observed that for a slow swelling hydrogel like polyvinyl alcohol, ISF transport in the hydrogel matrix was rate limiting. As the hydrogel system becomes fast swelling, the diffusivity of ISF in the hydrogel is higher than diffusivity in the skin and transport through skin becomes rate limiting. After this any improvement in the swelling of the hydrogel would make only incremental improvement in the ISF flow rate as the rate liming step shifted from the hydrogel to the dermis.

In case of hollow MNs or porous MNs, ISF at the surface was instantaneously absorbed. This maximized the concentration gradient in the dermis. Thus the rate limiting step is flow of ISF through the dermis. It is possible to increase the flow rate of ISF incrementally by increasing the surface area of the MN, which also has an upper bound because of the relatively small size of MNs and a limit on the number of MNs contained within a patch.

A micropore filled with an osmotic solution that has higher osmotic strength than surrounding ISF generates a pressure gradient that drives ISF towards the micropore. However, since the osmolyte itself is a small water soluble molecule, it diffuses into the dermis. Thus the osmotic pressure gradient decreases with time. A higher molecular weight osmolyte with lower diffusivity in dermis or presence of a semipermeable membrane that

prevents the back flow of osmolyte into the dermis might help to maintain the pressure gradient for longer times and thus increase the flow rate of ISF.

Finally exerting a convective force on the dermis to force ISF towards the micropores generates a steady pressure gradient that does not diminish with time. Hence, pressure driven convection gives the highest ISF sampling rates. The flow of ISF is limited by the flow conductivity of ISF in skin. Vacuum application can generate a maximum pressure gradient of 1 atm and there is no theoretical upper bound to the maximum positive pressure that can be applied to skin. However, skin tolerance to pressure for the time duration of pressure application may put a upper bound on this value. Overall, theoretical modelling of ISF in skin suggested that flow within the dermis was rate limiting, and to maximize ISF flow rate would require a high pressure gradient through the dermis.

Based on these observations, a vacuum based system was chosen as the optimum system to draw ISF through skin. MN insertion and immediate removal from skin created micropores over which vacuum application resulted in ISF flow to the surface. It was observed that the skin which contained the micropores needed to be either curved and placed over a firm support or stretched out in order to draw ISF to the surface. This is presumably because under the absence of tension, the micropores collapsed and closed the pathway for the ISF to flow towards the skin surface. Presence of any covering on the micropores during vacuum application, such as a gauze pad, hindered the flow of ISF towards the skin surface because of lowered pressure drop and surface tension drop. As the thickness of the covering was reduced, the flow of ISF to the surface improved and the

highest ISF flow was obtained when the micropores had no covering during vacuum application.

This system was tested on human participants to sample ISF, and multiple microliters of ISF were extracted from skin of human volunteers. It was seen that concentrations of glucose and total protein in ISF and companion plasma samples correlated and were similar in both fluids. Thus commonly measured analytes can be detected in ISF and ISF can be used as an alternative to blood for monitoring these biomarkers.

In addition to development of a MN patch to sample the ISF, it was important to evaluate the composition of ISF and establish ISF as a body fluid of clinical value. Previous studies have studied the proteomics of ISF and compared it to plasma. However, the small molecule composition of ISF has not been significantly studied before. Therefore, a metabolomic analysis was carried out on suction blister ISF obtained from 10 healthy adult participants and compared with plasma samples obtained from those participants. Analysis by mass spectrometry revealed that a total of 7044 *m/z* features were present in in all samples of which 79% were common between ISF and plasma, 15% were unique to suction blister ISF and 6% were unique to plasma. In general, plasma had a higher proportion of hydrophobic molecules and ISF had a greater percentage of hydrophilic molecules. Most endogenous metabolites were found in both fluids.

The metabolites in ISF included common clinical biomarkers such as glucose, cholesterol, creatinine, and urea. Also present were metabolites associated with amino acid metabolism, lipid metabolism, purine/pyrimidine metabolism, and several exogenous

compounds such as pesticides, phytochemicals and dietary compounds. This shows that ISF is a source of endogenous as well as exogenous metabolites and has great potential as a source of valuable biomarkers. Several clinically relevant molecules were identified to be unique or elevated in ISF compared to plasma. These compounds fell into several groups – phospholipids, purines, spermidines, methionine related compounds, and dietary derived compounds. This indicates the potential to use ISF to measure clinically relevant biomarkers in ISF that are are not easily detected in plasma. Dermatologically relevant molecules such as urocaninc acid were found uniquely in ISF which indicates the potential of dermal ISF in drug development and drug monitoring of dermatological drugs.

Similarly, we found that several biomarkers were correlated between ISF and plasma. Notably these include several amino acids, nucleic acids, and neurotransmitter related metabolites. Pathways associated with protein biosynthesis, betaine metabolism, methionine metabolism, and glycine, serine, and threonine metabolism were overrepresented among correlated metabolites. This indicates that several biomarkers that are currently monitored in blood can also be detected in ISF reliably. Overall, this study established metabolomics as a useful technique to study the composition and evaluate the value of ISF as a source of biomarkers. The understanding of similarities and differences between ISF and plasma can further enable the research and use of ISF for diagnostic applications.

Having developed a method ex-vivo to sample ISF using MNs and having established to potential of ISF as a valuable diagnostic fluid, we next adapted the MN system to reliably sample ISF from human participants. Ideally this method should be simple, minimally

invasive, be able to sample 1-10 µl within 20 min and the sampled ISF should match the composition of ISF in unperturbed skin. First, we optimized the system of MN application and vacuum application to reliably sample a clean ISF sample from skin within 20 min. Human skin is highly vascularized and MN application to create micropores damages blood vessels. Upon vacuum application, the blood from the damaged vessels effuses out leading to contamination of the ISF with blood. Lowering the MN length from 750 µm to 250 µm reduced the amount of bleeding but did not stop it completely. Lowering the maximum vacuum applied further reduced the amount of blood but also proportionately reduced the amount of ISF that could be collected. Finally, slowly ramping up the vacuum to the maximum value instead of a spontaneous vacuum application was seen to eliminate any contamination with blood, giving a clean ISF sample.

Using this, ISF was sampled from a cohort of 21 participants using up to 50 kPa vacuum for 20 min. Along with ISF, companion plasma samples from venipuncture as well as suction blister ISF from suction blisters were also obtained. Of all the features detected, around 2/3rd were common between MN ISF and plasma. This indicates that MN ISF can be used as a surrogate for plasma in some scenarios. Targeted analysis of 90 established biomarkers determined that 76 were found in at least one body fluid. Of these, 57 were found in more than 50% of all ISF and plasma samples. 7 metabolites were less common in plasma compared to ISF. These include tryptophan, sphingosine, leukotriene, hypoxanthine, xanthine, pantothenic acid (Vitamin B5), and tertahydrofolic acid. This indicates that ISF may be better than plasma to monitor certain biomarkers as they are more common or more elevated than in plasma. Others like taurodeoxycholic acid, acetyl-

cartinine, cortisol, methyl-histidine were found more commonly in plasma compared to ISF, indicating that ISF may not be suitable to monitor certain biomarkers.

We also found certain metabolites that were uniquely found in ISF. These include micronutrients such as gamma-tocopherol, citicholine, acetyl-glucosamine; several important endogenous metabolites such as glycogen, nebularine, angiotensin, estradiol cypionate; and other exogenous biomarkers such as barbaloin, diethanolamine, tributyltin chloride. A few of these biomarkers are not found in suction blister ISF suggesting that this method samples fluid from the skin surface that are not accessed by suction blister ISF. Thus this method of collecting ISF has the potential to access and monitor unique biomarkers, increasing the diagnostic value of this fluid.

In addition to detecting the presence and absence of certain biomarkers, we also studied the dynamic changes in biomarker concentration in ISF as compared to plasma from fingersticks. Caffeine was chosen as a model biomarker which was ingested orally by 9 participants at time zero. The levels of caffeine in ISF and plasma were monitored over a period of 8 h. The concentration of caffeine in ISF followed the concentration in plasma very closely with a steady rise in concentration for the first 2 h, followed by a steady decay for the next 6 h and no evidence of any lag time (when sampling every 30 min). Measured pharmacokinetic parameters such as C_{max}, t_{max}, $AUC_{0\text{-}8h}$, $t_{1/2}$ and clearance were similar in ISF and plasma. Thus, ISF using MNs can capture dynamic variations in biomarkers that could be used for continuous monitoring or therapeutic drug monitoring.

To assess the pain, skin tolerability and acceptability of the MN treatment we evaluated the pain experienced by the participants, studied skin tolerability up to 5 days after MN treatment and asked for participant feedback on the sensations experienced during MN treatment. The pain experienced from MN treatment was not statistically different to the pain experienced with suction blisters, venipuncture or fingerstick. In contrast, the pain experienced with suction blisters was significantly higher than the pain with venipuncture. The pain associated with MN treatment could mostly be attributed to MN application rather than vacuum application. This pain could be reduced by better design of the MN patch backing.

MN treatment was in general well-accepted by the skin. Mild erythema was observed at the site of MN treatment that generally resolved within 4 days. The erythema was contained within the area of MN treatment. No pain and minimal tenderness were felt at the site 3 days after MN treatment by some participants. Any swelling resolved within 24 h. In contrast, pain at site of fingerstick was felt by some participants up to 24 h after treatment and tenderness was felt up to 5 days after treatment. Suction blisters generated higher intensity erythema in higher percentage of participants. The pain and tenderness at the skin site after the procedure was also seen in higher percentage of participants.

When asked, the sensations experienced during MN application, participants reported pain and stinging as the dominant sensations. A similar response was seen for fingersticks. In general participants said that they were comfortable with all the sensations experienced with MN applications for 47% of the time as opposed to 53% with fingersticks. Overall these results suggest that MN treatment is comparable to other sampling technologies like

fingerstick and venipuncture with respect to pain and other sensations. MNs are well tolerated compared to suction blisters because of milder erythema, pain, tenderness and also the absence of any pigmentation/dark spots a few days after MN treatment. Given the acceptability of these methods, it is expected that a MN based method would also be well-accepted clinically for diagnostic applications.

In sum, we have developed a reliable method to sample ISF through skin based on a thorough experimental and theoretical evaluation of ISF transport in skin and of different MN designs. Using pressure driven convection as a result of vacuum application, we successfully sampled microliter volumes of ISF from skin of human participants. We established ISF as a body fluid of interest and a source of valuable biomarkers by evaluating its composition using metabolomics. Using the MN system, we further explored ISF composition from MNs and showed that the system could be used reliably for novel biomarker detection. We also established the acceptability and skin tolerability of MN treatment. We believe this technology can become a platform for greater exploration of ISF for research as well as for its future application in the clinic as a novel diagnostic fluid.

8 CHAPTER 8: FUTURE WORK

8.1 Miniaturization and adaptation of microneedle system for clinical use

The current system design is effective to reliably sample ISF through skin. However, it is not practical or adaptable for clinical use in the current form. Future work needs to be done to engineer the system to become simpler.

8.1.1 MN patch design

The current MN design requires manual insertion to create micropores. The MN patch needs to be designed such that the needles insert to the desired depth with one single push using a thumb or an applicator. The shape of the backing and the geometry of the MNs can be optimized such that the MNs insert painlessly and create sufficiently large micropores for ISF transport. Ideally this would involve a 2-D MN array that has ~100 MNs in a square centimeter area and can create 100 micropores with one insertion instead of repeated MN insertions required in this study.

8.1.2 Wearable vacuum chamber

The system for vacuum application is bulky and not directly adaptable for clinical applications. Design of a smaller suction cup that ramps up the vacuum over a set time period would be ideal in a clinical setting. Current devices such as handheld vacuum pumps used for cupping therapy, or vacutainer blood collection tubes can be adapted to modify the current setup. This could greatly accelerate the clinical acceptability of this MN system for diagnostic applications.

8.1.3 One step process

The current MN treatment includes MN application and vacuum application – which is a two- step process. To adapt the system for clinical use, a simpler portable system and a one-step process will be beneficial. This could be done by designing a spring loaded application system that is integrated into the suction cup, and that inserts and removes MNs creating micropores. Otherwise, MNs can be integrated on the suction cup such that vacuum is generated by the action of pressing MNs on the skin. Converting the current system to a simpler one-step system could greatly aid in increasing the practicability and adaptability of this system to clinical applications.

8.2 Expanding the scope of microneedle patches to point-of-care diagnostic systems

A major portion of this work has been to develop a method to sample ISF from skin of human participants and show a first demonstration of the utility of the MNs and ISF towards clinical applications. A major advantage of MN based devices is their ease of use, cost-effectiveness, and portability which makes it ideal for point-of-care applications. Thus, the next step for MN development is to develop a point-of-care system with MNs that is able to diagnose disease.

The first step is to assess ISF for diagnosis of a disease. This would require testing of the system in two populations – a diseased population vs. a healthy population. A detailed understanding of the relation between concentration of relevant biomarkers in ISF vs plasma needs to be established. Other important factors to consider are the variations in biomarker levels between subjects and their effect on the accuracy of detection, presence

of false positives or negatives. The current system relies on Na+ measurement to calibrate the volume of ISF sampled. The variability with this method needs to be studied and a robust method for internal calibration needs to be developed to improve the accuracy of the process.

The next step would be to integrate MN patch and ISF detection in a point-of-care system. Recent techniques such as lab-on-a-chip microprocessors, paper microfluidics, Raman spectroscopy can enable point of care testing. Combining these technologies with ISF sampling using a MN patch can truly enable point-of-care diagnosis with MNs.

These advances would establish the use of MN systems and ISF for diagnostic purposes and could accelerate the development of this technology for clinical applications.

8.3 Evaluation of factors affecting interstitial fluid flow after microneedle treatment in humans

8.3.1 Age and ethnicity

Applications of MN-based diagnostic device could be for a wide population range – these include people of different ages, ethnicities and hence different skin types. It is important to evaluate the efficacy of ISF sampling on these different skin types. It is important that the optimized MN device design should have equal efficacy for people of all ages and ethnicities.

8.3.2 Hydration levels

Hydration levels of an individual may affect the water content in the dermis and hence the volume of ISF available for sampling. There is a need to establish correlations between hydration and ISF sampled by modifying the water intake of individuals or artificially hydrating the skin prior to MN treatment.

A thorough evaluation of the various factors affecting ISF flow in humans and identification of the important parameters will enable the development of a robust MN system that can function well in all populations even under extreme conditions.

8.4 Evaluation of prolonged wear of microneedles on skin tolerability

Use of MNs for monitoring applications may need prolonged wear of the device – especially in cases of continuous monitoring. It is important to consider the pain, safety, acceptability, and tolerability of the MN system for prolonged wear. In the current study, MNs were quickly inserted and removed, and vacuum was kept in place for a maximum of 20 min.

Although pain experienced with vacuum application is shown to be minimal, prolonged application of vacuum may increase the pain and discomfort associated with the procedure. Also, prolonged vacuum application even at lower levels may lead to skin tissue damage. It is important to assess in-vivo the changes in skin physiology that occur as a result of prolonged wear. Different populations such as the children or the elderly may have different skin maturity and may react differently to MN treatment. Thus studying the effects of vacuum application becomes especially important while considering these susceptible populations.

Similarly, micropores that remain open for longer periods of time are more susceptible to infection. To evaluate the possibility of infection with micropore creation, challenge studies need to be carried out. It may be necessary to integrate anti-microbial agents into the system to minimize infection risk during prolonged wear.

This study would allow for a thorough assessment of the safety of MN patches and help improve the acceptability of this technique by a broader research and clinical community.

9 CHAPTER 9: CONCLUSIONS

Diagnosis and monitoring of disease is often done by measuring biomarkers found in blood, urine, saliva and other bodily fluids. Another rich source of biomarkers is the ISF that surrounds cells and tissues in the body, but difficulty in accessing this fluid has limited its use in research and medicine. In this study, we conducted experimental studies coupled with theoretical modeling to design a MN patch that penetrates into superficial layers of skin and thereby enables withdrawal of ISF through micropores in a simple, minimally-invasive manner. We have shown that this MN based system can sample multiple microliters of ISF within 20 min.

By exploring the metabolomic profile of ISF, we have shown that ISF can be used as a surrogate for blood in some cases or also to detect valuable biomarkers that are unique or elevated in ISF compared to blood. The MN patch can be used to detect these unique biomarkers in ISF and also to detect dynamics of biomarker variations as is currently done using plasma. This patch can help researchers access ISF to advance discovery of novel biomarkers and enable doctors to use ISF for possible future diagnosis and monitoring of disease.

APPENDIX A

SUPPORTING INFORMATION FOR CHAPTER 4

A.1.1. ISF content in skin

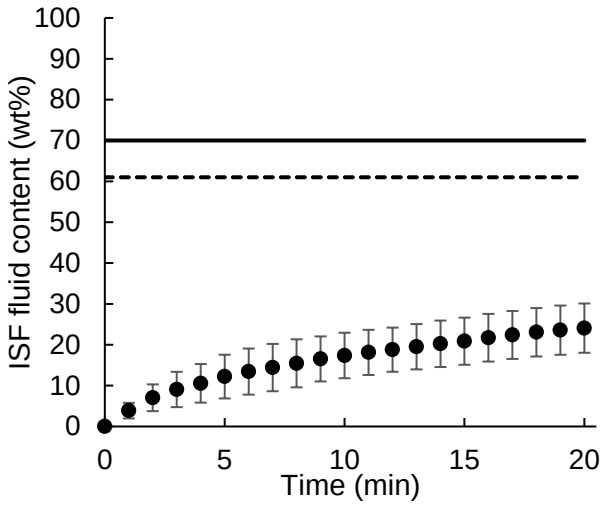

Figure A. 1: Estimation of ISF content in skin: Total ISF content reported in literature (solid line, 70 wt% (1)), total ISF content was determined by lyophilizing skin (dashed line, 61 ± 10 wt%). Mobile ISF loss (data points) is plotted over time, reaching a value of 20 wt% after 20 min. Mobile ISF loss is the amount of ISF that could be removed from the dermis and was not otherwise bound or encapsulated. To estimate this, pig skin ex vivo measuring 4 cm2 was placed under 8.9 kg weight, and skin mass was measured periodically. Data show mean ± SD (n = 3).

A.1.2. Effect of osmotic driving force on ISF collection over time

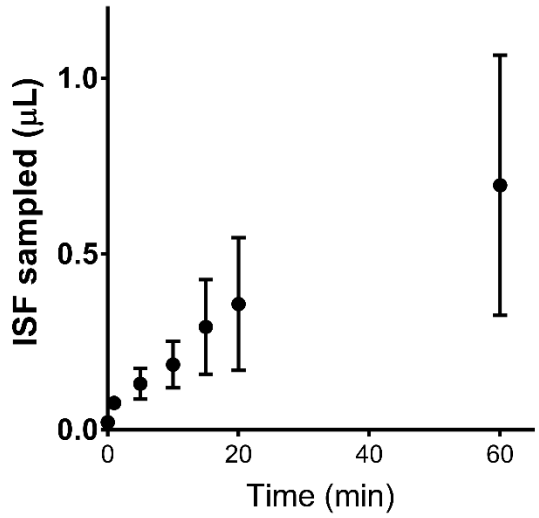

Figure A. 2: ISF volume sampled from pig skin ex vivo over time by osmosis. An array of 10 uncoated, metal MNs was used to create micropores in skin. A 400 mg/mL solution of maltose was then placed on the skin surface to provide an osmotic driving force. Data show mean ± SD (n=4).

A.1.3. Effect of number of MNs on ISF volume collected by osmosis

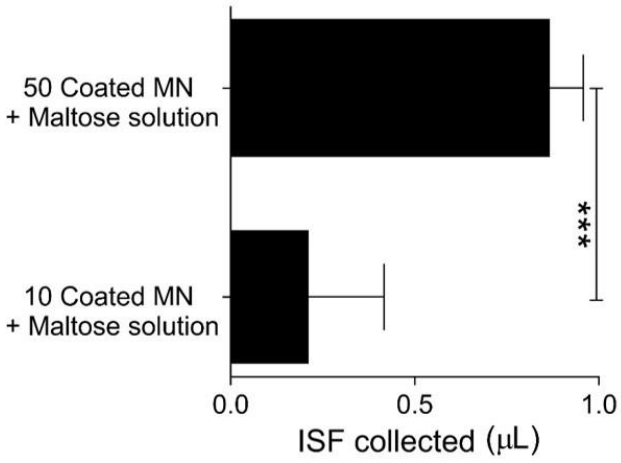

Figure A. 3: ISF volume sampled from pig skin ex-vivo by osmosis. An array of 10 or 50 coated, metal MNs was used to create micropores in the skin. A 400 mg/mL solution of maltose was then placed on the skin surface to provide an osmotic driving

force. The volume of ISF sampled increases with increasing number of MNs. Data show mean±SD (n=4). *** p-value<0.001

A.1.4. Effect of number of MNs on ISF sample volume

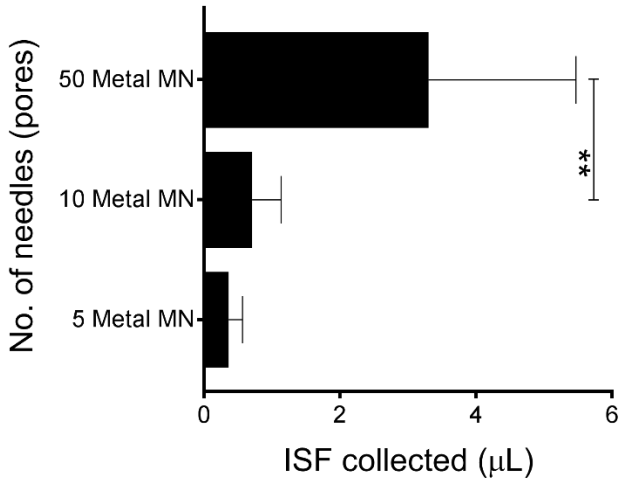

Figure A. 4: ISF sample volume collected from pig skin ex vivo using suction (-85 kPa) after puncture with different numbers of metal MNs measuring 750 µm in length. Data show mean ± SD (n≥3).

A.1.5. Effect of MN length on ISF sample volume

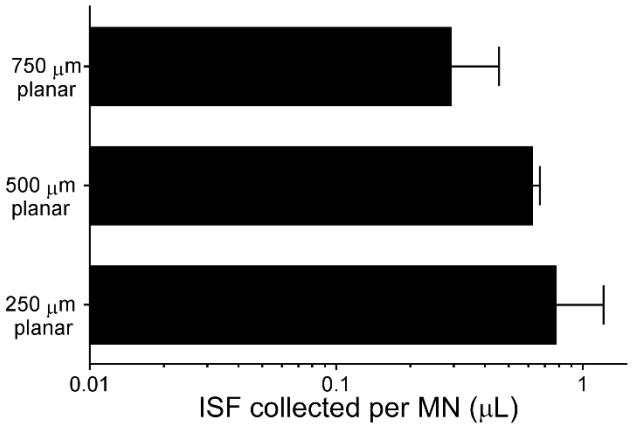

Figure A. 5: ISF sample volume collected from pig skin ex vivo using suction for three different lengths of metal MNs on 10-MN patches. Data show mean ± SD (n≥3).

A.1.6. Effect of MN geometry on ISF sample volume

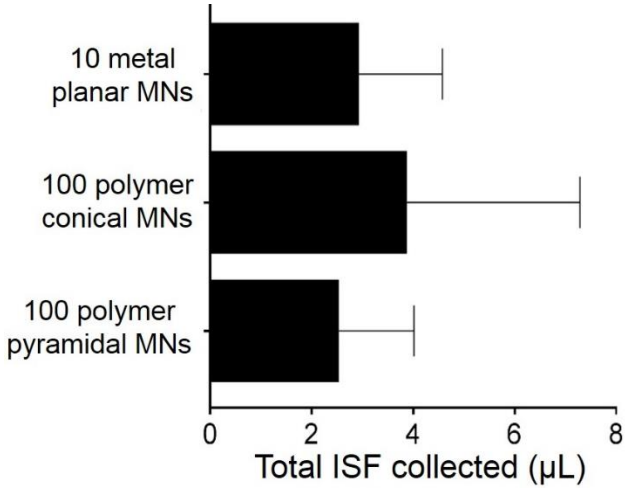

Figure A. 6: ISF sample volume collected from pig skin ex vivo using -85 kPa suction for MNs with different geometries. The planar metal MNs constitute a 2 x 5 array of MNs measuring 750 µm in length and 200 µm by 25 µm in cross section at the base. The conical polymer MNs constitute a 10 x 10 array of MNs measuring 600 µm in length and 300 µm in diameter at the base. The pyramidal polymer MNs constitute a 10 x 10 array of MNs measuring 500 µm in length and 250 µm by 250 µm in cross section at the base. Data show mean ± SD (n≥3).

A.1.7. Effect of skin configuration on ISF sample volume

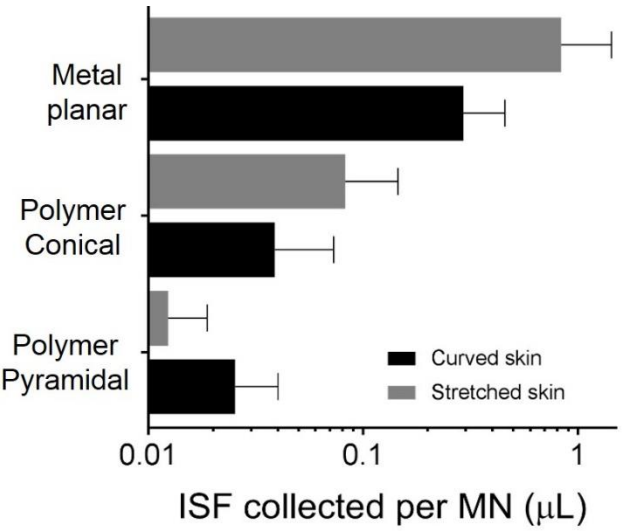

Figure A. 7: ISF sample volume collected from pig skin ex vivo using -85 kPa suction for different pig skin configurations using MNs with different geometries. The MNs were the same as described in Figure A. 6. Curved skin had a radius of curvature of 5 mm. Stretched skin had a strain of ~100%. Data show mean ± SD (n≥3).

A.1.8. Schematic of positive pressure application for ISF sample collection

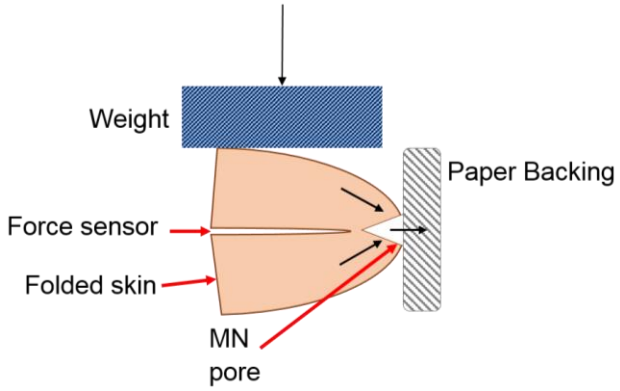

Figure A. 8: A schematic showing how positive pressure was applied to pig skin ex vivo to sample ISF to simulate pinching the skin. After application of MNs, the skin was folded with the micropores at the apex of curvature, and a weight was rested on the upper skin surface while the lower skin surface was placed on a rigid surface. Force applied to skin was detected via a sensor placed between the skin layers. ISF eluted from skin was collected using a paper strip on the skin surface.

A.1.9. Microneedle design and apparatus for vacuum application to skin of human participants

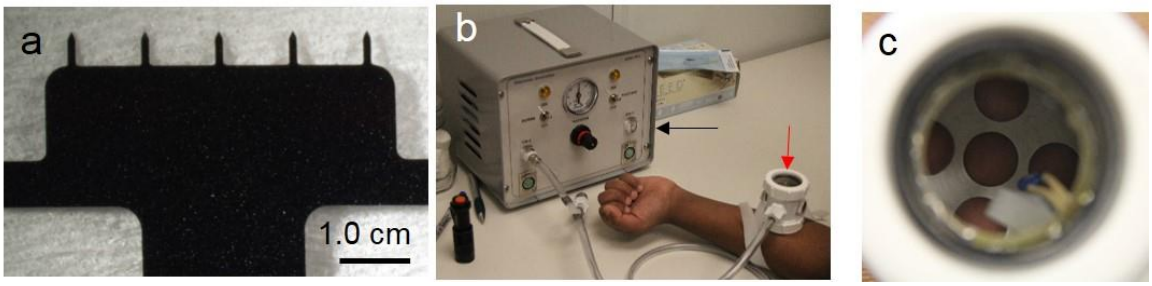

Figure A. 9: Microneedle design and apparatus for vacuum application to skin of human participants. (a) MN patch configuration used for insertion into skin to create micropores. (b) Suction apparatus used to create vacuum on the skin site (red arrow indicates the suction cup, black arrow indicates the vacuum pump and regulator). (c) Top view of skin sites through the suction cup as vacuum is being applied to skin (each of the five regions of exposed skin have a diameter of ~1 cm).

A.1.10. Correlations between concentrations of glucose and total protein in ISF and plasma of human participants

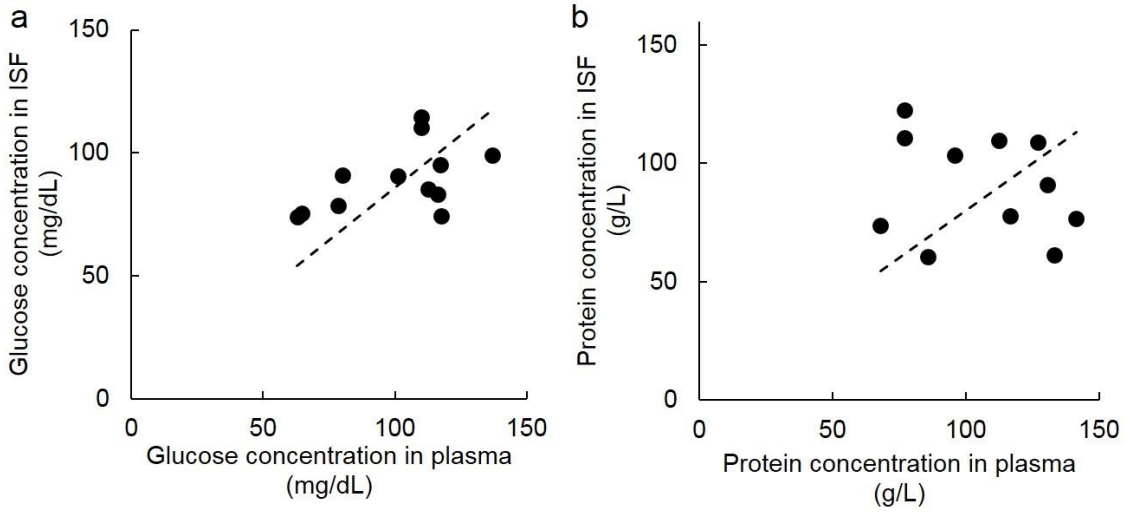

Figure A. 10: Concentration of analytes in ISF vs. plasma of 11 healthy human participants. (a) Concentration of glucose in ISF vs. plasma. Dotted line indicates best fit. (b) Concentration of total protein in ISF vs. plasma. Dotted line indicates best fit.

A.2. Theoretical model to predict ISF collection rates

A.2.1. ISF collection by diffusion into hydrogel microneedles

In this section we model two different hydrogel systems: physically crosslinked PVA hydrogel MNs developed in this study and chemically crosslinked rapidly swelling, methacrylated hyaluronic acid (MeHA) hydrogel MNs recently published by Chang et al. [169].

ISF collection using hydrogel MNs involves ISF first diffusing through dermis and then, upon partitioning into the hydrogel, diffusing through the hydrogel matrix. Diffusive transport in dermis is modeled using Fick's second law [252, 253]

$$\frac{\partial \mathrm{C}}{\partial \mathrm{t}} = \mathrm{D}_{\mathrm{derm}} \frac{\partial^2 \mathrm{C}}{\partial \mathrm{x}^2}. \quad (1)$$

with the following boundary conditions: $\mathrm{C}(\mathrm{x}, 0) = \mathrm{C}_0$, $\mathrm{C}(0, \mathrm{t}) = \mathrm{C}_{\mathrm{derm}}^{\mathrm{inter}}$, $\mathrm{C}(\infty, \mathrm{t}) = \mathrm{C}_0$, where C is ISF concentration in dermis, $\mathrm{D}_{\mathrm{derm}}$ is ISF diffusivity in dermis (8.72×10^{-10} m^2/s, see Eq. 2), $\mathrm{C}_{\mathrm{derm}}^{\mathrm{inter}}$ is ISF concentration in dermis at the MN interface, C_0 is ISF concentration in unperturbed dermis (0.7 g/mL) [71], t is time and x is position.

Diffusivity of ISF in dermis was estimated using values for permeability of water through dermis. Permeability (K) of a porous medium to a diffusing solute is given by

$$K = \frac{\varphi D_{derm}}{L} \quad (2)$$

where φ is the solute partition coefficient (ratio of concentration of solute in porous medium to free solution in the dermis, 0.7 (1)), D_{derm} is diffusivity of ISF, L is thickness of the barrier (thickness of dermis = 1.7 mm) and K is water permeability in dermis (6.11 x 10^{-7} m/s, [254]). Substituting the values into Eq. 2 gives D_{derm} = 8.72 x 10^{-10} m^2/s.

Integrating Eq. 1 and applying the boundary conditions, we get ISF flow rate at the dermis-MN interface as [255]

$$\dot{Q}_x\big|_{x=0} = -D_{derm}\frac{\partial C}{\partial x}\Big|_{x=0} A = \sqrt{\frac{D_{derm}}{\pi t}}\left(C_0 - C_{derm}^{inter}\right)A \qquad (3)$$

where A is MN surface area, which is 5.12 x 10^{-8} m^2 for the PVA MN, based on inserted MN dimensions of 100 µm x 100 µm at the base with 250 µm height and a pyramidal shape, and is 7.6 x 10^{-8} m^2 for the MeHA MN, based on inserted MN dimensions of 125 µm x 125 µm at the base with 300 µm height and a pyramidal shape.

ISF diffusion in the hydrogel MN is similarly modeled using Fick's second law

$$\frac{\partial C}{\partial t} = D_{MN}\frac{\partial^2 C}{\partial x^2}. \qquad (4)$$

with the following boundary conditions: $C(x,0) = 0,\ C(0,t) = C_{MN}^{inter},\ C(\infty,t) = 0,$ where C is ISF concentration in MN, C_{MN}^{inter} is ISF concentration in the MN at the dermis interface and D_{MN} is ISF diffusivity in MN. D_{MN} for PVA hydrogels is 1.8 x 10^{-11} m^2/s (4) and D_{MN} for rapidly swelling MeHA hydrogels can be approximated as equal to self-diffusivity of water, ~2.3 x 10^{-9} m^2/s [256].

Integrating Eq. 4 and applying the boundary conditions, we get ISF flow rate at the dermis-MN interface as [255]

$$\dot{Q}_{ISF}\big|_{x=0} = -D_{MN}\frac{\partial C}{\partial x}\Big|_{x=0} A = \sqrt{\frac{D_{MN}}{\pi t}}\, C_{MN}^{inter} A \tag{5}$$

Since ISF flow leaving the dermis equals ISF entering the MNs, Eqs. 3 and 5 are equal. C_{MN}^{inter} and C_{derm}^{inter} are related to each other by the partition coefficient, which is the ratio of equilibrium concentration of ISF in the MN (0.67 g/mL, obtained experimentally by measuring weight before and after equilibrium swelling of PVA hydrogel) and the dermis (0.7 g/mL, [71]).

$$\frac{C_{MN}^{inter}}{C_{derm}^{inter}} = k = 0.96 \tag{6}$$

Flow into the MNs was calculated over regular time intervals of 1 min. The predicted ISF concentration profiles and collection rate for PVA MNs are shown in Figure A. 11a,b. This analysis predicts a sample volume collected by a 100-MN PVA patch over 12 h to be 0.029 µL. The experimental value is 0.003±0.001 µL. The predicted value is ~10 fold larger than the predicted value, but is in reasonable agreement, given the simplified theoretical analysis with no fitted parameters. Because the diffusivity of ISF in the hydrogel is smaller than in the dermis, this results in the rate-limiting step for uptake being the diffusion of ISF within the hydrogel (Figure A. 11a).

For rapidly swelling MeHA hydrogel MNs, the analysis predicts a sample volume collected by a 100-MN MeHA hydrogel patch over 20 min to be 3.7 µL. The experimental value

determined by Chang et al. [169] is ~2.5 µL over 20 min, which is in good agreement with the predicted value. In this case, the diffusivity in the dermis is smaller than in the hydrogel, and hence flow through the dermis is the rate-limiting step.

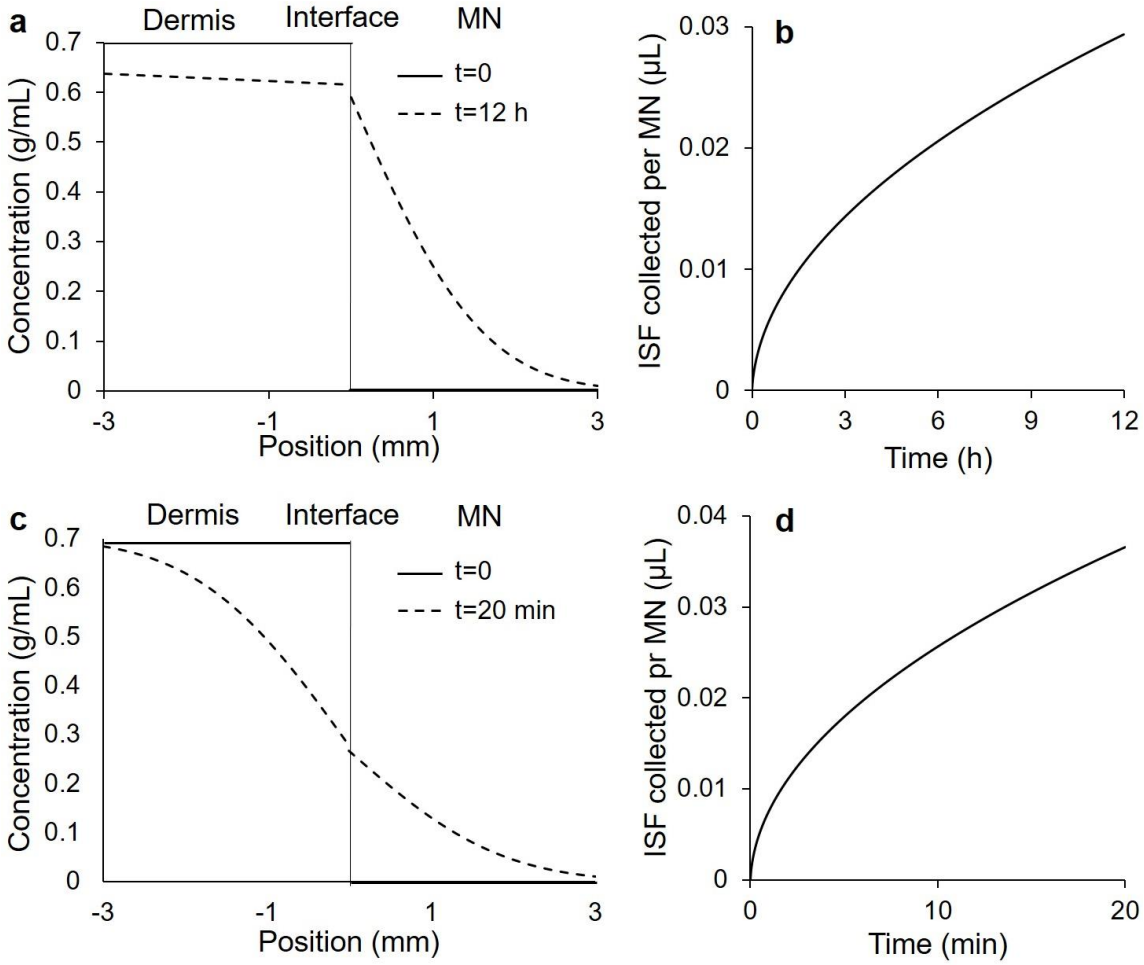

Figure A. 11: Model predictions of ISF collection by diffusion into hydrogel microneedles. (a) Concentration profile of ISF in the dermis and PVA MN at time 0 min (black line) and 12 h (dotted line). (b) ISF volume collected from skin into PVA MNs over time (c) Concentration profile of ISF in the dermis and MeHA MN at time 0 min (black line) and 20 min (dotted line). (d) ISF volume collected from skin into MeHA MNs over time

A.2.2. ISF collection by diffusion into micropores

ISF collection by diffusion into micropores is modelled in the same way as ISF collection by diffusion into hydrogel MNs, except the ISF diffusivity in the micropore is taken to be that of water self-diffusivity, ~2.3 x 10^{-9} m^2/s [256] and the micropore geometry differs from that of the hydrogel MN, such that the micropore-dermis interfacial area, A is 5 x 10^{-8} m^2 (based on 500 µm MN insertion depth, MN pore cross sectional dimensions of 50 µm x 10 µm and assuming the MN pore retracts ~4 fold after removing the MN with original cross-sectional area of 200 µm x 25 µm [123]).

The predicted ISF concentration profiles and collection rate for micropores are shown in Figure A. 12. This analysis predicts a sample volume collected by 10 micropores over 20 min to be 0.15 µL. The experimental value is 0.039±0.035 µL, which is ~4-fold lower than the predicted value, but is in reasonable agreement, given the simplified theoretical analysis with no fitted parameters.

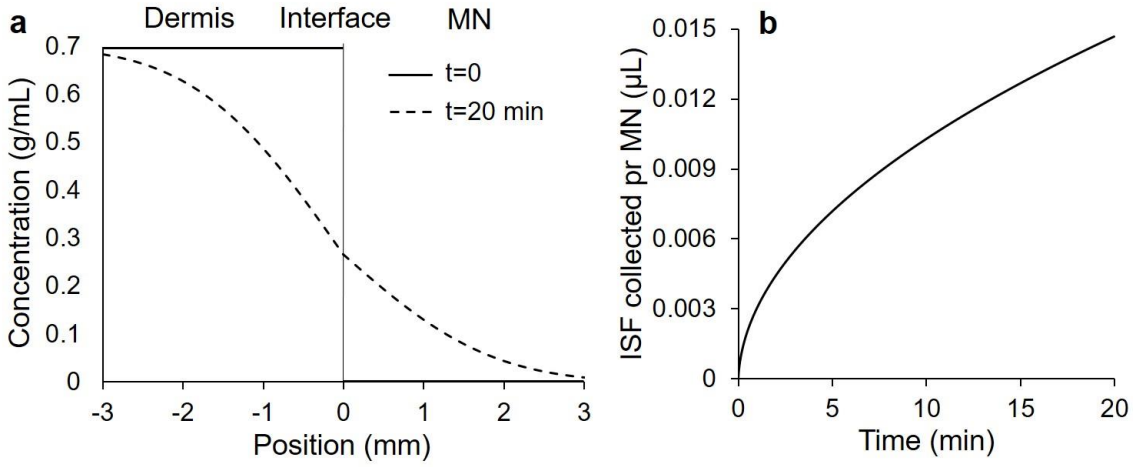

Figure A. 12: Model predictions of ISF collection by diffusion into micropores. (a) Concentration profile of ISF in the dermis and micropore at time 0 min (black line) and 20 min (dotted line). (b) ISF volume collected from skin into micropores

A.2.3. ISF collection by capillary flow into porous microneedles and hollow microneedles

Collection of ISF by capillary action involves two steps: (i) flow through dermis towards the MN or micropore and (ii) uptake and flow in the MN or micropore.

The rate of flow of ISF through a capillary can be estimated by the Hagen Poiseuille equation.

$$Q = \frac{\Delta P}{L}\frac{\pi R^4}{8\mu} \quad (7)$$

where Q is flow rate of ISF, ΔP is pressure difference across the capillary, L is length of capillary (500 μm), and μ is viscosity of ISF (assumed to be similar to plasma viscosity, 0.0012 Pa.s [257]).

The pressure difference can be estimated by the Lucas Washburn equation

$$\Delta P = \frac{2\gamma}{R}\cos\emptyset \quad (8)$$

where γ is surface tension of ISF (assumed to be similar to water 0.072 N/m at 37^0C) and ∅ is contact angle between ISF and MN (assumed to be 0^0).

Estimated flow after 20 min through a capillary with radius ~ 5 µm (corresponding to a single pore in filter paper, which is contains many porous pathways) or 130 µm (corresponding to a 25G needle) is 14 µl or 250 ml, respectively..

Since the experimental ISF collection values are much lower than flow rates through the bore of a hollow needle or that expected through a large network of capillaries in a porous paper MN, uptake of ISF by porous filter paper or a hollow MN can be considered instantaneous. As confirmation of this expectation, when 20 µl of water was pipetted onto the porous paper MNs, the water was absorbed into the paper within seconds. Therefore, we assumed that ISF coming to the dermis-MN interface is absorbed instantaneously and the concentration of ISF at the interface is 0.

The flow of ISF in dermis can be modeled by Fick's second law of diffusion.

$$\frac{\partial \mathrm{C}}{\partial \mathrm{t}} = D_{derm} \frac{\partial^2 \mathrm{C}}{\partial \mathrm{x}^2} \tag{9}$$

with the following boundary conditions: $\mathrm{C}(\mathrm{x}, 0) = \mathrm{C}_0$, $\mathrm{C}(0, \mathrm{t}) = 0$, $\mathrm{C}(\infty, \mathrm{t}) = \mathrm{C}_0$ where C is concentration of ISF in dermis, D_{derm} is ISF diffusivity in dermis (8.72×10^{-10} m^2/s, see above) and C_0 is ISF concentration in unperturbed dermis (0.7 g/mL).

Substituting the boundary conditions in the equation, we get flow rate into the MN [255]

$$\dot{\mathrm{Q}}_{\mathrm{ISF}} = -\mathrm{D} \frac{\partial \mathrm{C}}{\partial \mathrm{x}}\Big|_{\mathrm{x}=0} \mathrm{A} = \sqrt{\frac{\mathrm{D}}{\pi \mathrm{t}}} \mathrm{C}_0 \mathrm{A} \tag{10}$$

The exposed outer surface area of a porous paper MN sandwiched between two metal MNs is 2.7×10^{-8} m^2 (based on MN dimensions of 50 µm x 200 µm cross-sectional area and 400 µm insertion depth and void fraction of 68%) and area of the open tip of a hollow 25G MN is 5.3×10^{-8} m^2 (based on an inner diameter of 260 µm) (see Fig 2). Substituting these values in the flux equations, the predicted ISF concentration profiles and collection rate are obtained and shown in Figure A. 13.

The predicted ISF volume collected by each MN over 20 min follows. For a porous paper MN it is 0.021 µL and for a hollow 25G MN is 0.041 µL. The experimentally observed flow rates for porous paper MN is 0.0033±0.0031 µL and for a hollow 25G MN is 0.025±0.019 µL. The predicted values are 6.4 and 1.6 times larger than the experimental values, which represents reasonable agreement given the simplifying assumptions of this analysis with no fitted parameters. Since the rate of transport through MN capillaries is much faster than through dermis, the rate of ISF uptake is limited by the diffusion of ISF through the dermis.

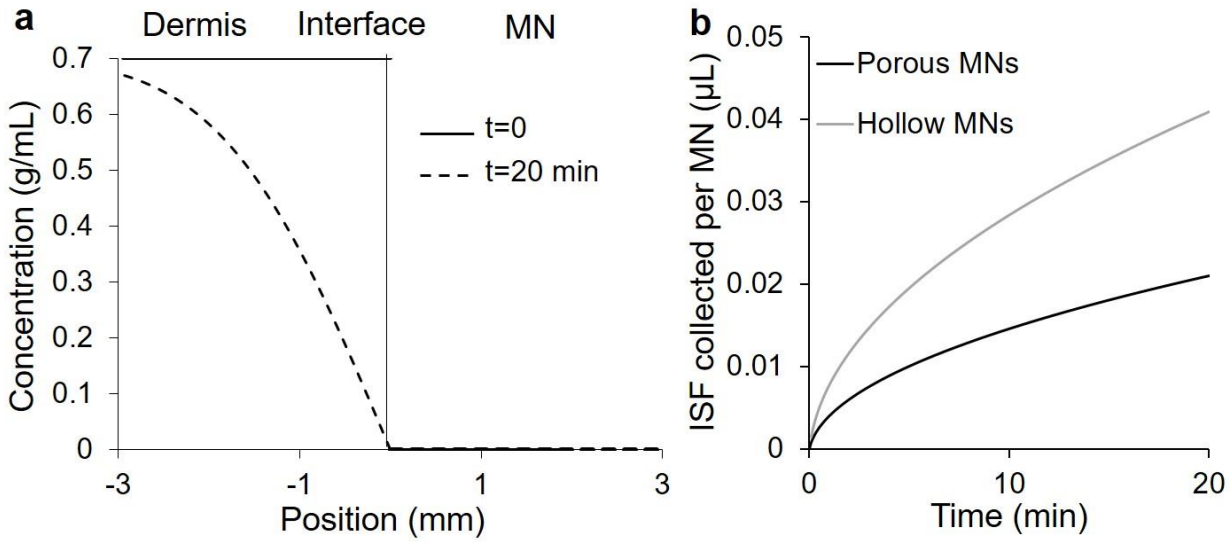

Figure A. 13: Model predictions of ISF collection by capillary flow into porous and hollow microneedles (MNs). (a) Concentration profile of ISF in the dermis and MN at time 0 min (grey line) and 12h (dashed line). (b) ISF volume entering MNs over time for porous and hollow MNs

A.2.4. ISF collection by osmotically driven flow through micropores

Flow of ISF from the dermis towards a micropore filled with an osmolyte is mediated by an osmotic pressure gradient. This pressure gradient is proportional to the concentration gradient of the osmolyte on both sides of the micropore-dermis interface. In our MN system, there is no semipermeable membrane separating the osmolyte from the dermis. Hence, the osmolyte diffuses out of the micropore. We modeled this system by simultaneously solving for diffusion of the osmolyte (maltose) out of the micropore and

osmotically driven convection into the micropore. We assume that within the micropore, mixing is instantaneous and concentration of maltose is uniform.

Maltose diffusing into the dermis can be modelled by Fick's second law

$$\frac{\partial C_M}{\partial t} = D_{mal} \frac{\partial^2 C_{Mal}}{\partial x^2} \quad (11)$$

with the following boundary conditions: $C_{Mal}(x, 0) = 0, C_{Mal}(0, t) = C^{inter}_{Mal\,derm}, C_{Mal}(\infty, t) = 0$ where C_M is concentration of maltose in dermis, $C^{inter}_{Mal\,derm}$ is concentration of maltose in the dermis at the micropore interface, D_{mal} is diffusivity of maltose in dermis (2.6×10^{-10} m^2/s [258]).

Substituting the boundary conditions in the equation we get flow rate into the micropore (6)

$$\dot{Q}^{Diff}_{Mal} = \sqrt{\frac{D_{mal}}{\pi t}} C^{inter}_{Mal\,derm} A \quad (12)$$

where Q^{Diff}_{Mal} is the rate of maltose diffusing out of the micropore, t is time and A is surface area of the micropore (1.3×10^{-7} m^2, based on micropore dimensions of 100 µm base width and 600 µm length). $C^{inter}_{Mal\,derm}$ is related to concentration of maltose in the micropore by a partition coefficient k=0.7 (10). The initial concentration of maltose in the micropore is 400 mg/mL (1.17 M). Osmotic pressure of 1.17 M maltose solution is 2.6 MPa [259]).

Diffusion of maltose out of the micropore and into the dermis creates a concentration gradient of maltose (and therefore an osmotic pressure gradient) across the dermis. This

gradient decreases over time as the maltose continues to diffuse deeper into the dermis (Figure A. 14). This pressure gradient is responsible for osmotic flow of ISF into the micropore. The rate of ISF coming into the micropore by osmosis can be calculated by combining Darcy's Law for flow of ISF in a porous medium (i.e., dermis) [260] with Van't Hoff's equation for relating concentrations to osmotic pressure [261].

$$\dot{Q}_{ISF} = \frac{\kappa}{\mu}\frac{(P^{Osmotic}_{Mal\ at\ interface} - P^{Osmotic}_{Mal\ at\ dermis})}{L}A = \frac{\kappa}{\mu}\frac{(RTC^{inter}_{Mal\ derm} - RTC_{Mal\ derm})}{L}A \qquad (13)$$

where $\dot{Q}_{ISF}$ is flow rate of ISF into the micropore, κ is flow conductivity of ISF in dermis, μ is viscosity of ISF ($\frac{\kappa}{\mu} = 10^{-15}\frac{m^2}{Pa.s}$ [45, 262]), $P^{Osmotic}_{Mal}$ is osmotic pressure of maltose, L is the characteristic length (here the length of dermis required to drop maltose concentration to 1% of wall concentration, $1.82\sqrt{4D_{mal}t}$, as determined by analytical solution for concentration obtained from Ficks second law and fixing the ratio of $C/C^{inter}_{Mal\ derm}$ at 0.01), $C^{inter}_{Mal\ derm}$ is the concentration of maltose at the micropore-dermis interface.

The $C^{inter}_{Mal\ derm}$ and $\dot{Q}_{ISF}$ were computed over time iterations of 1s. The predicted ISF concentration profiles and collection rate are shown in Figure A. 14. The predicted amount of ISF absorbed by each micropore over 20 min is 0.036 µL. The experimental flow rate is 0.021±0.020 µL/ µpore, which is in good agreement. Predicted ISF flow rate decreases over time as more maltose diffuses out of the micropore. The decrease of osmotic pressure over time as the osmolyte diffuses into the dermis limits the pressure gradient and ultimately the flow rate of ISF into the micropore.

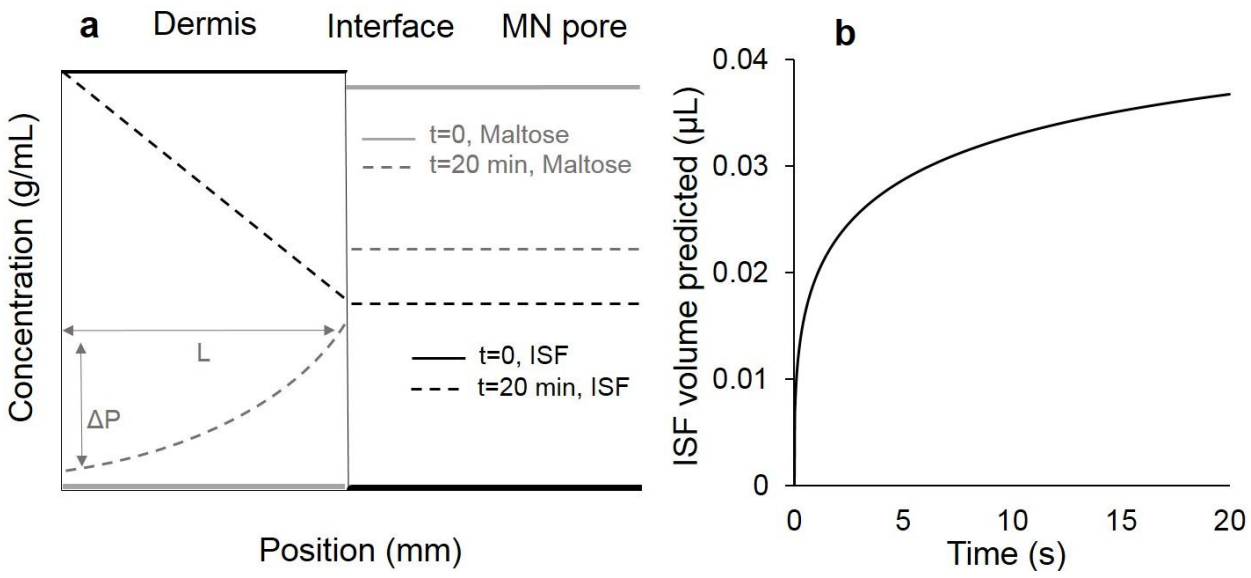

Figure A. 14: Model predictions of ISF collection by osmotically driven flow through micropores. (a) Concentration profile of ISF (black lines) and maltose (gray lines) in the dermis and micropore at time 0 min (solid lines) and 20 min (dashed lines). (b) ISF volume entering a micropore over time.

A.2.5. ISF collection by pressure-driven convection via micropores

Flow under pressure through the dermis can be modelled as flow through a porous medium under pressure by Darcy's law.

$$\dot{Q}_{ISF} = \frac{\kappa}{\mu}\frac{\Delta P}{L}A \qquad (14)$$

where Q_{ISF} is the flow rate of ISF through dermis, κ is the flow conductivity of dermis under pressure, μ is the viscosity of ISF ($\frac{\kappa}{\mu} = 5\times10^{-15}\,\frac{m^2}{Pa.s}$) [262], L is the characteristic length (here thickness of dermis, L=0.0017 m), ΔP is the applied pressure difference (85 kPa for vacuum and 51 kPa for applied pressure), A is surface area of a micropore (3.9 x

10^{-7} m^2, based on micropore dimensions of 200 µm x 100 µm cross-sectional area and 650 µm length). Flow rate of ISF through the micropore can be estimated by the Hagen-Poiseulle equation and is found to be much greater than the flow rate through dermis (calculation not shown). Thus, the rate of ISF collection is limited by the applied pressure drop and the flow conductivity of dermis.

The predicted ISF concentration profiles and collection rates are shown in Figure A. 15. For application of suction, the predicted flow rate for a 10-MN array over 20 min is 0.2 µL, as compared to the experimental value of 0.84±0.60 µL. F or positive pressure application, the predicted flow rate is 0.12 µL, as compared to the experimental flow rate of 0.29±0.20 µL. These predictions are in reasonable agreement with experiments, given the simplified theoretical analysis with no fitted parameters

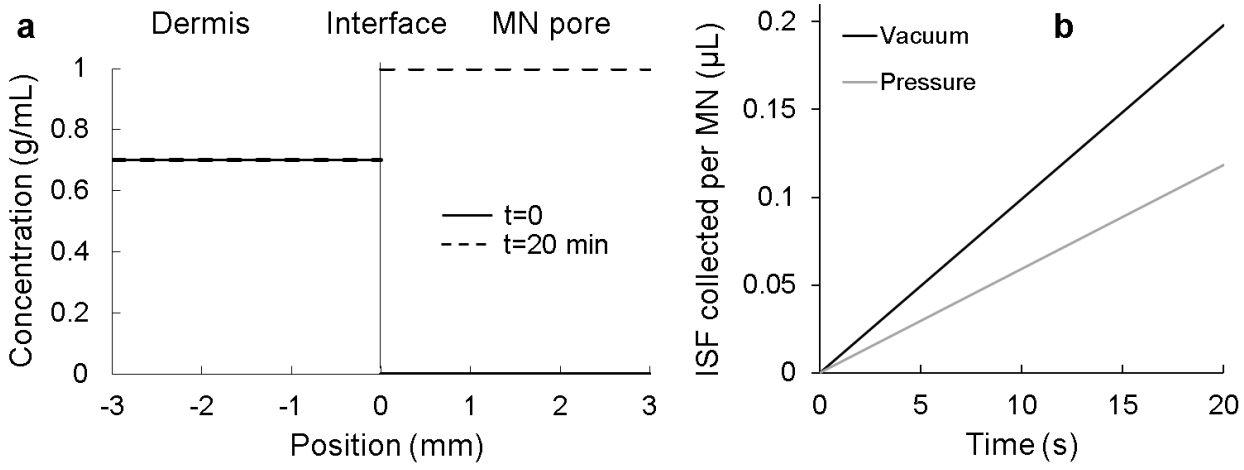

Figure A. 15: Model predictions of ISF collection by pressure-driven convection via micropores. (a) Concentration profile of ISF in the dermis and micropore at time 0 min (solid black line) and 12 h (dashed black line). (b) ISF volume entering micropores over time for vacuum and pressure application.

A.2.6. Correlation between experimental values

The predicted values match the experimentally observed values for volume of ISF collected over 20 min reasonably well, especially given the simplified theoretical analysis with no fitted parameters, and are often within the error bars of the data. The volume of ISF is largest for pressure-driven convection, followed by osmosis, use of capillary flow in hollow or porous MNs and diffusion into hydrogel MNs or micropores.

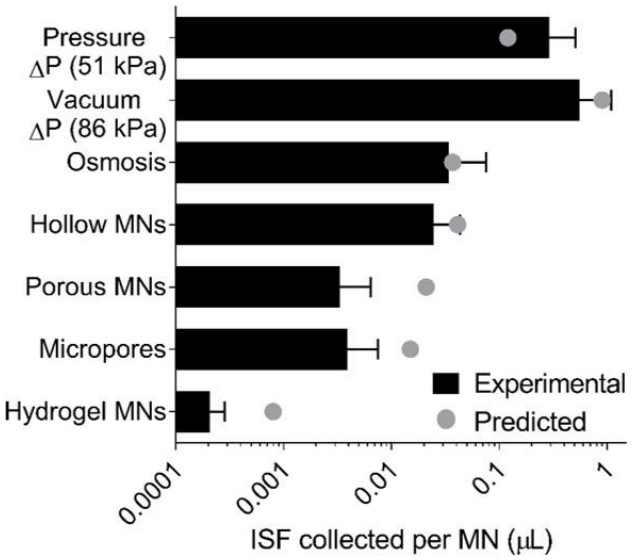

Figure A. 16: Predicted (grey dots) and experimental (black bars) values for ISF volume collected from skin over 20 min for each of the mechanisms discussed. (ISF sampled for hydrogel MNs is interpolated for 20 min.)

A.3. Materials and methods

A.3.1 Microneedle fabrication

Hydrogel microneedles: Hydrogel MNs were prepared by dissolving PVA (31-50 kDa, 99% hydrolyzed, Sigma Aldrich, St. Louis, MO) in water at 95°C to make a 15% (w/v) solution. The solution was cast onto silicone (Sylgard 184, Dow Corning, Midland, MI) molds containing a 10 x 10 array of cavities in the inverse shape of MNs, and vacuum was applied for 30 min to allow the solution to enter the mold cavities, as described previously [263]. The filled molds were kept at 80°C for 3 – 4 h to crosslink the PVA. The molds were then dried overnight at room temperature (20 – 25°C) and humidity (20 – 50 % rh), after which the dried MN arrays were peeled from the molds (Fig. 1a,b). The resulting MNs were 520 µm tall and 220 µm by 220 µm at the base, tapering to a sharp tip. The MNs were arranged in a 10 x 10 array in an area of 0.50 cm^2.

Solid metal microneedles: Stainless steel microneedles were fabricated as five-needle planar arrays (Tech-Etch, Plymouth, MA). Each microneedle was 750 µm tall, with a cross-sectional area of 200 µm by 25 µm (Fig 1d).

Porous microneedles: To make porous MNs, a sheet of filter paper (Whatman #1 chromatography paper, GE Healthcare, Chicago, IL) was adhered to an array of solid metal MNs using double-sided adhesive tape (Hi-Tack Medical Transfer Adhesive 1, 504XL, 4.0 mil, 62# Liner, 3M, St. Paul, MN). With the metal side up, the stainless steel acted as a protective mask during etching with a raster laser beam (Versa Laser VLS 3.50, Universal Laser Systems, Scottsdale, AZ) that cut away any paper not shielded by the metal. The

resulting metal-paper MN array was attached to another metal MN array with adhesive tape, effectively sandwiching the paper between two metal MN arrays. The metal MNs provided mechanical strength, while the filter paper provided the porous medium for collection of ISF (Fig. 2a).

Hollow metal microneedles: To make hollow MNs, hypodermic needles (25, 30 and 33 gauge, Becton Dickinson, Franklin Lakes, NJ) were shortened to ~1.5 mm in length from the luer-lock hub by cutting the needle using a cordless rotary tool (Dremel 800, Robert Bosch Tool Corporation, Mount Prospect, IL), as described previously [264]. The needle was further shortened to ~750 µm in length and the bevel was produced by grinding the shortened needle at a 60° angle against the sanding band attachment of the rotary tool. A constant stream of water was flowed through the needle bore to prevent heat buildup and the metal from melting (Fig 2c).

10-MN arrays: To make solid MNs in 10-MN arrays, two planar arrays of solid metal MNs were aligned with a sheet of filter paper adhered using double-sided tape between their base plates but not between the MNs themselves (Fig. 1d).

Coated metal microneedles: Coated MNs were made by dipping solid metal MNs five times into an aqueous solution of 40% (w/v) maltose (Sigma Aldrich, St. Louis, MO) (Fig 3a) using a process described previously [99].

A.3.2. Measurement of ISF content in skin

Pig ear skin was obtain freshly excised from feeder pigs (generously provided by Hollifield Farms, Conyers, GA) and then frozen at –80°C until use. To measure ISF content in the skin, pieces of skin were pre-weighed (0.10-0.15 g per piece) and lypophilized (Freezone 6 liter freeze dryer, Labconco, Kansas City, MO), as described previously [265]. The weight loss after lyophilization was taken to equal the ISF content in the skin, assuming complete water removal by lyophilization. Use of pig skin in this study was exempt from review by the Georgia Tech Institutional Animal Care and Use Committee.

To measure the amount of ISF that could be removed from the skin under pressure, pre-weighed pieces of pig skin (2.0-2.5 g per piece) were placed on a benchtop over tissue paper (Kim-wipes, Kimberly-Clark, Neenah, WI). A load of 9.1 kg was placed on the skin, which applied a pressure of ~220 kPa over the ~4 cm^2 of skin surface area. The weight loss of the skin was measured periodically for 20 min.

A.3.3. Measurement of ISF collection from skin during microneedle-based protocols

Skin preparation: Pig ear skin was sandwiched in a Franz diffusion cell between the donor and receiver chambers using a clamp (PermeGear, Hellertown, PA). The system was sealed using Parafilm (Bemis Company, Neenah, WI). The receiver chamber was filled with a 1 mg/mL solution of sodium fluorescein (Sigma-Aldrich) in phosphate-buffered saline. The setup was kept overnight at 37°C to equilibrate the skin with the fluorescein solution. The skin was then used for testing of ISF collection during MN-based protocols. To verify that the concentration of fluorescein in ISF was 1 mg/mL, a sample of ISF after pig skin

equilibration was taken by removing the epidermis and micropipetting out ISF from the dermis. Fluorescein concentration in this ISF was 1.1 ± 0.4 mg/mL.

ISF collection using hydrogel microneedles: Hydrogel MN arrays were inserted into porcine skin on a benchtop by pressing the MNs into the skin using the back of the thumb. The MN arrays were secured to the skin using adhesive tape (3M, St. Paul, MN). The skin with the MN patch was again sandwiched in Franz cells as described above, and left in place for 12 h at 37^0C to allow the MNs to extract ISF.

ISF collection using capillary action: Three methods were used. 1) The porous MN arrays were inserted into pig skin on a benchtop, and left in skin for 20 min to allow MNs to absorb surrounding ISF. The MNs were then removed and the two stainless steel layers were separated to expose the paper. 2) To make micropores in skin, a 10-MN patch was inserted into pig skin and removed immediately to create an 2x5 array of 10 micropores. The skin was left for 20 min to allow the micropores to absorb surrounding ISF. Fluid on the skin was wiped off using a tissue-paper wipe (Kim-wipe, Kimberly Clark, Neenah, WI). 3) The hollow MNs were attached to a 3mL syringe and inserted into pig skin. The MNs were left in place for 20 min, after which the MNs were removed and ISF inside the hollow MNs was collected for further analysis.

ISF collection enhanced by osmosis: Two methods were used. 1) The coated MN patch was inserted into pig skin and left in skin for 5 min to allow the maltose to dissolve off the MNs in the skin. The patch was removed to create 10 micropores in the skin filled with concentrated maltose solution. After 20 min, the fluid on the skin surface was collected

with a tissue-paper wipe. 2) To fill micropores with osmolyte solution, the plain/coated stainless steel MNs were inserted into skin to create micropores. 10 µL of maltose solution was pipetted on the skin site. The system was left for 20 min to allow the micropores to take up ISF. Fluid on the skin surface was collected with tissue-paper wipes.

ISF collection by pressure-driven convection through micropores: For suction, a 10-MN array was inserted into skin and removed immediately to create micropores. The micropores were covered with paper: tissue-paper wipes (Kim-wipes), gauze pads (Johnson and Johnson, New Brunswick, NJ) or plasma treated gauze pads (Plasma Cleaner PDC-32G, Harrick Plasma, Ithaca, NY). A suction cup attached to a vacuum pump (Laboport Series N840.1.2FTP Pump, KNF Neuberger, Trenton, NJ) was placed over the micropores, and suction was applied for the desired amount of time. After stopping the vacuum pump, the MN pore covering was removed and soaked in 1 mL of DI water for 24 h to elute out the ISF contents. To make a curvature on the skin surface, a curved disc (Skittles, Wrigley Company, Chicago, IL) was placed beneath the skin and the skin was secured to a wooden board under mild tension. To stretch out the skin, the ends of the skin piece were stretched out by hand and secured to a wooden board.

For MNs utilizing pressure, a 10-MN patch was inserted into pig skin and removed immediately to make micropores. The skin piece was folded in half with the pores at the apex, and placed horizontally on the benchtop (Figure A. 8b in Appendix A). The micropores were covered with a tissue-paper wipe to absorb the ISF that eluted out. Pressure was applied using different cast-iron weights (Body Solid, Forest Park, IL) to apply the desired load. Applied force was measured by a tactile pressure sensor (Flexiforce

10N, Tekscan, South Boston, MA). The load was kept for the desired amount of time. After the load was taken off, the ISF absorbed by the issue-paper wipe was collected.

Quantification of ISF volume extracted ex vivo: To elute out all the ISF components absorbed using MN patches, the MNs or the tissue paper or gauze used to collect the ISF was soaked in DI water for 24 h. The concentration of fluorescein in the samples was measured against a standard calibration curve of fluorescein on a standard 96 well plate (Costar Black Polypropylene, Corning, Corning, NY). The plates were analyzed in a plate reader (Synergy MX, BioTek Instruments, Winooski, VT) at an emission wavelength of 525 nm and absorption wavelength of 590 nm. The amount of ISF absorbed was calculated based on the detected concentration in the unknown samples and the known fluorescein concentration in skin at 1mg/mL.

Collection of ISF from skin of human volunteers: ISF was collected from selected skin sites of 6 human volunteers. The cohort consisted of 5 males aged 24 ± 2 years and 3 females aged 26 ± 1 years. Before MN application, the site was disinfected using an antiseptic solution (Hibiclens Antiseptic Skin Cleanser, Mölnlycke Health Care US, Norcross Georgia) and alcohol swabs (Becton Dickinson), and then marked using a pen and template. Solid metal MNs were terminally sterilized using ethylene oxide treatment and inserted into the skin at the marked sites and then removed within 30 s. To avoid possible contamination of ISF with blood, capillaries damaged by MNs were allowed to repair for ≤ 20 min after MN insertion. Suction was applied at –34-68 kPa to the skin site (NP-2, NPCSS, Electronic Diversities, Finksburg, MD) for 20 min to withdraw ISF from the skin [247, 248]. After removing the suction device, ISF on the skin surface was collected using

sterile gauze pads (Johnson and Johnson), which were then soaked in 0.5 mL DI water to elute out the contents absorbed by the gauze. All human volunteers provided informed consent. This study was approved by the Georgia Tech Institutional Review Board.

Determination of ISF volume and biomarkers collected from skin in vivo: The ISF volume collected was measured by determining the sodium ion concentration in the collected fluid. Sodium ion concentration was determined using a sodium ion sensitive electrode (perfectION comb NA, Mettler Toledo, Columbus, OH). The sodium ion content in the samples was normalized against a standard sodium ion concentration in ISF of 135 mmol/L [48]. This technique has been used in the past to calibrate analyte levels for an individual when variable volumes of body fluid are sampled [89]. The amount of glucose in the sample was measured using a glucose assay (Amplex® Red Glucose Assay Kit, Thermo Fisher Scientific, Waltham, MA) and divided by the volume of ISF collected to obtain concentration. The total protein content was detected using a micro BCA assay (Micro BCA Protein Assay Kit, Thermo Fisher Scientific) and divided by the volume of ISF collected to obtain concentration.

A.3.4 Statistics

Statistical analysis was performed using Graphpad Prism 7 software (Graphpad Software, La Jolla, CA). Statistical significance was assessed using t-tests. P-value<0.05 was taken to be statistically significant.

APPENDIX B

SUPPORTING INFORMATION FOR CHAPTER 5.

B.1. Supplementary methods

B.1.1. Obtaining plasma and ISF samples

The study was conducted using 10 healthy human volunteers and was approved by the Institutional Review Board (IRB) at the Georgia Institute of Technology. Written informed consent was obtained from all volunteers. The cohort consisted of 7 males aged 24 ± 6 years and 3 females aged 27 ± 7 years. Blood samples were taken from the forearm by venipuncture. The blood samples were collected into K3 EDTA tubes (Vacutainer Blood Collection Tube, Becton Dickinson, Franklin Lakes, NJ) and spun down at 9,000 rpf for 15 min (5702 RH centrifuge, Eppendorf, Hamburg, Germany) to separate the plasma. Plasma was collected in LoBind Protein tubes (Eppendorf) and stored at -80°C.

Skin suction blister fluid was collected from suction blisters generated on the thigh by the method developed by Kiistala.[73] The skin was first disinfected with alcohol wipes and then suction was applied using a NP-2 Negative Pressure Cutaneous Suction System (Electronic Divestities, Ridge Road, Finksburg, MD). The sterile orifice plates with 5 circular holes (8 mm diameter each) along with the suction cup was firmly attached to the skin using straps. Suction at 50 – 70 kPa below atmospheric pressure was applied at a temperature of 40°C for ~45 min until blister formation was complete. Fluid from intact

and hemoglobin-free blisters was collected using a Micro-Fine syringe (Becton Dickinson). The fluid was stored in LoBind Proetin tubes (Eppendorf) at -80˚C.

B 1.2. High-resolution metabolomics

Plasma and ISF samples were prepared for HRM analysis using established methods.[185, 266, 267] Because only 15 μL of ISF was available for HRM, all ISF samples were diluted to 50 μL using LC-MS grade water prior to sample preparation. Stored aliquots were first thawed on ice, and then 50 μL of biofluid (plasma or diluted ISF) was added to 100 μL of acetonitrile containing a mixture of stable isotopic standards, vortexed and allowed to equilibrate for 30 min. Proteins were precipitated by centrifuge (16.1 × *g* at 4°C for 10 min), and extracts were stored in a refrigerated autosampler until analysis (<24 h). Triplicate 10 μL aliquots were analyzed using reverse-phase C_{18} liquid chromatography (Ultimate 3000, Dionex, Sunnyvale, CA) and Fourier transform mass spectrometry (Q Exactive, Thermo Scientific, Waltham, MA) operated in positive electrospray ionization mode, resolution (FWHM) of 70,000 and mass-to-charge (*m/z*) range of 85-1,250[268, 269]. All samples were analyzed in one batch, with a pooled plasma quality control reference sample included at the beginning and end of the run. Raw data files were extracted and processed (e.g., peak picking and retention time alignment) using apLCMS[225] with modifications by xMSanalyzer,[226] with each unique mass-to-charge (*m/z*) feature defined by *m/z*, retention time and ion abundance.

B1.3. Statistical analysis

Statistical analyses were conducted using the metabolite "feature table," a spreadsheet produced after data extraction and alignment. The feature table contains information on all *m/z* features, with the first and second columns containing feature *m/z* values and retention times, respectively, and subsequent columns containing the metabolite intensities in the study samples. The "presence" or "absence" of a metabolite feature in a sample was defined by its "missingness" in the feature table (i.e., value of 0), which reflects whether the feature was detected or not detected, respectively.

Metabolite features that were elevated in ISF compared to plasma were identified using a paired fold change analysis. This was assessed on the raw dataset by first replacing missing values with one-half the minimum value for each feature, then calculating the $\log_2$-fold changes (ISF/plasma) within each pair for each feature; here, features with $\log_2$-paired fold changes > 1.0 (equivalent to raw fold changes > 2.0) in at least 8 of 10 sample pairs were considered significant and selected for further characterization.

Correlations of *m/z* feature intensities between plasma and ISF samples were assessed on the raw dataset using Spearman rank-order correlation coefficients. The *m/z* features that were strongly correlated between plasma and ISF (Spearman rho > 0.7, $p < 0.10$) and were present in at least 4 out of 10 sample pairs were selected for further characterization by manual annotation.

B1.4. Metabolite feature identification

B1.4.1. Dataset-wide annotation

Initial annotation of metabolites present in ISF and plasma (**Tables S1** and S**2**) was completed using a data-driven approach that combined Kyoto Encyclopedia of Genes and Genomes (KEGG)[187] database matching (± 5 ppm) with a custom dataset-wide deconvolution and identification algorithm; metabolites with two or more associated adducts/isotopes (adduct groups) were selected for further characterization. Matches were curated to remove unlikely peak groupings and/or biologically-implausible compounds so that each adduct group was matched uniquely to a single chemical compound. Metabolites were also identified by comparing features to an in-house library of metabolites from authentic reference standards run under identical assay conditions;[249] study features were matched to reference standard metabolites using an accurate mass threshold of 5 ppm and retention time threshold of 30 s.

B1.4.2. Manual annotation

We used a manual annotation scheme to annotate features from the fold change and correlation analyses. To accurately identify features elevated in a biofluid, we used a custom grouping algorithm to attempt to assign features to adduct groups by parent monoisotopic mass, and we removed all features that were not the most intense peaks (i.e., 'base peaks') within their adduct groups. For strongly-correlated features identified in the correlation analysis, we also used the grouping algorithm to assign these features to adduct groups. If multiple features from the same metabolite were found among the list of strongly-correlated features, the feature with the strongest correlation was retained for further characterization. Manual compound matching was then conducted in the Human Metabolomics Database (HMDB)[270] (± 5 ppm) using the adduct type for each feature

(if the feature was successfully assigned to an adduct group) or $[M+H]^+$, $[M+Na]^+$, and $[M+K]^+$ (if the feature was not assigned to an adduct group).

Final curated annotation tables reflect metabolite features with a unique database match, or when multiple matches were found, the most biologically-likely match. Putative annotations were assigned confidence scores (1-4, where 4 is highest): an annotation with a score of 4 reflects that the metabolite feature was successfully assigned to a metabolite cluster and the monoisotopic mass had a unique compound match in HMDB; score of 3, the feature was assigned to a metabolite cluster, but the annotation was selected as the most biologically- plausible match from ≥ 2 possible compounds; score of 2, the feature was not assigned to a cluster, but the feature had a unique compound match for $[M+H]^+$, $[M+Na]^+$, and $[M+K]^+$; and score of 1, the feature was not assigned to a cluster and the annotation was selected from multiple compound matches for $[M+H]^+$, $[M+Na]^+$, and $[M+K]^+$. Compounds were assigned to categories based on biological knowledge of metabolite structures and/or functions.

B1.5. Network and pathway analysis

Biological functions of metabolites correlated between plasma and ISF were characterized by Mummichog,[271] which unifies network and pathway analysis to predict metabolite identities and functional metabolic changes in untargeted metabolomic datasets. Briefly, the Spearman correlation results were entered into Mummichog, with the requirement that the $[M+H]^+$ ion was present for a predicted compound. The resulting metabolic activity network, as presented in Figure B. 1,

represents the high-confidence metabolites identified from a combined network module analysis and pathway analysis; subnetworks in the activity network with ≤ 3 nodes were omitted from the figure. All metabolic pathways significant at an adjusted $p < 0.01$ were included in Figure B. 1. To assess the biological roles of the metabolites identified in the network modules, all KEGG IDs from significant modules were searched in the KEGG BRITE database[187] to find common biological functions.

B1.6. Metabolite set enrichment analysis

Metabolite set enrichment analysis (MSEA) was conducted in MetaboAnalyst 3.0.[272] Briefly, MSEA works by comparing a list of compounds from a study against a collection of defined metabolite sets (i.e., covering metabolic pathways, disease states), and "overrepresented" metabolite sets within the study metabolite list are identified.[273] In the current study, lists of curated, putatively-identified compounds (by HMDB ID) were used for MSEA; overrepresented pathways were assessed using the pathway-associated metabolite set library (88 metabolite sets); metabolite sets consisting of < 3 metabolites were excluded from the analysis.

Table B. 1: Metabolites detected in ISF.

Category	Compound	Identification[4]	Detected, plasma	Detected, ISF
Clinical/health indicators	Cholesterol	RS	10	10
	Creatinine	DD/RS	10	10
	Glucose	DD/RS	10	10
	Urea	DD	10	10
Amino acid metabolism	Alanine	DD/RS	10	10
	Arginine	DD/RS	10	10
	Asparagine	DD/RS	10	10
	Aspartate	DD	7	9
	Aspartate 4-semialdehyde	DD	10	10
	Betaine	DD	10	10
	Cucurbitine	DD	10	10
	Citrulline	DD/RS	10	10
	Glutamate	DD/RS	10	10
	Glutamine	DD/RS	10	10
	Histidine	DD/RS	10	10
	Kynurenine	RS	10	9
	(Iso)leucine	DD/RS	10	10

[4] DD: data-driven annotation by accurate mass; RS: matched to *m/z* and retention time of reference standard

Table B.1 continued

	Lysine	DD/RS	10	10
	Methionine	DD/RS	10	10
	Ornithine	DD	10	10
	Oxoproline	RS	10	10
	Phenylalanine	DD/RS	10	10
	Pipecolate	DD	9	10
	Proline	DD/RS	10	10
	Serine	DD/RS	10	10
	Threonine	RS	10	10
	Tryptophan	DD/RS	10	10
	Tyrosine	DD/RS	10	10
	Valine	DD	10	10
Lipids	2-Aminoethylphosphocholate	DD	10	10
	3-Dehydroteasterone	DD	10	10
	3-Oxododecanoic acid	DD	10	10
	Dodecanamide	DD	10	9
	Glycodeoxycholate	DD	10	4
	Lauric acid	RS	3	7
	Linolenic acid	RS	4	1
	LysoPC(16:1)	RS	10	10
	LysoPC(18:0)	RS	7	10
	LysoPC(20:3)	RS	10	10

Table B.1 continued

	PC(34:2)	RS	10	10
	PC(36:2)	RS	10	10
	PC(36:3)	RS	10	10
	PC(36:4)	RS	10	10
	PC(38:4)	RS	10	10
	Prostaglandin G2	DD	8	3
	sn-glycero-3-Phosphocholine	RS	10	10
Arginine/proline metabolism	4-Aminobutanoate	DD	10	10
	5-Amino-2-oxopentanoic acid	DD	10	10
	Creatine	DD/RS	9	10
Carnitine metabolism	Acetylcarnitine	RS	10	10
	Crotonobetaine	DD	10	10
	Octanoylcarnitine	DD	10	7
	O-Decanoyl-L-carnitine	DD	10	7
	Palmitoylcarnitine	DD/RS	10	2
Histidine metabolism	Histamine	DD	10	10
	Methylhistamine	DD	10	10
	N-Acetylhistamine	DD	10	10
	Urocanic acid	DD	0	10

Table B.1 continued

Linoleic acid metabolism	13(S)-HPODE	DD	10	7
	9(10)-EpOME	DD	10	10
	Linoleic acid	DD	10	9
Pyrimidine metabolism	5,6-Dihydrothymine	DD	10	10
	5,6-Dihydrouracil	DD	10	10
	5-Methylcytosine	DD	10	10
	Thymine	DD	10	10
Purine metabolism	Deoxyadenosine	DD	5	9
	Hypoxanthine	DD/RS	10	10
	Uric acid	DD/RS	10	10
	Xanthine	RS	10	3
Sphingosine metabolism	Ethanolamine phosphate	DD	1	8
	Sphingosine	DD/RS	10	6
Other endogenous	2,5-Dichloro-4-oxohex-2-enedioate	DD	10	10
	Butanoylphosphate	DD	10	9
	Calcium L-aspartate	DD	10	1
	Formyl phosphate	DD	9	4
	Fructose	DD	10	7
	Indole	DD	10	10

	Harmalol	DD	10	9
	Hydantoin	DD	10	10
	Lenticin	DD	9	7
	N1,N12-Diacetylspermine	DD	10	6
	Taurine	DD	10	10
	Tetrahydropteridine	DD	10	10
	Toxopyrimidine	DD	10	10
	Trimethylamine N-oxide	DD	10	10
	Tryptophol	DD	9	7
Pesticides	2-Hydroxybiphenyl	DD	10	3
	alpha-Naphthylthiourea	DD	10	7
	Athidathion	DD	10	10
	Bis(4-chlorophenyl)methane	DD	9	7
	Carbendazim	DD/RS	6	7
	Chlorthiophos	DD	10	10
	Demeton-S-methyl	DD	10	2
	Diisopropyl phosphate	DD	10	10
	Fenuron-TCA	DD	10	10
	Fosamine	DD	8	10
	Metaldehyde	DD	10	7
	Methamidophos	DD/RS	10	3
	Prohydrojasmon	DD	10	10
	Sesamex	DD	10	8

Aromatic compounds	1-Methylnaphthalene	DD	10	7
	Benzoic acid	RS	10	1
	4-Fluorocyclohexadiene-cis,cis-1,2-diol	DD	10	7
Carcinogens	2-Naphthylamine	DD	10	10
	N-Nitrosodiethylamine	DD	10	10
	3-Chloro-4-(dichloromethyl)-5-hydroxy-2(5H)-furanone (Mutagen X)	DD	10	10
Phytochemicals	Lophophorine	DD	10	9
	Otonecine	DD	10	10
	Piperidine	DD	10	10
	Piperine	DD	10	4
	trans-Cinnamate	DD	10	10
Other exogenous	2,2-Dimethyl-3-4-(acetyloxy)phenyl-4-ethyl-2H-1-benzopyran-7-ol acetate	DD	6	1
	2,5,6-Tribromo-1-methylgramine	DD	2	10
	7-Hydroxymethyl-1,2-methylbenzaanthracene sulfate	DD	10	8
	Botrydial	DD	10	4
	Dibromobisphenol A	DD	10	8
	Dodecanedioic acid	DD	10	9

	N-Cyclohexylformamide	DD	1	10
	N-Ethylammelide	DD	10	9
	Octachlorostyrene	DD	10	9
	Rhododendrin	DD	10	8
	Triethanolamine	DD	0	10
	Tritriacontane	DD	0	9

Table B. 2: Metabolites not detected in ISF.

Category	Putative compound	Identification[5]	Detected, plasma	Detected, ISF
Exogenous chemicals	2-Amino-5-chloromuconate 6-semialdehyde	DD	10	0
	Aflatrem	DD	9	0
	Ammelide	DD	10	0
	Bisphenol A bis(chloroformate)	DD	10	0
	Malathion	DD/RS	10	0
	Nabam	DD	9	0
	Triadimefon	DD/RS	10	0
	Trp-P-1	DD	10	0
	Tuliposide B	DD	10	0

[5] DD: data-driven annotation by accurate mass; RS: matched to *m/z* and retention time of reference standard

Table B.2 continued

Lipids	alpha-D-Galactosyl-diphosphoundecaprenol	DD	9	0
	3-Oxooctanoyl-CoA	DD	8	0
Porphyrin metabolism	5-Aminolevulinate	DD	10	0
	Hydroxymethylbilane	DD	8	0
Plasma collection artifacts	EDTA	DD	10	0
	Iodine	DD	10	0
	Iodoform	DD	10	0
Other endogenous	4,8-Dihydroxyquinoline	DD	10	0
	alpha-Ketoglutaramate	DD	9	0
	Inosine 5-diphosphate	DD	9	0

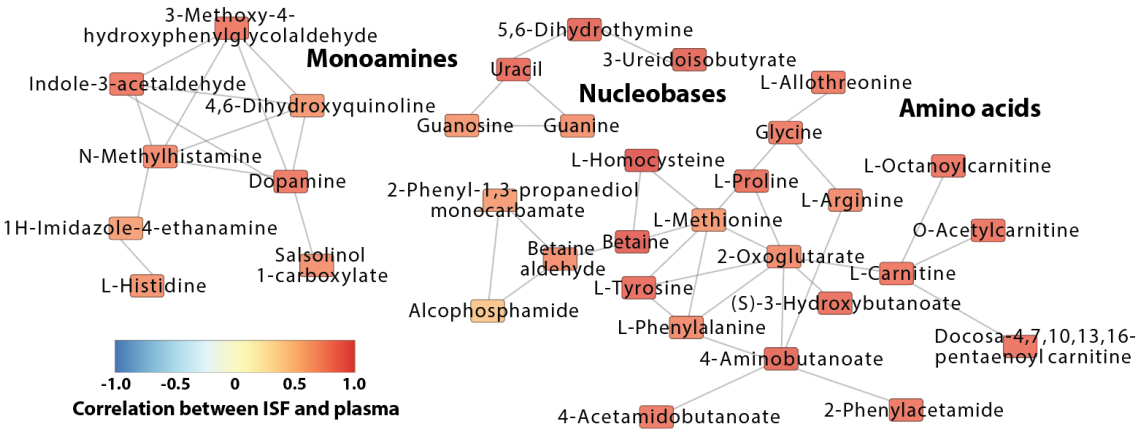

Figure B. 1:Mummichog activity network for metabolites correlated between ISF and plasma.

Activity network displays biologically-connected metabolites matched to significant features with high confidence, with the strength of correlation between ISF and plasma for each metabolite denoted by the color scale. For clarity, only subnetworks with ≥ 4 metabolites are displayed.

APPENDIX C

SUPPORTING INFORMATION FOR CHAPTER 6

C.1. Microneedle insertion and vacuum application to skin

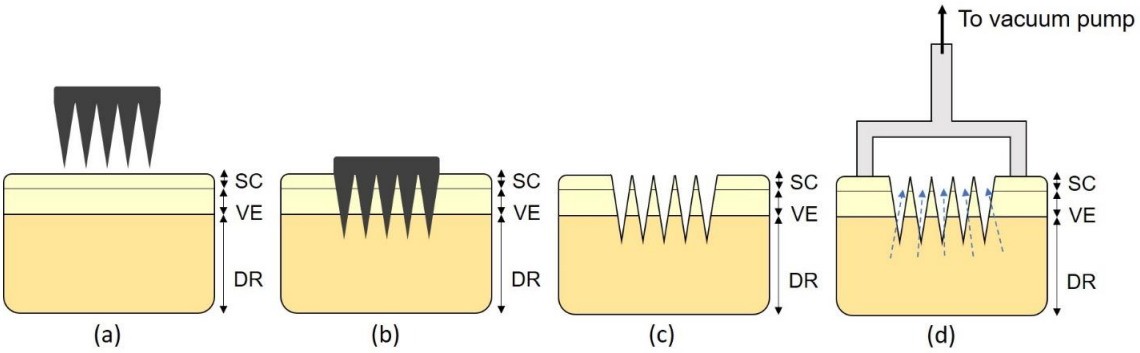

Figure C. 1: Schematic of microneedle (MN) insertion and vacuum application to skin: (a) Stainless steel MN patch ready for insertion into skin comprising SC-stratum corneum, VE-viable epidermis, DR-dermis. (b) MN patch inserted into skin across epidermis and into superficial dermis. (c) Micropores created in skin after MN removal. (d) Vacuum applied over the micropores draws ISF to the skin surface (dashed blue arrows).

C.2. Optimization of ISF sampling method

ISF sampling method was optimized to enable reliable collection of ISF that minimized contamination with blood, the objective was to develop a method that reliably and reproducibly samples 1-10 µL of pure ISF from skin within 20 min. To achieve this outcome, key design parameters such as MN length, vacuum pressure, and timing of vacuum application were varied and optimized in a small study in five human participants.

Blood vessels may break due to contact with MNs and/or applied vacuum, which can lead to blood contaminating the ISF. Since blood vessels are present to a greater extent deeper in dermis [71], more shallow depth of MN insertion and weaker vacuum should reduce bleeding. We found that insertion of MN of three different lengths (250 µm, 450 µm and 650 µm) followed immediately by application of vacuum at -34 kPa or -50 kPa (gauge) resulted in bleeding onto the skin surface (Fig. S.2). Vacuum at -17 kPa (gauge) also led to bleeding when preceded by treatment with 650 µm long MNs, but the chances of bleeding decreased at shorter MN lengths, although 40% of participants still bleed when using 250 µm MNs (Fig S.2.) We did not reduce MN length below 250 µm because insertion of shorter MNs into skin is unreliable because of skin elasticity during insertion [274].

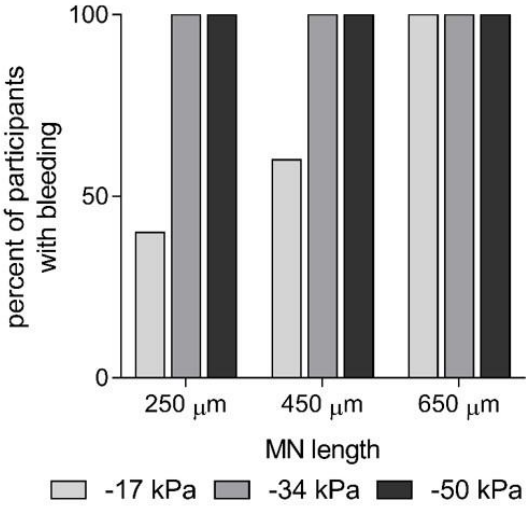

Figure C. 2: Effect of microneedle (MN) length and vacuum pressure on bleeding from the skin of 5 human participants.

We found that ISF collection varied dramatically among individual micropores in an array that all received the same MN and vacuum treatment. In general, the large majority of micropores remained dry. For example, after treatment with 250 µm-long MN and -17 kPa (gauge) vacuum, typically 5-10 micropores produced small droplets of blood and 5-20 micropores produced clear ISF among the 100 micropores in the array (data not shown). This resulted in 3.7±3.4 µL of blood and 1.5±2.7 µL of ISF being collected (Fig S.2). The heterogeneity of micropores with blood is probably due to the small odds of a given MN hitting a capillary to cause highly localized bleeding at the site of the micropore. The cause of heterogeneity of micropores producing ISF is less clear.

As a further attempt to eliminate bleeding, we delayed the onset of vacuum application in order to let broken capillaries reseal through the process of blood coagulation that starts within a few seconds [275]. Delaying application of vacuum at -50 kPa (gauge) for up to 10 min had no effect on bleeding; 7-8 µL of blood came out with little or no ISF (Fig S.3a). We finally tried to slowly increase the vacuum from 0 kPa to -50 kPa (gauge) over the course of ~3 min. This reduced the amount of bleeding to almost zero and allowed us to collect 2.3±2.6 µL of ISF based on experiments repeated three times on every participant (i.e., n=15 replicates).

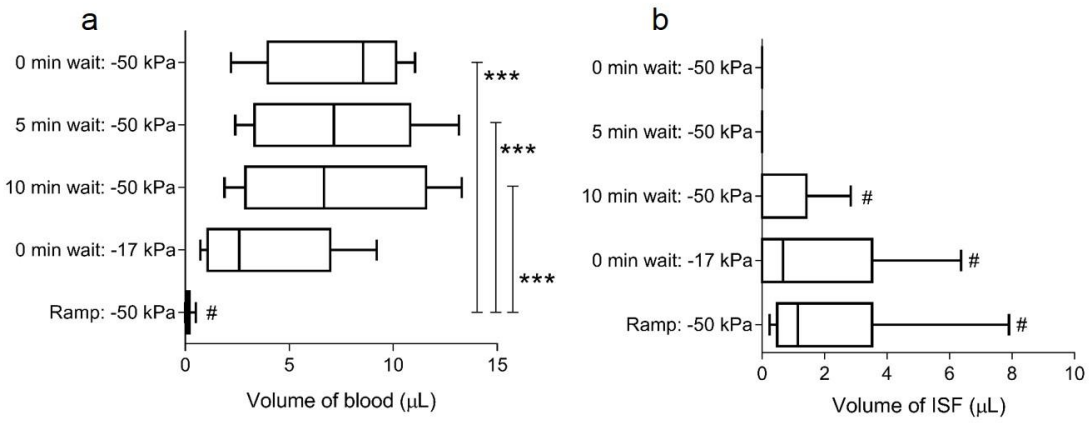

Figure C. 3: Effect of timing of vacuum application on bleeding and ISF sampling from the skin of 5 human participants. (a) Volume of blood collected from skin within 15 s and (b) volume of ISF collected after vacuum application at -17 or -50 kPa (gauge) either 0, 5 or 10 min after MN patch treatment. # indicates blood was collected over 20 min (not just 15 s). MN patches comprised 250 µm long MNs that were used to generate 100 micropores. Box plots show 5th, 25th, 50th, 75th and 95th percentiles (n = 5 replicates)

C.3. Detection of biomarkers in interstitial fluid, suction blister fluid and plasma

Analysis of ISF from MN treatment, SBF from suction blisters and plasma from venipuncture from a cohort of 20 participants using high-resolution metabolomics using liquid chromatography-mass spectrometry (LC-MS) detected 10,338 features with hydrophilic interaction chromatography (HILIC), which better detects lipophilic compounds and 7,703 features with reverse-phase C18 chromatography, which better detects polar compounds. Among features found in HILIC and C18, 63% and 50% were respectively common to all three body fluids; 79% and 60% were respectively common to plasma and ISF, suggesting that these metabolite measurements in ISF may be a surrogate for plasma; and 1% and 14% were respectively unique to ISF, suggesting that these

biomarkers can be uniquely assayed in ISF (Fig. 3). Comparing the 10,208 and 7,255 features found respectively in ISF or SBF, only 72% and 64% were respectively common to both fluids, which demonstrates that ISF and SBF are not identical fluids, probably because of their different methods of sampling.

To better interpret differences between ISF and SBF, a swab was wiped across intact skin and analyzed for biomarkers. Because ISF was collected from the skin surface, it may contain more epidermal and skin surface biomarkers than SBF. Consistent with this expectation, among 1,740 and 1,880 features detected in ISF and absent from SBF by HILIC and C18, respectively, 58% and 79% were respectively found in the skin wipe. Among 1,102 and 732 features detected in SBF and absent from ISF, respectively, 65% and 36% were respectively found in the skin wipe (Fig S.4). However, it should also be noted that 70% and 46% of features detected in skin swabs were respectively also found in plasma (Fig S.5), indicating that biomarkers found on the skin surface are not necessarily contaminants.

Table C. 1: Demographics of 21 participants in ISF, SBF, and plasma metabolomics study

Age (years)	
Mean (SD)	28.4 (7.1)
Median (IQR)	26 (24-31)
Sex	
Male (%)	10 (48%)
Female (%)	11 (52%)
Ethnic origin[†]	
White (%)	9.5 (45%)
Black (%)	4.5 (21%)
Asian (%)	7 (33%)
BMI (kg/m^2)[§]	
Mean (SD)	23.1 (3.4)
Median (IQR)	22.4 (20.4-25.6)

[†]Ethnic origin was self-reported, participants were allowed to select multiple options (for subjects that chose multiple ethnicities, the calculated fraction was assigned to each ethnicity); [§]Height and weight were self-reported; SD = standard deviation; IQR = interquartile range.

Table C. 2: Demographics of 20 participants in ISF, SBF, and plasma metabolomics study

Age (years)	
Mean (SD)	28.4 (7.3)
Median (IQR)	26 (23-31)
Sex	
Male (%)	10 (50%)
Female (%)	10 (50%)
Ethnic origin[†]	
White (%)	9.5 (47.5%)
Black (%)	3.5 (17.5%)
Asian (%)	7 (35%)
BMI (kg/m^2)[§]	
Mean (SD)	23.1 (3.5)
Median (IQR)	22.3 (20.2-25.6)

[†]Ethnic origin was self-reported, participants were allowed to select multiple options; [§]Height and weight were self-reported; SD = standard deviation; IQR = interquartile range.

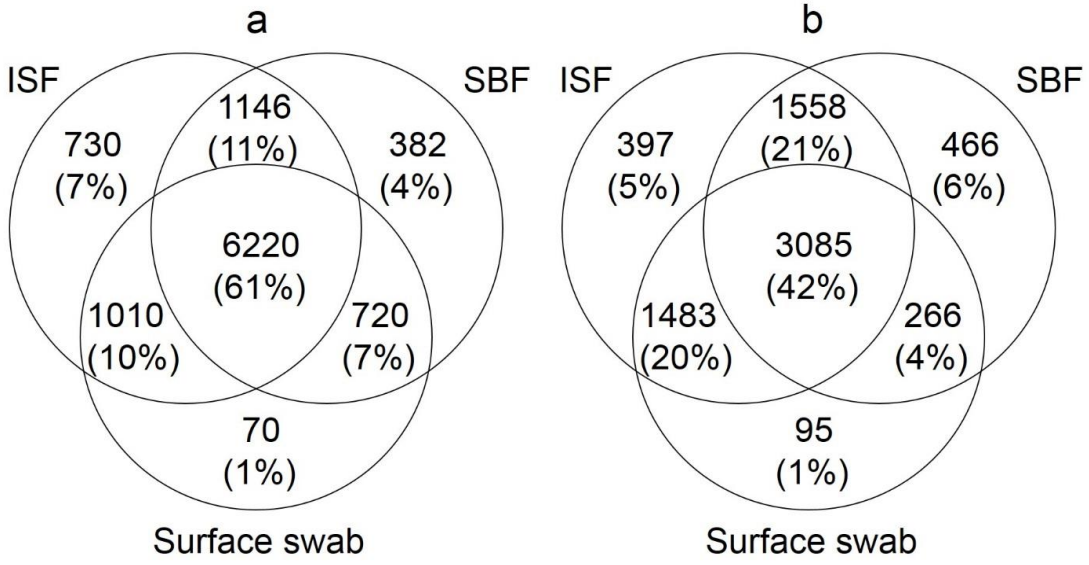

Figure C. 4: Venn diagram showing overlap of features in ISF from MN treatment, suction blister fluid and surface swab. Samples were analyzed using (a) hydrophilic interaction chromatography (HILIC) and (b) reverse-phase C18 liquid chromatography. Features (i.e., ion peaks) were first screened for detection in ≥ 10 of 20 subjects in at least one sample type. After filtering, a total of 10,316 features were detected. After filtering, a feature was considered "present" in a fluid if the feature was detected in that fluid in greater than 10% of samples (≥ 3 of 20 samples). Figure not to scale.

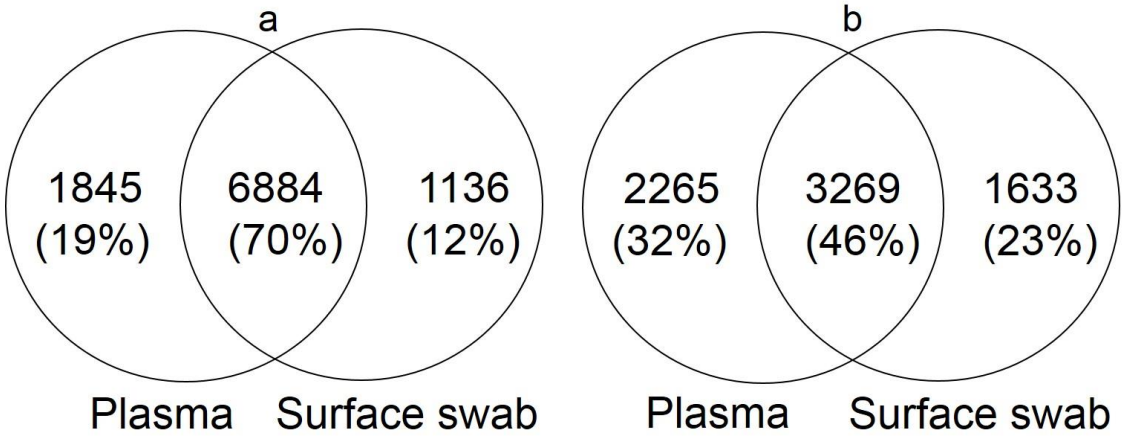

Figure C. 5: Venn diagram showing overlap of features in plasma and surface swab. Samples were analyzed using (a) hydrophilic interaction chromatography (HILIC) and (b) reverse-phase C18 liquid chromatography. After filtering, a feature was

considered "present" in a fluid if the feature was detected in that fluid in greater than 10% of samples (≥ 3 of 20 samples). Figure not to scale.

Table C. 3: Prevalence of selected clinically relevant biomarkers in ISF, SBF and plasma in matched samples from 20 human participants.

Biomarker	**Prevalence of biomarker**[†]		
	Plasma	ISF	SBF
Amino Acid Metabolites			
5-Hydroxy-l-trytophan	45%	60%	15%
Hippurate	85%	85%	90%
Kynurenine	90%	80%	95%
Methionine sulfoxide	100%	100%	100%
Methyl-histidine	80%	25%	55%
Oxoproline	100%	100%	100%
Amino Acids			
Alanine	100%	100%	100%
Arginine	100%	100%	100%
Aspartic acid	100%	100%	100%
Citrulline	100%	100%	100%
Cystine	100%	100%	100%
Glutamic acid	100%	100%	100%
Glutamine	100%	100%	100%
Histidine	100%	100%	100%
Lysine	100%	100%	100%

Table C.3 continued

Methionine	100%	100%	100%
Ornithine	100%	100%	100%
Phenylalanine	100%	100%	100%
Proline	100%	100%	100%
Serine	100%	100%	100%
Sum Leucine, Isoleucine	100%	100%	100%
Taurine	100%	100%	100%
Threonine	100%	100%	100%
Tryptophan	100%	100%	100%
Tyrosine	85%	100%	100%
Valine	100%	100%	100%
Clinical Markers			
Cholesterol	100%	80%	100%
Cortisol	100%	30%	80%
Creatinine	100%	100%	100%
Homocysteine	20%	55%	55%
Urea	100%	100%	100%
Glucose	100%	100%	100%
Lactic acid	75%	100%	100%
Uric acid	100%	100%	100%
Fatty Acid Metabolism			
Acetyl-carnitine	85%	40%	100%

Table C.3 continued

Carnitine	100%	100%	100%
11,14-Eicosadienoic acid	100%	100%	100%
Adrenic acid	100%	100%	100%
alpha-Linolenic acid	100%	95%	95%
Arachidonic acid	100%	90%	100%
Docosahexaenoic acid	100%	95%	100%
Docosapentaenoic acid	100%	95%	100%
Eicosapentanoic acid	100%	100%	100%
gamma-Linolenic acid	100%	95%	95%
Gondoic acid	100%	100%	100%
homo-gamma-Linolenic acid	100%	100%	100%
Linoleic acid	100%	95%	100%
Margaric acid	60%	100%	25%
Myristic acid	90%	100%	75%
Myristoleic acid	85%	100%	45%
Oleic acid	100%	100%	100%
Palmitic acid	95%	100%	75%
Palmitoleic acid	90%	100%	55%
Stearic acid	75%	100%	15%
Lipid Metabolism			
sn-glycero-3-Phosphocholine	100%	100%	100%
Sphingosine	10%	100%	50%

Table C.3 continued

Leukotriene B4	50%	100%	50%
Resolvin E2	100%	100%	75%
Nucleotide-related Metabolism			
Hypoxanthine	0%	80%	100%
Xanthine	25%	90%	100%
Uridine	100%	100%	100%
Sterol Metabolism			
Deoxycholic acid	100%	55%	100%
Taurodeoxycholic acid	100%	50%	100%
TCA Cycle			
Citric acid	100%	100%	100%
Malic acid	100%	100%	100%
Pyruvic acid	100%	100%	100%
Vitamins and Cofactors			
Choline	100%	100%	100%
Pantothenic acid	50%	60%	95%
Tetrahydrofolic acid	40%	60%	30%

[†]Prevalence among 20 samples analyzed by HILIC

Table C. 4: Prevalence of clinically relevant biomarkers detected uniquely or predominately in ISF compared to plasma in matched samples from 20 human participants.

Biomarker	**Medical significance**	**Prevalence of biomarker**[§]		
		Plasma	ISF	SBF
Urocanic acid[*]	photocarcinogenesis, UV chromophore [196]	0%	100%	100%
N-Acetyl-D-glucosamine	micronutrient and drug, suppresses immune response, used to treat autoimmune diseases [276]	10%	100%	90%
Glycogen	energy storage [277]	10%	100%	60%
Diethanolamine[*]	cosmetic formulations, carcinogen [278]	5%	100%	60%
Sphingosine[*]	signaling molecule in skin [279]	10%	100%	50%
Nebularine	nucleoside	0%	100%	20%
Tributyltin chloride	environmental pollutant used as antifouling agent, now largely banned [280, 281]	10%	100%	10%
Citicoline	naturally occuring and also a nutrient supplement [282, 283]	10%	100%	5%
Angiotensin (5-8)	angiotensin cascade modulates vasoconstriction	5%	100%	5%
Pentadecanoic acid	marker for intake of milk fat [284]	10%	100%	0%
Gamma Tocopherol	form of vitamin E, micronutrient [285]	5%	100%	0%
Estradiol cypionate	natural form of estrogen - plays a role in reproduction, lactation [286]	0%	100%	0%
Arginosuccinic acid	biomarker for urea cycle disorder [287]	0%	95%	25%

Table C.4 continued

Porphobilinogen	biomarker for acute porphyrias, currently urine based detection [288]	10%	95%	20%
N^1,N^{12}-Diacetylspermine	cancer biomarker [289]	0%	95%	15%
Triethanolamine*	commonly used in skin care products [290]	0%	90%	0%
Prostanoic acid	basic building block of prostaglandins [291]	5%	85%	55%
6-Ethylchenodeoxycholic acid	bile acid derivative - reduces liver fat and fibrosis [292]	0%	85%	0%
Inosine	cardiac disease biomarker [293, 294]	5%	80%	100%
Hypoxanthine	cardiac disease biomarker [293]	0%	80%	100%
Barbaloin	product of aloe vera - anti-inflammatory, cathartic properties [295]	0%	70%	10%
AMPA	neurological biomarker [296]	10%	65%	90%
Bromochloroacetic acid	present in brominated disinfected water and may cause adverse reproductive outcomes [297]	5%	65%	10%
20-COOH-Leukotriene B4	Involved in vasodilation [298]	5%	55%	5%

§Prevalence among 20 samples; *Biomarker has dermatological significance.

Table C. 5: Metabolites identified unique to suction blister fluid (SBF) compared to microneedle (MN) patch derived ISF.

Biomarker	**Prevalence of biomarker**[†]		
	Plasma	ISF	SBF
1-Methylpyrrolinium	0%	0%	95%
Coniine	5%	10%	95%
N-Methyl-L-histidine	0%	5%	100%
Octamethyltrisiloxane	10%	5%	75%
sn-Glycero-3-phosphoethanolamine	5%	5%	100%
Guanosine	10%	10%	100%
Corticosterone [299]	0%	0%	100%
2-Arachidonoylglycerol [238]	0%	5%	95%
Riboflavin	0%	0%	95%
Hyperforin	0%	0%	95%
2,3,6-Trichlorohydroquinone	70%	0%	55%
Dichlorprop	0%	0%	80%
Chlorethoxyfos	0%	0%	95%
Bilirubin	100%	5%	100%

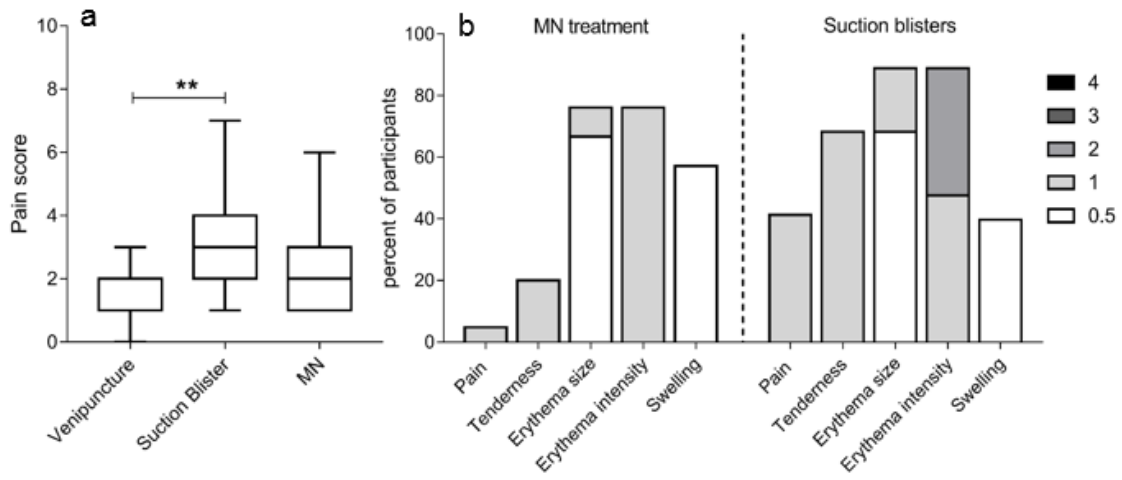

Figure C. 6: Tolerability of biofluid sampling methods in 21 human participants. (a) Pain associated with venipuncture, suction blister and MN treatment reported using a Visual Analog Scale (0 – 10) by 21 human participants. (b) Skin tolerability was assessed immediately after sampling by MN treatment or suction blister. All parameters rated on a scale of 0 to 4 (see Table S.5 in Appendix C).

C.4. Skin tolerability measurements

Table C. 6: Grading scale for skin tolerability measurements.

Local reaction to patch	Grade 0	Grade 0.5*	Grade 1	Grade 2	Grade 3	Grade 4
Pain**	Pain is absent	N/A	Mild pain that does not interfere with activity	Repeated use of non-narcotic pain reliever > 24 hours or interferes with activity	Any use of narcotic pain reliever or prevents daily activity	Emergency room (ER) visit or hospitalization
Tenderness**	No discomfort to touch	N/A	Mild discomfort to touch	Discomfort with movement	Significant discomfort at rest	ER visit or hospitalization
Erythema (Size)	0 cm	1.– 1 cm [erythema less than or equal to patch size ≤ 1 cm]	1.– 5 cm [erythema spreading beyond patch site > 1cm]	5.1 – 10 cm	> 10 cm	Necrosis or exfoliative dermatitis
Erythema (Intensity)	No erythema	N/A	Very slight erythema (barely perceptible)	Well-defined erythema	Moderate to severe erythema	Severe erythema (beet redness)
Induration/ Swelling	0 cm	1. – 1 cm [swelling less than or equal to patch size ≤ 1 cm]	1.1 – 5 cm and does not interfere with activity [swelling spreading beyond patch size > 1cm]	5.1 – 10 cm or interferes with activity	> 10 cm or prevents daily activity	Necrosis

* Used only with erythema (size) and induration/swelling.

** Pain and tenderness scored based on the response from the subject

C.5. Pharmacokinetics of caffeine in interstitial fluid and plasma

Table C. 7: Demographics of 9 participants in caffeine pharmacokinetics study

Age (years)	
Mean (SD)	28 (4)
Median (IQR)	26 (24-31)
Sex	
Male (%)	6 (67%)
Female (%)	3 (33%)
Ethnic origin[†]	
White (%)	3 (33%)
Black (%)	2 (22%)
Asian (%)	4 (44%)
BMI (kg/m^2) [§]	
Mean (SD)	22.7 (2.2)
Median (IQR)	22.4 (21.0-23.8)

[†]Ethnic origin was self-reported, participants were allowed to select multiple options;

[§]Height and weight were self-reported

C.6. Acceptability and tolerability of ISF connection by MN patch and plasma collection by fingerstick.

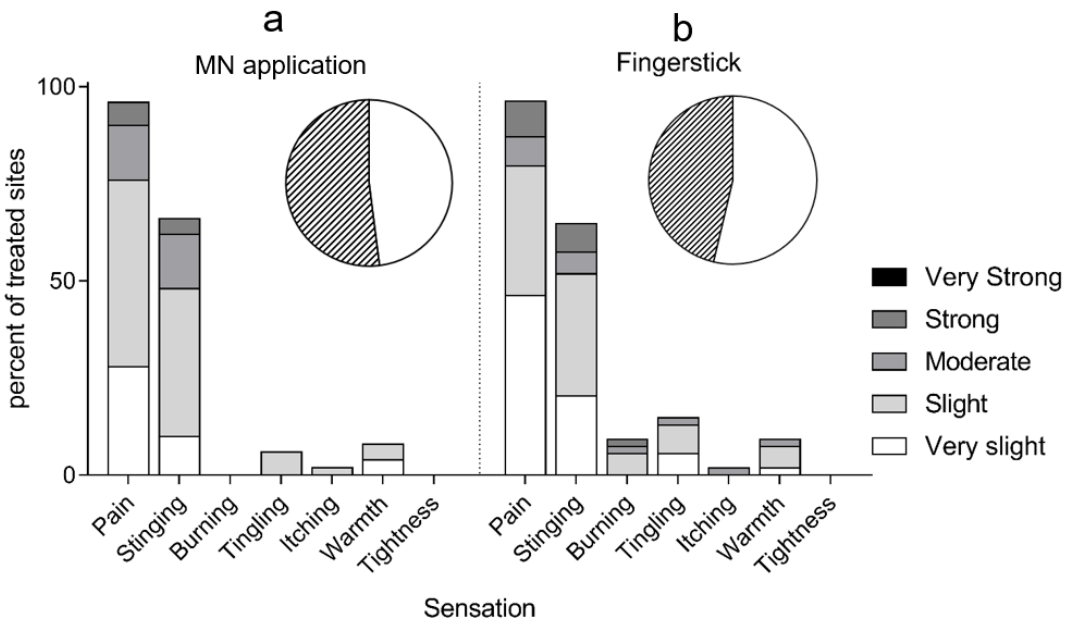

Figure C. 7: Sensory perceptions reported by 9 human participants during MN treatment and fingerstick blood collection. Sensory perception of pain, stinging, burning, tingling, itching, warmth and tightness were reported by participants at five levels: very slight, slight, moderate, strong, and very strong. The pie chart displays the percent of treatments that participants reported that all sensations associated with the treatment were comfortable (white) or at least one was reported as not comfortable (striped). (a) MN application. (b) Fingerstick.

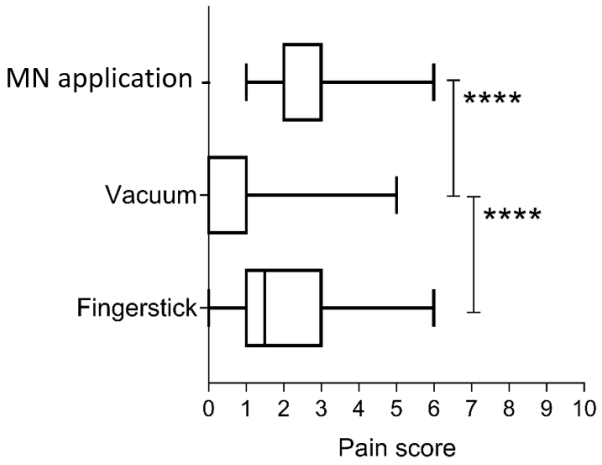

Figure C. 8: Pain of microneedle (MN) patch application, vacuum (following MN patch application) and fingerstick as reported by 5 participants on a scale of 0 (no pain) to 10 (worst possible pain). **** p<0.0001.

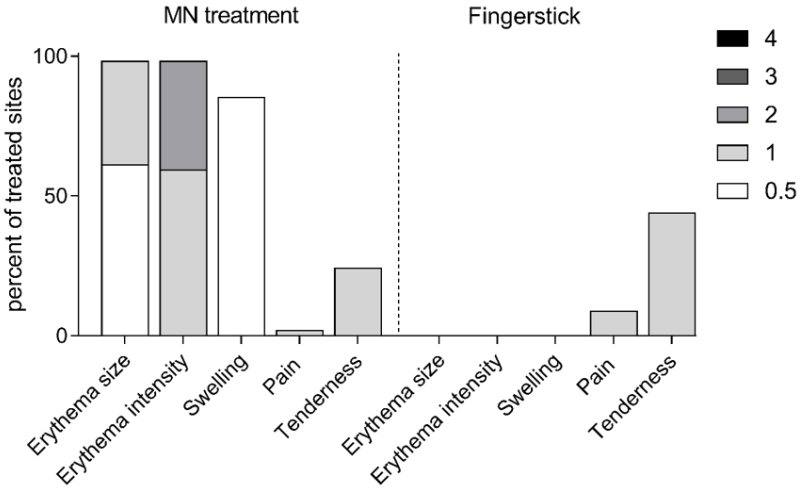

Figure C. 9: Skin tolerability measurements made after microneedle (MN) patch treatment and fingerstick in 9 human participants. Skin tolerability parameters – erythema size, erythema intensity, swelling, pain and tenderness – were measured on a scale of 0 to 4 based on the scale described in Table S.5.

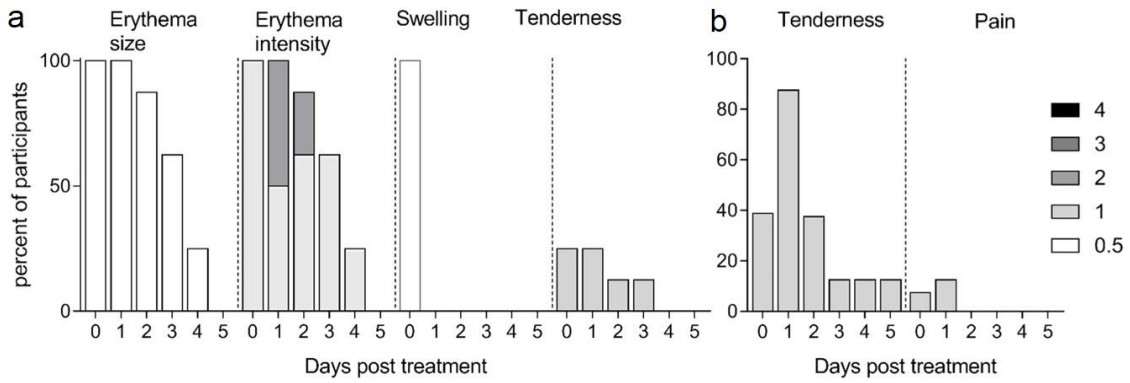

Figure C. 10: Skin tolerability over 5 days after microneedle (MN) treatment and fingerstick in 9 human participants. Skin was assessed for erythema size, erythema intensity, swelling and tenderness and pain. (a) Skin tolerability after MN treatment. No participants reported on-going pain. (b) Skin tolerability after fingerstick. No participants experienced erythema or swelling.

REFERENCES

1. Nichols, J.H., *Evidence based practice for point of care setting*, J.H. Nichols, Editor. 2006, American Association for Clinical Chemistry. p. 203.

2. Chin, C.D., V. Linder, and S.K. Sia, *Commercialization of microfluidic point-of-care diagnostic devices.* Lab Chip, 2012. **12**(12): p. 2118-34.

3. *Biomarkers and risk assessment: Concepts and principles.* WHO International Programme on Chemical Safety, 1993.

4. *Guide to early cancer diagnosis.* Geneva: World Health Organization, 2017: p. Licence: CC BY-NC-SA 3.0 IGO.

5. Etzioni, R., et al., *The case for early detection.* Nat Rev Cancer, 2003. **3**(4): p. 243-52.

6. Leifer, B.P., *Early diagnosis of Alzheimer's disease: clinical and economic benefits.* Journal of the American Geriatrics Society, 2003. **51**(5s2).

7. Inzucchi, S.E., et al., *Management of hyperglycaemia in type 2 diabetes: a patient-centered approach. Position statement of the American Diabetes Association (ADA) and the European Association for the Study of Diabetes (EASD).* Diabetologia, 2012. **55**(6): p. 1577-1596.

8. Matchar, D.B., et al., *The impact of frequency of patient self-testing of prothrombin time on time in target range within VA Cooperative Study# 481: The Home INR Study (THINRS), a randomized, controlled trial.* Journal of thrombosis and thrombolysis, 2015. **40**(1): p. 17-25.

9. Rifai, N., M.A. Gillette, and S.A. Carr, *Protein biomarker discovery and validation: the long and uncertain path to clinical utility.* Nature biotechnology, 2006. **24**(8).

10. Diamandis, E.P., *Mass spectrometry as a diagnostic and a cancer biomarker discovery tool opportunities and potential limitations.* Molecular & Cellular Proteomics, 2004. **3**(4): p. 367-378.

11. Miller, D.T., et al., *Consensus Statement: Chromosomal Microarray Is a First-Tier Clinical Diagnostic Test for Individuals with Developmental Disabilities or Congenital Anomalies.* The American Journal of Human Genetics, 2010. **86**(5): p. 749-764.

12. Tissari, P., et al., *Accurate and rapid identification of bacterial species from positive blood cultures with a DNA-based microarray platform: an observational study.* The Lancet, 2010. **375**(9710): p. 224-230.

13. Wittner, B.S., et al., *Analysis of the MammaPrint breast cancer assay in a predominantly postmenopausal cohort.* Clinical Cancer Research, 2008. **14**(10): p. 2988-2993.

14. Mook, S., et al., *Individualization of therapy using MammaPrint® ì: From development to the MINDACT Trial.* Cancer Genomics-Proteomics, 2007. **4**(3): p. 147-155.

15. Bodenlenz, M., et al., *Open Flow Microperfusion as a Dermal Pharmacokinetic Approach to Evaluate Topical Bioequivalence.* Clinical Pharmacokinetics, 2017. **56**(1): p. 91-98.

16. Mitchell, P.S., et al., *Circulating microRNAs as stable blood-based markers for cancer detection.* Proceedings of the National Academy of Sciences, 2008. **105**(30): p. 10513-10518.

17. Frantzi, M., et al., *Development and validation of urine-based peptide biomarker panels for detecting bladder cancer in a multi-center study.* Clinical Cancer Research, 2016. **22**(16): p. 4077-4086.

18. Hendriks, R., et al., *383 Multicenter validation study of a urine-based molecular biomarker algorithm to predict high-grade prostate cancer.* European Urology Supplements, 2016. **15**(3): p. e383.

19. Gao, W., et al., *Fully integrated wearable sensor arrays for multiplexed in situ perspiration analysis.* Nature, 2016. **529**(7587): p. 509-514.

20. Malamud, D., *Saliva as a diagnostic fluid.* Dental Clinics of North America, 2011. **55**(1): p. 159-178.

21. Nunes, S., et al., *Clinical and diagnostic utility of saliva as a non-invasive diagnostic fluid: a systematic review.* Biochemia medica, 2015. **25**(2): p. 177-192.

22. St John, A. and C.P. Price, *Existing and Emerging Technologies for Point-of-Care Testing.* The Clinical Biochemist Reviews, 2014. **35**(3): p. 155-167.

23. Dalton, L., *Sticking Points*. 2016, ACS Publications.

24. Olansky, L. and L. Kennedy, *Finger-Stick Glucose Monitoring: Issues of accuracy and specificity.* Diabetes Care, 2010. **33**(4): p. 948-949.

25. Gnoth, C. and S. Johnson, *Strips of hope: accuracy of home pregnancy tests and new developments.* Geburtshilfe und Frauenheilkunde, 2014. **74**(07): p. 661-669.

26. Behre, H., et al., *Prediction of ovulation by urinary hormone measurements with the home use ClearPlan® Fertility Monitor: comparison with transvaginal ultrasound scans and serum hormone measurements.* Human Reproduction, 2000. **15**(12): p. 2478-2482.

27. Perrier, E., et al., *Circadian variation and responsiveness of hydration biomarkers to changes in daily water intake.* Eur J Appl Physiol, 2013. **113**(8): p. 2143-51.

28. Giskeødegård, G.F., et al., *Diurnal rhythms in the human urine metabolome during sleep and total sleep deprivation.* Scientific Reports, 2015. **5**: p. 14843.

29. Pfaffe, T., et al., *Diagnostic potential of saliva: current state and future applications.* Clinical chemistry, 2011. **57**(5): p. 675-687.

30. Pai, N.P., et al., *Supervised and unsupervised self-testing for HIV in high-and low-risk populations: a systematic review.* PLOS medicine, 2013. **10**(4): p. e1001414.

31. Bandodkar, A.J., et al., *Epidermal tattoo potentiometric sodium sensors with wireless signal transduction for continuous non-invasive sweat monitoring.* Biosensors and Bioelectronics, 2014. **54**(Supplement C): p. 603-609.

32. Warwick, W.J., *Cystic Fibrosis Sweat Test.* Encyclopedia of Medical Devices and Instrumentation, 2006.

33. Korte, B., *Point-of-Care Diagnostic Testing*. 2010, National Institutes of Health.

34. Vikas, *Global market for point-of-care diagnostics to reach $16.5 billion in 2014.*, in *BCC Research*. 2012, BCC Research LLC: Wellesley, Massachusetts.

35. Yager, P., G.J. Domingo, and J. Gerdes, *Point-of-care diagnostics for global health.* Annu Rev Biomed Eng, 2008. **10**: p. 107-44.

36. Gubala, V., et al., *Point of care diagnostics: status and future.* Anal Chem, 2012. **84**(2): p. 487-515.

37. Holland, C.A. and F.L. Kiechle, *Point-of-care molecular diagnostic systems--past, present and future.* Curr Opin Microbiol, 2005. **8**(5): p. 504-9.

38. Chan, M., et al., *Smart wearable systems: Current status and future challenges.* Artificial Intelligence in Medicine, 2012. **56**(3): p. 137-156.

39. Lamkin, P., *Wearable tech market to treble in next five years*, in *Forbes Tech*. 2015.

40. Steinmetz, L.M. and A. Jones, *Sensing a revolution.* Molecular Systems Biology, 2016. **12**(4): p. n/a-n/a.

41. Pantelopoulos, A. and N.G. Bourbakis, *A survey on wearable sensor-based systems for health monitoring and prognosis.* IEEE Transactions on Systems, Man, and Cybernetics, Part C (Applications and Reviews), 2010. **40**(1): p. 1-12.

42. Bandodkar, A.J., I. Jeerapan, and J. Wang, *Wearable Chemical Sensors: Present Challenges and Future Prospects.* ACS Sensors, 2016. **1**(5): p. 464-482.

43. K Aukland, G.N., *Interstitial fluid volume: local regulatory mechanisms.* Physiological Reviews, 1981. **61**(3): p. 556-643.

44. Scallan J., H.V.H., Korthuis R.J., *Capillary Fluid Exchange: Regulations, Function and Pathology*, in *Colloquium Lectures on Integrated Systems Physiology-FromMolecules to Function*, G.J.P. Granger D.N., Editor. 2010, Morgan & Claypool life sciences publishers. p. 1-33.

45. Aukland, K. and G. Nicolaysen, *Interstitial fluid volume: local regulatory mechanisms.* Physiological Reviews, 1981. **61**(3): p. 556-643.

46. Scallan J., H.V.H., Korthuis R.J., *Capillary fluid exchange: Regulations, function and pathology*, in *Colloquium Lectures on Integrated Systems Physiology- From Molecules to Function*, G.J.P. Granger D.N., Editor. 2010, Morgan & Claypool life sciences publishers. p. 1-33.

47. Wiig, H., R.K. Reed, and O. Tenstad, *Interstitial fluid pressure, composition of interstitium, and interstitial exclusion of albumin in hypothyroid rats.* American Journal of Physiology - Heart and Circulatory Physiology, 2000. **278**(5): p. H1627-H1639.

48. Fogh-Andersen, N., et al., *Composition of interstitial fluid.* Clin Chem, 1995. **41**(10): p. 1522-5.

49. Bauer, J. and C. Brooks, *Body-fluid composition in normal and hypertensive man.* Clinical Science, 1982. **62**(1): p. 43-49.

50. Kool, J., et al., *Suction blister fluid as potential body fluid for biomarker proteins.* Proteomics, 2007. **7**(20): p. 3638-50.

51. Muller, A.C., et al., *A comparative proteomic study of human skin suction blister fluid from healthy individuals using immunodepletion and iTRAQ labeling.* J Proteome Res, 2012. **11**(7): p. 3715-27.

52. Lunt, S.J., et al., *Interstitial fluid pressure in tumors: therapeutic barrier and biomarker of angiogenesis.* Future Oncol, 2008. **4**(6): p. 793-802.

53. Gullino, P.M., S.H. Clark, and F.H. Grantham, *The Interstitial Fluid of Solid Tumors.* Cancer Research, 1964. **24**(5): p. 780-797.

54. Celis, J.E., et al., *Proteomic characterization of the interstitial fluid perfusing the breast tumor microenvironment: a novel resource for biomarker and therapeutic target discovery.* Mol Cell Proteomics, 2004. **3**(4): p. 327-44.

55. Pugin, J., et al., *Diagnosis of Ventilator-associated Pneumonia by Bacteriologic Analysis of Bronchoscopic and Nonbronchoscopic "Blind" Bronchoalveolar Lavage Fluid.* American Review of Respiratory Disease, 1991. **143**(5_pt_1): p. 1121-1129.

56. Wattiez, R. and P. Falmagne, *Proteomics of bronchoalveolar lavage fluid.* Journal of Chromatography B, 2005. **815**(1–2): p. 169-178.

57. Zetterberg, H., D.H. Smith, and K. Blennow, *Biomarkers of mild traumatic brain injury in cerebrospinal fluid and blood.* Nature Reviews Neurology, 2013. **9**(4): p. 201-210.

58. Parnetti, L., et al., *Cerebrospinal fluid biomarkers in Parkinson disease.* Nat Rev Neurol, 2013. **9**(3): p. 131-140.

59. Blennow, K., et al., *Clinical utility of cerebrospinal fluid biomarkers in the diagnosis of early Alzheimer's disease.* Alzheimer's & Dementia, 2015. **11**(1): p. 58-69.

60. Klimowicz, A., S. Farfał, and S. Bielecka-Grzela, *Evaluation of skin penetration of topically applied drugs in humans by cutaneous microdialysis: acyclovir vs. salicylic acid.* Journal of clinical pharmacy and therapeutics, 2007. **32**(2): p. 143-148.

61. Holmgaard, R., J.B. Nielsen, and E. Benfeldt, *Microdialysis sampling for investigations of bioavailability and bioequivalence of topically administered drugs: current state and future perspectives.* Skin pharmacology and physiology, 2010. **23**(5): p. 225-243.

62. Kastellorizios, M. and D.J. Burgess, *Continuous metabolic monitoring based on multi-analyte biomarkers to predict exhaustion.* Sci Rep, 2015. **5**: p. 10603.

63. Windmiller, J.R. and J. Wang, *Wearable electrochemical sensors and biosensors: a review.* Electroanalysis, 2013. **25**(1): p. 29-46.

64. Klonoff, D.C., *Continuous Glucose Monitoring.* Roadmap for 21st century diabetes therapy, 2005. **28**(5): p. 1231-1239.

65. Matuleviciene, V., et al., *A clinical trial of the accuracy and treatment experience of the Dexcom G4 sensor (Dexcom G4 system) and Enlite sensor (guardian REAL-time system) tested simultaneously in ambulatory patients with type 1 diabetes.* Diabetes Technol Ther, 2014. **16**(11): p. 759-67.

66. Calhoun, P., et al., *Performance comparison of the medtronic sof-sensor and enlite glucose sensors in inpatient studies of individuals with type 1 diabetes.* Diabetes Technol Ther, 2013. **15**(9): p. 758-61.

67. Vashist, S.K., *Non-invasive glucose monitoring technology in diabetes management: A review.* Analytica chimica acta, 2012. **750**: p. 16-27.

68. Wiig, H., R.K. Reed, and O. Tenstad, *Interstitial fluid pressure, composition of interstitium,and interstitial exclusion of albumin in hypothyroid rats.* Am J Physiol Heart Circ Physiol, 2000. **278**: p. H1627–H1639,.

69. Montagna, W. and P.F. Parakkal, *The structure and function of skin*. 3 ed. 1974, London, UK: Academic Press Inc. 432.

70. Harding, C.R., *The stratum corneum: Structure and function in health and disease.* Dermatologic Therapy, 2004. **17**: p. 6-15.

71. Pierre Agache, P.H., *Measuring the skin*, ed. M. Philipp. 2004: Springer-Verlag Berlin Heidelberg New York. 784.

72. Amirlak, B. *Skin Anatomy*. Medscape References: Drugs, Diseases and Procedures 2013; Available from: http://emedicine.medscape.com/article/1294744-overview.

73. Kiistala, U., *Suction blister device for separation of viable epidermis from dermis.* The Journal of Investigative Dermatology, 1968. **15**(2): p. 129-137.

74. Alexis, A.F., et al., *Reassessment of the suction blister model of wound healing: introduction of a new higher pressure device.* Int J Dermatol, 1999. **38**(8): p. 613-7.

75. Krawczyk, W.S., *A pattern of epidermal cell migration during wound healing.* The Journal of cell biology, 1971. **49**(2): p. 247-263.

76. Meinardi, M.M.H.M., et al., *Cyclosporin A levels in suction-blister fluid of patients with psoriasis treated systemically.* British Journal of Dermatology, 1990. **122**(5): p. 671-676.

77. Hatchome, N., T. Kato, and H. Tagami, *Therapeutic success of epidermal grafting in generalized vitiligo is limited by the Koebner phenomenon.* Journal of the American Academy of Dermatology, 1990. **22**(1): p. 87-91.

78. Kayashima S, et al., *Suction effusion fluid from skin and constituent analysis: new candidate for interstitial fluid.* Am J Physiol Heart Circ Physiol 1992. **263**: p. H1623-7.

79. Schnetz, E. and M. Fartasch, *Microdialysis for the evaluation of penetration through the human skin barrier — a promising tool for future research?* European Journal of Pharmaceutical Sciences, 2001. **12**(3): p. 165-174.

80. Schmidt, S., et al., *Clinical Microdialysis in Skin and Soft Tissues: An Update.* The Journal of Clinical Pharmacology, 2008. **48**(3): p. 351-364.

81. Lonnroth, P., P.A. Jansson, and U. Smith, *A microdialysis method allowing characterization of intercellular water space in humans.* American Journal of Physiology - Endocrinology and Metabolism, 1987. **253**(2): p. E228-E231.

82. Krogstad, A.L., et al., *Microdialysis methodology for the measurement of dermal interstitial fluid in humans.* British Journal of Dermatology, 1996. **134**(6): p. 1005-1012.

83. Pieber, T., et al., *Open flow microperfusion: an alternative method to microdialysis?*, in *Microdialysis in Drug Development* 2013, Springer: New York, NY. p. 283-302.

84. Bodenlenz, M., et al., *Clinical applicability of dOFM devices for dermal sampling.* Skin Res Technol, 2013. **19**(4): p. 474-83.

85. Bodenlenz, M., et al., *Open flow microperfusion as a dermal pharmacokinetic approach to evaluate topical bioequivalence.* Clin Pharmacokinet, 2017. **56**(1): p. 91-98.

86. Mark R. Prausnitz, C.S.L., Cindy H. Liu, Judy C. Pang, Tej-Preet Singh, Robert Langer, James C. Weaver, *Transdermal transport efficiency during skin electroporation and iontophoresis.* J Controlled Release, 1996. **38**: p. 205-217.

87. Sieg, A., R.H. Guy, and M. Begoña Delgado-Charro, *Electroosmosis in Transdermal Iontophoresis: Implications for Noninvasive and Calibration-Free Glucose Monitoring.* Biophysical Journal, 2004. **87**(5): p. 3344-3350.

88. Potts, R.O., J.A. Tamada, and M.J. Tierney, *Glucose monitoring by reverse iontophoresis.* Diabetes Metab Res Rev, 2002. **18 Suppl 1**: p. S49-53.

89. Sieg, A., R.H. Guy, and M.B. Delgado-Charro, *Noninvasive glucose monitoring by reverse iontophoresis in vivo: application of the internal standard concept.* Clin Chem, 2004. **50**(8): p. 1383-90.

90. Samir Mitragotri, M.C., Joseph Kost, Robert Langer, *Analysis of ultrasonically extracted interstitial fluid as a predictor of blood glucose levels.* Journal of Applied Physiology, 2000. **89**: p. 961-966.

91. Luijf, Y.M., et al., *Accuracy and reliability of continuous glucose monitoring systems: a head-to-head comparison.* Diabetes Technol Ther, 2013. **15**(8): p. 722-7.

92. Gowda, G.N. and D. Djukovic, *Overview of mass spectrometry-based metabolomics: opportunities and challenges.* Mass Spectrometry in Metabolomics: Methods and Protocols, 2014: p. 3-12.

93. Dettmer, K., P.A. Aronov, and B.D. Hammock, *MASS SPECTROMETRY-BASED METABOLOMICS.* Mass spectrometry reviews, 2007. **26**(1): p. 51-78.

94. Mikami, T., M. Aoki, and T. Kimura, *The application of mass spectrometry to proteomics and metabolomics in biomarker discovery and drug development.* Curr Mol Pharmacol, 2012. **5**(2): p. 301-16.

95. Hadrévi, J., et al., *Comparative metabolomics of muscle interstitium fluid in human trapezius myalgia: an in vivo microdialysis study.* European Journal of Applied Physiology, 2013. **113**(12): p. 2977-2989.

96. Celis, J.E., et al., *Identification of extracellular and intracellular signaling components of the mammary adipose tissue and its interstitial fluid in high risk breast cancer patients toward dissecting the molecular circuitry of epithelial-adipocyte stromal cell interactions.* Molecular & cellular proteomics, 2005. **4**(4): p. 492-522.

97. Kim, Y.C., J.H. Park, and M.R. Prausnitz, *Microneedles for drug and vaccine delivery.* Adv Drug Deliv Rev, 2012. **64**(14): p. 1547-68.

98. Henry, S., et al., *Microfabricated microneedles: a novel approach to transdermal drug delivery.* J Pharm Sci, 1998. **87**(8): p. 922-5.

99. Gill, H.S. and M.R. Prausnitz, *Coated microneedles for transdermal delivery.* J Control Release, 2007. **117**(2): p. 227-37.

100. Martanto, W., et al., *Microinfusion using hollow microneedles.* Pharm Res, 2006. **23**(1): p. 104-13.

101. Gupta, J., E.I. Felner, and M.R. Prausnitz, *Minimally invasive insulin delivery in subjects with type 1 diabetes using hollow microneedles.* Diabetes Technol Ther, 2009. **11**(6): p. 329-37.

102. Sullivan, S.P., et al., *Dissolving polymer microneedle patches for influenza vaccination.* Nat Med, 2010. **16**(8): p. 915-20.

103. Norman, J.J., et al., *Microneedle patches: usability and acceptability for self-vaccination against influenza.* Vaccine, 2014. **32**(16): p. 1856-62.

104. Arya, J., et al., *Tolerability, usability and acceptability of dissolving microneedle patch administration in human subjects.* Biomaterials, 2017. **128**: p. 1-7.

105. El-Laboudi, A., et al., *Use of microneedle array devices for continuous glucose monitoring: a review.* Diabetes Technol Ther, 2013. **15**(1): p. 101-15.

106. Miller, P.R., R.J. Narayan, and R. Polsky, *Microneedle-based sensors for medical diagnosis.* Journal of Materials Chemistry B, 2016. **4**(8): p. 1379-1383.

107. Ventrelli, L., L. Marsilio Strambini, and G. Barillaro, *Microneedles for Transdermal Biosensing: Current Picture and Future Direction.* Adv Healthc Mater, 2015. **4**(17): p. 2606-40.

108. Kobayashi, K. and H. Suzuki, *A sampling mechanism employing the phase transition of a gel and its application to a micro analysis system imitating a mosquito.* Sensors and Actuators B: Chemical, 2001. **80**(1): p. 1-8.

109. Suzuki H., e.a., *A disposable 'intelligent mosquito' with a reversible sampling mechanism usint the volume-phase transition of a gel.* Sensors and Actuators B: Chemical, 2002. **83**: p. 53-59.

110. Suzuki, H., et al., *A disposable on-line microsystem for continuous sampling and monitoring of glucose.* Sensors and Actuators B: Chemical, 2004. **97**(1): p. 90-97.

111. Gattiker, G.E., K.V.I.S. Kaler, and M.P. Mintchev, *Electronic Mosquito: designing a semi-invasive Microsystem for blood sampling, analysis and drug delivery applications.* Microsystem Technologies, 2005. **12**(1-2): p. 44-51.

112. Tsuchiya K., e.a., *Development of Blood Extraction System for Health Monitoring System.* Biomedical Microdevices, 2005. **7**(4): p. 347-353.

113. Nicolau, D.V., et al., *Design of painless microneedle for blood extraction system.* 2007. **6799**: p. 67990Q-67990Q-11.

114. Chakraborty, S. and K. Tsuchiya, *Development and fluidic simulation of microneedles for painless pathological interfacing with living systems.* Journal of Applied Physics, 2008. **103**(11): p. 114701.

115. Mukerjee, E.V., et al., *Microneedle array with integrated microchannels for transdermal sample extraction and in situ analysis*, in *The 12th International Conference on Solid Stale Sensors, Actuators and Micmystems*. 2003, IEEE: Boston, MA. p. 1439-1441.

116. Mukerjee, E.V., et al., *Microneedle array for transdermal biological fluid extraction and in situ analysis.* Sensors and Actuators A: Physical, 2004. **114**(2-3): p. 267-275.

117. Ebah, L.M., *Extraction and Analysis of Interstitial fluid and characterisation of the interstitial compartment in kidney disease*, in *School pf Biomedicine*. 2012, University of Manchester. p. 303.

118. Miller, P.R., et al., *Integrated carbon fiber electrodes within hollow polymer microneedles for transdermal electrochemical sensing.* Biomicrofluidics, 2011. **5**(1): p. 013415.

119. Windmiller, J.R., et al., *Microneedle array-based carbon paste amperometric sensors and biosensors.* Analyst, 2011. **136**(9): p. 1846-51.

120. Miller, P.R., et al., *Multiplexed microneedle-based biosensor array for characterization of metabolic acidosis.* Talanta, 2012. **88**: p. 739-42.

121. Miller, P.R., et al., *Microneedle-Based Transdermal Sensor for On-Chip Potentiometric Determination of K+.* Advanced Healthcare Materials, 2014. **3**(6): p. 876-881.

122. Keum, D.H., et al., *Microneedle Biosensor for Real-Time Electrical Detection of Nitric Oxide for In Situ Cancer Diagnosis During Endomicroscopy.* Advanced Healthcare Materials, 2015: p. n/a-n/a.

123. Wang P.M., C.M., Prausnitz M. R., *Minimally invasive extraction of dermal interstitial fluid for glucose monitoring using microneedles.* Diabetes Technology and Therapeutics, 2005. **7**(1): p. 131-141.

124. Li, C.G., et al., *An optimized hollow microneedle for minimally invasive blood extraction.* Biomed Microdevices, 2013. **15**(1): p. 17-25.

125. Biosystems, S.S., *Tap Technology*, in *Seventh Sense Biosystems*. 2012, Seventh Sense Biosystems, Inc. .

126. Bloomfield, D. *Blood-Drawing Startup Seventh Sense Seeks Pain-Free Profits*. Bloomberg 2016 April 1, 2016 [cited 2016 July 18]; Available from: http://www.bloomberg.com/news/articles/2016-04-01/blood-drawing-startup-seventh-sense-seeks-pain-free-profits.

127. Zimmermann, S., et al., *In-device enzyme immobilization: wafer-level fabrication of an integrated glucose sensor.* Sensors and Actuators B: Chemical, 2004. **99**(1): p. 163-173.

128. Zimmermann S., F.D., Stoeber B., Flounders A.W., Liepmann D., *A microneedle-based glucose monitor fabricated on a wafer level using in device enzyme immobilization.* IEEE, 2003.

129. Chua, B., et al., *Effect of microneedles shape on skin penetration and minimally invasive continuous glucose monitoring in vivo.* Sensors and Actuators A: Physical, 2013. **203**: p. 373-381.

130. Jina, A., et al., *Design, Development, and Evaluation of a Novel Microneedle Array-based Continuous Glucose Monitor.* J Diabetes Sci Technol, 2014. **8**(3): p. 483-487.

131. Invernale, M.A., et al., *Microneedle electrodes toward an amperometric glucose-sensing smart patch.* Adv Healthc Mater, 2014. **3**(3): p. 338-42.

132. Valdés-Ramírez, G., et al., *Microneedle-based self-powered glucose sensor.* Electrochemistry Communications, 2014. **47**: p. 58-62.

133. Yu, J., et al., *Microneedle-array patches loaded with hypoxia-sensitive vesicles provide fast glucose-responsive insulin delivery.* Proceedings of the National Academy of Sciences, 2015. **112**(27): p. 8260-8265.

134. Corrie, S.R., et al., *Surface-modified microprojection arrays for intradermal biomarker capture, with low non-specific protein binding.* Lab Chip, 2010. **10**(20): p. 2655-8.

135. Muller, D.A., et al., *Surface modified microprojection arrays for the selective extraction of the dengue virus NS1 protein as a marker for disease.* Anal Chem, 2012. **84**(7): p. 3262-8.

136. Lee, K.T., et al., *Capture of the Circulating Plasmodium falciparum Biomarker HRP2 in a Multiplexed Format, via a Wearable Skin Patch.* Analytical Chemistry, 2014. **86**(20): p. 10474-10483.

137. Sato, T., et al., *Measurement of glucose area under the curve using minimally invasive interstitial fluid extraction technology: evaluation of glucose monitoring concepts without blood sampling.* Diabetes Technol Ther, 2011. **13**(12): p. 1194-200.

138. Sakaguchi, K., et al., *A minimally invasive system for glucose area under the curve measurement using interstitial fluid extraction technology: evaluation of the accuracy and usefulness with oral glucose tolerance tests in subjects with and without diabetes.* Diabetes Technol Ther, 2012. **14**(6): p. 485-91.

139. Donnelly, R.F., et al., *Hydrogel-Forming Microneedles Increase in Volume During Swelling in Skin, but Skin Barrier Function Recovery is Unaffected.* Journal of Pharmaceutical Sciences, 2014. **103**(5): p. 1478-1486.

140. Donnelly, R.F., et al., *Microneedle-Mediated Minimally Invasive Patient Monitoring.* Therapeutic Drug Monitoring, 2014. **36**(1): p. 10-17.

141. Donnelly, R.F., et al., *Hydrogel-forming microneedles prepared from "super swelling" polymers combined with lyophilised wafers for transdermal drug delivery.* PLoS One, 2014. **9**(10): p. e111547.

142. Caffarel-Salvador, E., et al., *Hydrogel-Forming Microneedle Arrays Allow Detection of Drugs and Glucose <italic>In Vivo</italic>: Potential for Use in Diagnosis and Therapeutic Drug Monitoring.* PLoS ONE, 2016. **10**(12): p. e0145644.

143. Romanyuk, A.V., et al., *Collection of Analytes from Microneedle Patches.* Analytical Chemistry, 2014. **86**(21): p. 10520-10523.

144. Lee J.W., P.J.H., Prausnitz M.R., *Dissolving Microneedles for Transdermal Drug Delivery.* Biomaterials, 2008. **29**(13): p. 2113-24.

145. Chang, H., et al., *A Swellable Microneedle Patch to Rapidly Extract Skin Interstitial Fluid for Timely Metabolic Analysis.* Adv Mater, 2017.

146. Zahn J.D., e.a., *Microdialysis microneedles for continuous medical monitoring.* Biomedical Microdevices, 2005. **7**(1): p. 59-69.

147. Zahn, J.D., D. Trebotich, and D. Liepmann. *Microfabricated microdialysis microneedles for continuous medical monitoring*. in *Microtechnologies in Medicine and Biology, 1st Annual International, Conference On. 2000*. 2000.

148. Jeffrey D. Zahn, A.A.D., Alexandros P. Papavasiliou, Albert P. Pisano, Dorian Liepmann. *An integrated microfluidic device for the continuous sampling and analysis of biological fluids*. in *Proceedings of 2001 ASME International Mechanical Engineering Congress and Exposition*. 2001. New York, NY.

149. Venugopal, M., et al., *A realtime and continuous assessment of cortisol in ISF using electrochemical impedance spectroscopy.* Sensors and Actuators A: Physical, 2011. **172**: p. 154-160.

150. Palacios, G., et al., *Biomarkers of physical activity and exercise.* Nutr Hosp, 2015. **31 Suppl 3**: p. 237-44.

151. Ezzati, M., *Cardiovascular disease, chronic kidney disease, and diabetes mortality burden of cardiometabolic risk factors from 1980 to 2010: a comparative risk assessment.* The Lancet Diabetes & Endocrinology, 2014. **2**(8): p. 634-647.

152. Fassett, R.G., et al., *Biomarkers in chronic kidney disease: a review.* Kidney Int, 2011. **80**(8): p. 806-21.

153. Vasan, R.S., *Biomarkers of cardiovascular disease: molecular basis and practical considerations.* Circulation, 2006. **113**(19): p. 2335-62.

154. Esser, N., N. Paquot, and A.J. Scheen, *Inflammatory markers and cardiometabolic diseases.* Acta Clin Belg, 2015. **70**(3): p. 193-9.

155. Combs, G.F., Jr., et al., *Biomarkers in nutrition: new frontiers in research and application.* Ann N Y Acad Sci, 2013. **1278**: p. 1-10.

156. Hedrick, V.E., et al., *Dietary biomarkers: advances, limitations and future directions.* Nutr J, 2012. **11**: p. 109.

157. Ken Sexton, L.L.N., James L. Pirkle, *Human biomonitoring of environmental chemicals.* American Scientist, 2004. **92**: p. 38-45.

158. Baker, M., *In biomarkers we trust?* Nature biotechnology, 2005. **23**(3): p. 297.

159. Bond, M.M. and R.R. Richards-Kortum, *Drop-to-Drop Variation in the Cellular Components of Fingerprick Blood.* American journal of clinical pathology, 2015. **144**(6): p. 885-894.

160. Slupsky, C.M., et al., *Investigations of the effects of gender, diurnal variation, and age in human urinary metabolomic profiles.* Analytical chemistry, 2007. **79**(18): p. 6995-7004.

161. Gromov, P., et al., *Tumor interstitial fluid—a treasure trove of cancer biomarkers.* Biochimica et Biophysica Acta (BBA)-Proteins and Proteomics, 2013. **1834**(11): p. 2259-2270.

162. Prausnitz, M.R., *Engineering microneedle patches for vaccination and drug delivery to skin.* Annual Review of Chemical and Biomolecular Engineering, 2017. **8**: p. 177-200.

163. Parikh, P., H. Mochari, and L. Mosca, *Clinical utility of a fingerstick technology to identify individuals with abnormal blood lipids and high-sensitivity C-reactive protein levels.* American Journal of Health Promotion, 2009. **23**(4): p. 279-282.

164. Garg, S.K., et al., *Correlation of fingerstick blood glucose measurements with GlucoWatch biographer glucose results in young subjects with type 1 diabetes.* Diabetes Care, 1999. **22**(10): p. 1708-1714.

165. Loewenstein, D., C. Stake, and M. Cichon, *Assessment of using fingerstick blood sample with i-STAT point-of-care device for cardiac troponin I assay.* Am J Emerg Med, 2013. **31**(8): p. 1236-9.

166. Aukland, K. and G. Nicolaysen, *Interstitial fluid volume: local regulatory mechanisms.* Physiol Rev, 1981. **61**(3): p. 556-643.

167. Wang, J., et al., *Hydrophobic sol-gel channel patterning strategies for paper-based microfluidics.* Lab Chip, 2014. **14**(4): p. 691-5.

168. Gribble, C.M., et al., *Porometry, porosimetry, image analysis and void network modelling in the study of the pore-level properties of filters.* Chemical Engineering Science, 2011. **66**(16): p. 3701-3709.

169. Chang, H., et al., *A swellable microneedle patch to rapidly extract skin interstitial fluid for timely metabolic analysis.* Adv Mater, 2017. **DOI: 10.1002/adma.201702243**.

170. Santos, D., et al., *A review of the effects of external pressure on skin blood flow.* The Foot, 2003. **13**(4): p. 185-189.

171. Miller, P.R., et al., *Hollow Microneedle-based Sensor for Multiplexed Transdermal Electrochemical Sensing.* Journal of Visualized Experiments : JoVE, 2012(64): p. 4067.

172. Caffarel-Salvador, E., et al., *Hydrogel-forming microneedle arrays allow detection of drugs and glucose: Potential for use in diagnosis and therapeutic drug monitoring.* PLoS ONE, 2016. **10**(12): p. e0145644.

173. Broccardo, C.J., et al., *Peeling off the layers: skin taping and a novel proteomics approach to study atopic dermatitis.* J Allergy Clin Immunol, 2009. **124**(5): p. 1113-5.e1-11.

174. Matsui, T., et al., *Identification of novel keratinocyte-secreted peptides dermokine-α/-β and a new stratified epithelium-secreted protein gene complex on human chromosome 19q13. 1.* Genomics, 2004. **84**(2): p. 384-397.

175. Bal, S., et al., *In vivo visualization of microneedle conduits in human skin using laser scanning microscopy.* Laser Physics Letters, 2010. **7**(3): p. 242.

176. Cao, H., X. Li, and J. Liu, *An updated review of the efficacy of cupping therapy.* PloS one, 2012. **7**(2): p. e31793.

177. Crouch, J.D., S.M. Smith, and J.C. Leguen-Perez, *Hand-held and conversion vacuum cleaner with adapter* USPTO, Editor. 2014: USA.

178. Apelqvist, J., et al., *EWMA Document: Negative Pressure Wound Therapy.* J Wound Care, 2017. **26**(Sup3): p. S1-s154.

179. Mark R. Prausnitz, J.A.M., Michel Cormier, and a.A.K. Andrianov, *Microneedle-Based Vaccines,* in *Vaccines for Pandemic Influenza* R.W. Compans and W.A. Orenstein, Editors. 2009, Springer. p. 370-393.

180. Kelchen, M.N., et al., *Micropore closure kinetics are delayed following microneedle insertion in elderly subjects.* J Control Release, 2016. **225**: p. 294-300.

181. Mayeux, R., *Biomarkers: Potential Uses and Limitations.* NeuroRx, 2004. **1**(2): p. 182-188.

182. Wiig, H. and M.A. Swartz, *Interstitial fluid and lymph formation and transport: physiological regulation and roles in inflammation and cancer.* Physiol Rev, 2012. **92**(3): p. 1005-60.

183. Celis, J.E., et al., *Proteomic characterization of the interstitial fluid perfusing the breast tumor microenvironment A novel resource for biomarker and therapeutic target discovery.* Molecular & Cellular Proteomics, 2004. **3**(4): p. 327-344.

184. Jones, D.P., *Sequencing the exposome: A call to action.* Toxicology Reports, 2016. **3**: p. 29-45.

185. Go, Y.M., et al., *Reference Standardization for Mass Spectrometry and High-resolution Metabolomics Applications to Exposome Research.* Toxicol Sci, 2015. **148**(2): p. 531-43.

186. Go, Y.-M., et al., *Reference Standardization for Mass Spectrometry and High-resolution Metabolomics Applications to Exposome Research.* Toxicological Sciences, 2015. **148**(2): p. 531-543.

187. Kanehisa, M., et al., *KEGG for integration and interpretation of large-scale molecular data sets.* Nucleic Acids Research, 2012. **40**(Database issue): p. D109-D114.

188. Miao, H., et al., *Simultaneous Determination of Melamine, Ammelide, Ammeline, and Cyanuric Acid in Milk and Milk Products by Gas Chromatography-tandem Mass Spectrometry.* Biomedical and Environmental Sciences, 2009. **22**(2): p. 87-94.

189. Wishart, D.S., et al., *HMDB 3.0--The Human Metabolome Database in 2013.* Nucleic Acids Res, 2013. **41**(Database issue): p. D801-7.

190. Safer, D., et al., *Urocanic acid is a major chemoattractant for the skin-penetrating parasitic nematode Strongyloides stercoralis.* Proceedings of the National Academy of Sciences, 2007. **104**(5): p. 1627-1630.

191. Li, S., et al., *Predicting Network Activity from High Throughput Metabolomics.* PLOS Computational Biology, 2013. **9**(7): p. e1003123.

192. Xia, J., et al., *MetaboAnalyst 3.0--making metabolomics more meaningful.* Nucleic Acids Res, 2015. **43**(W1): p. W251-7.

193. Wang, Z., et al., *Prognostic value of choline and betaine depends on intestinal microbiota-generated metabolite trimethylamine-N-oxide.* European Heart Journal, 2014. **35**(14): p. 904-910.

194. Tang, W.H.W., et al., *Intestinal Microbial Metabolism of Phosphatidylcholine and Cardiovascular Risk.* New England Journal of Medicine, 2013. **368**(17): p. 1575-1584.

195. Mazzafera, P., *Trigonelline in coffee.* Phytochemistry, 1991. **30**(7): p. 2309-2310.

196. Gibbs, N.K. and M. Norval, *Urocanic Acid in the Skin: A Mixed Blessing?* Journal of Investigative Dermatology, 2011. **131**(1): p. 14-17.

197. El Baze, P., et al., *Polyamine levels in normal human skin. A comparative study of pure epidermis, pure dermis, and suction blister fluid.* Arch Dermatol Res, 1983. **275**(4): p. 218-21.

198. Minois, N., *Molecular basis of the 'anti-aging' effect of spermidine and other natural polyamines - a mini-review.* Gerontology, 2014. **60**(4): p. 319-26.

199. Giskeødegård, G.F., et al., *Spermine and Citrate as Metabolic Biomarkers for Assessing Prostate Cancer Aggressiveness.* PLOS ONE, 2013. **8**(4): p. e62375.

200. Le-Niculescu, H., et al., *Discovery and validation of blood biomarkers for suicidality.* Molecular Psychiatry, 2013. **18**(12): p. 1249-1264.

201. Miolo, G., et al., *Pharmacometabolomics study identifies circulating spermidine and tryptophan as potential biomarkers associated with the complete pathological response to trastuzumab-paclitaxel neoadjuvant therapy in HER-2 positive breast cancer.* Oncotarget, 2016. **7**(26): p. 39809-39822.

202. Wyss, M. and R. Kaddurah-Daouk, *Creatine and creatinine metabolism.* Physiological reviews, 2000. **80**(3): p. 1107-1213.

203. Pajares, S., et al., *Role of creatine as biomarker of mitochondrial diseases.* Mol Genet Metab, 2013. **108**(2): p. 119-24.

204. Shaham, O., et al., *A plasma signature of human mitochondrial disease revealed through metabolic profiling of spent media from cultured muscle cells.* Proceedings of the National Academy of Sciences, 2010. **107**(4): p. 1571-1575.

205. Bell, M.J., et al., *Interstitial adenosine, inosine, and hypoxanthine are increased after experimental traumatic brain injury in the rat.* J Neurotrauma, 1998. **15**(3): p. 163-70.

206. Farthing, D.E., C.A. Farthing, and L. Xi, *Inosine and hypoxanthine as novel biomarkers for cardiac ischemia: From bench to point-of-care.* Experimental Biology and Medicine, 2015. **240**(6): p. 821-831.

207. Patel, S. and S. Ahmed, *Emerging field of metabolomics: Big promise for cancer biomarker identification and drug discovery.* Journal of Pharmaceutical and Biomedical Analysis, 2015. **107**: p. 63-74.

208. Wurtman, R., *Biomarkers in the diagnosis and management of Alzheimer's disease.* Metabolism, 2015. **64**(3, Supplement 1): p. S47-S50.

209. Deepinder, F., H.T. Chowdary, and A. Agarwal, *Role of metabolomic analysis of biomarkers in the management of male infertility.* Expert Rev Mol Diagn, 2007. **7**(4): p. 351-8.

210. Otoki, Y., et al., *Plasma Phosphatidylethanolamine and Triacylglycerol Fatty Acid Concentrations are Altered in Major Depressive Disorder Patients with Seasonal Pattern.* Lipids, 2017. **52**(6): p. 559-571.

211. Bame, M., et al., *Amino acids as biomarkers in the SOD1(G93A) mouse model of ALS.* Biochim Biophys Acta, 2014. **1842**(1): p. 79-87.

212. Huang, M.-T., T. Ferraro, and C.-T. Ho, *Cancer Chemoprevention by Phytochemicals in Fruits and Vegetables*, in *Food Phytochemicals for Cancer Prevention I*. 1993, American Chemical Society. p. 2-16.

213. Tang, L., et al., *Total isothiocyanate yield from raw cruciferous vegetables commonly consumed in the United States.* Journal of functional foods, 2013. **5**(4): p. 1996-2001.

214. Shibata, T., et al., *Toll-like Receptors as a Target of Food-derived Anti-Inflammatory Compounds.* Journal of Biological Chemistry, 2014.

215. Lim, T., *Solanum torvum*, in *Edible Medicinal And Non-Medicinal Plants*. 2013, Springer. p. 429-441.

216. Green, R., *Indicators for assessing folate and vitamin B-12 status and for monitoring the efficacy of intervention strategies.* The American Journal of Clinical Nutrition, 2011. **94**(2): p. 666S-672S.

217. Ganguly, P. and S.F. Alam, *Role of homocysteine in the development of cardiovascular disease.* Nutrition Journal, 2015. **14**: p. 6.

218. Herrmann, W. and R. Obeid, *Homocysteine: a biomarker in neurodegenerative diseases.* Clin Chem Lab Med, 2011. **49**(3): p. 435-41.

219. Ueland, P.M., *Choline and betaine in health and disease.* J Inherit Metab Dis, 2011. **34**(1): p. 3-15.

220. Velasquez, M.T., et al., *Trimethylamine N-Oxide: The Good, the Bad and the Unknown.* Toxins, 2016. **8**(11): p. 326.

221. Lever, M., et al., *Betaine and Trimethylamine-N-Oxide as Predictors of Cardiovascular Outcomes Show Different Patterns in Diabetes Mellitus: An Observational Study.* PLOS ONE, 2014. **9**(12): p. e114969.

222. Wang, Z., et al., *Gut flora metabolism of phosphatidylcholine promotes cardiovascular disease.* Nature, 2011. **472**(7341): p. 57-63.

223. Lang, R., et al., *Identification of Urinary and Salivary Biomarkers for Coffee Consumption*, in *Recent Advances in the Analysis of Food and Flavors*. 2012, American Chemical Society. p. 13-25.

224. Uppal, K., D.I. Walker, and D.P. Jones, *xMSannotator: An R Package for Network-Based Annotation of High-Resolution Metabolomics Data.* Analytical Chemistry, 2017. **89**(2): p. 1063-1067.

225. Yu, T., et al., *Hybrid feature detection and information accumulation using high-resolution LC-MS metabolomics data.* J Proteome Res, 2013. **12**(3): p. 1419-27.

226. Uppal, K., et al., *xMSanalyzer: automated pipeline for improved feature detection and downstream analysis of large-scale, non-targeted metabolomics data.* BMC Bioinformatics, 2013. **14**: p. 15.

227. Team, R., *RStudio: Integrated Development for R.* 2015, RStudio, Inc.: Boston, MA.

228. Downing, G.J., *Biomarkers: Facing the Challenges at the Crossroads of Research and Health Care*, in *Pharmaceutical Sciences Encyclopedia*. 2010, John Wiley & Sons, Inc.

229. Deacon, B. and J. Abramowitz, *Fear of needles and vasovagal reactions among phlebotomy patients.* Journal of Anxiety Disorders, 2006. **20**(7): p. 946-960.

230. Fischbach, F.T. and M.B. Dinning, *A manual of laboratory and diagnostic tests*. 8th edition ed. 2009: Wolters Kluwer Health. 1283.

231. Renard, E., *Implantable continuous glucose sensors.* Current diabetes reviews, 2008. **4**(3): p. 169-174.

232. Herkenne, C., et al., *In vivo methods for the assessment of topical drug bioavailability.* Pharmaceutical Research, 2008. **25**(1): p. 87.

233. Wiig, H., et al., *Interstitial fluid: the overlooked component of the tumor microenvironment?* Fibrogenesis Tissue Repair, 2010. **3**: p. 12.

234. Haslene-Hox, H., et al., *A new method for isolation of interstitial fluid from human solid tumors applied to proteomic analysis of ovarian carcinoma tissue.* PLoS One, 2011. **6**(4): p. e19217.

235. Ranamukhaarachchi, S.A., et al., *Integrated hollow microneedle-optofluidic biosensor for therapeutic drug monitoring in sub-nanoliter volumes.* Scientific Reports, 2016. **6**: p. 29075.

236. Kiistala, U. and K.K. Mustakallio, *Dermo-Epidermal Separation with Suction: Electron Microscopic and Histochemical Study of Initial Events of Blistering on Human Skin*.* Journal of Investigative Dermatology, 1967. **48**(5): p. 466-477.

237. Kinn, P.M., et al., *Age-dependent variation in cytokines, chemokines, and biologic analytes rinsed from the surface of healthy human skin.* Scientific Reports, 2015. **5**: p. 10472.

238. Bíró, T., et al., *The endocannabinoid system of the skin in health and disease: novel perspectives and therapeutic opportunities.* Trends in pharmacological sciences, 2009. **30**(8): p. 411-420.

239. Terao, M. and I. Katayama, *Local cortisol/corticosterone activation in skin physiology and pathology.* Journal of Dermatological Science, 2016. **84**(1): p. 11-16.

240. Garza, C., *Pharmacology of Caffeine.*, in *Caffeine for the Sustainment of Mental Task Performance: Formulations for Military Operations.* 2001, Committee on Military Nutrition Research, Food and Nutrition Board, National Academies Press (US): Washington D.C. p. 172.

241. Liguori, A., J.R. Hughes, and J.A. Grass, *Absorption and subjective effects of caffeine from coffee, cola and capsules.* Pharmacology Biochemistry and Behavior, 1997. **58**(3): p. 721-726.

242. Jacobson, A.F., et al., *Serum caffeine levels after 24 hours of caffeine abstention: observations on clinical patients undergoing myocardial perfusion imaging with dipyridamole or adenosine.* European Journal of Nuclear Medicine and Molecular Imaging, 1994. **21**(1): p. 23-26.

243. Collomp, K., et al., *Effects of moderate exercise on the pharmacokinetics of caffeine.* European Journal of Clinical Pharmacology, 1991. **40**(3): p. 279-282.

244. Hammarlund-Udenaes, M., *Microdialysis as an Important Technique in Systems Pharmacology—a Historical and Methodological Review.* The AAPS Journal, 2017: p. 1-10.

245. Scuffi, C., *Interstitium Versus Blood Equilibrium in Glucose Concentration and its Impact on Subcutaneous Continuous Glucose Monitoring Systems.* Euro Endocrin, 2014. **10**(1): p. 36-42.

246. Gill, H.S., et al., *Effect of microneedle design on pain in human volunteers.* Clin J Pain, 2008. **24**(7): p. 585-94.

247. Powell, L., *Negative pressure cutaneous suction system*, in *Electronic Diversities,*. Finksburg MD. p. 1-5.

248. Powell, L. *Negative pressure instrument*. [cited 2013 8/7/2013]; Available from: http://www.electdiv.com/page4.html.

249. Go, Y.-M., et al., *Reference standardization for mass spectrometry and high-resolution metabolomics applications to exposome research.* Toxicological Sciences 2015. **148**(2): p. 531-543.

250. Yu, T., et al., *apLCMS—adaptive processing of high-resolution LC/MS data.* Bioinformatics, 2009. **25**(15): p. 1930-1936.

251. Uppal, K., et al., *xMSanalyzer: automated pipeline for improved feature detection and downstream analysis of large-scale, non-targeted metabolomics data.* BMC Bioinformatics, 2013. **14**(1): p. 15.

252. Scheuplein, R.J. and I.H. Blank, *Permeability of the skin.* Physiol Rev, 1971. **51**(4): p. 702-747.

253. Hill, D.J.T., A.K. Whittaker, and Zainuddin, *Water diffusion into radiation crosslinked PVA–PVP network hydrogels.* Radiation Physics and Chemistry, 2011. **80**(2): p. 213-218.

254. Galey, W.R., H. Lonsdale, and S. Nacht, *The in vitro permeability of skin and buccal mucosa to selected drugs and tritiated water.* Journal of Investigative Dermatology, 1976. **67**(6): p. 713-717.

255. Deen, W.M., *Analysis of Transport Phenomena* Vol. 3. 1998: Oxford University Press, New York.

256. Mills, R., *Self-diffusion in normal and heavy water in the range 1-45. deg.* The Journal of Physical Chemistry, 1973. **77**(5): p. 685-688.

257. Kesmarky, G., et al., *Plasma viscosity: a forgotten variable.* Clin Hemorheol Microcirc, 2008. **39**(1-4): p. 243-6.

258. Khalil, E., K. Kretsos, and G.B. Kasting, *Glucose partition coefficient and diffusivity in the lower skin layers.* Pharm Res, 2006. **23**(6): p. 1227-34.

259. Hamdan, M., et al., *Draw solutions for forward osmosis process: Osmotic pressure of binary and ternary aqueous solutions of magnesium chloride, sodium chloride, sucrose and maltose.* Journal of Food Engineering, 2015. **155**: p. 10-15.

260. Whitaker, S., *Flow in porous media I: A theoretical derivation of Darcy's law.* Transport in Porous Media, 1986. **1**(1): p. 3-25.

261. Van't Hoff, J.H., *The role of osmotic pressure in the analogy between solutions and gases.* Journal of Membrane Science, 1995. **100**(1): p. 39-44.

262. Bert, J.L. and R.K. Reed, *Flow conductivity of rat dermis is determined by hydration.* Biorheology, 1995. **32**(1): p. 17-27.

263. Chu, L.Y., S.O. Choi, and M.R. Prausnitz, *Fabrication of dissolving polymer microneedles for controlled drug encapsulation and delivery: Bubble and pedestal microneedle designs.* J Pharm Sci, 2010. **99**(10): p. 4228-38.

264. Chiang, B., et al., *Sustained reduction of intraocular pressure by supraciliary delivery of brimonidine-loaded poly(lactic acid) microspheres for the treatment of glaucoma.* J Control Release, 2016. **228**: p. 48-57.

265. Franzen, L., et al., *Freeze-drying as a preserving preparation technique for in vitro testing of human skin.* Experimental Dermatology, 2013. **22**(1): p. 54-56.

266. Park, Y.H., et al., *High-performance metabolic profiling of plasma from seven mammalian species for simultaneous environmental chemical surveillance and bioeffect monitoring.* Toxicology, 2012. **295**(1-3): p. 47-55.

267. Soltow, Q., et al., *High-performance metabolic profiling with dual chromatography-Fourier-transform mass spectrometry (DC-FTMS) for study of the exposome.* Metabolomics, 2013.

268. Accardi, C.J., et al., *High-Resolution Metabolomics for Nutrition and Health Assessment of Armed Forces Personnel.* Journal of Occupational and Environmental Medicine, 2016. **58**: p. S80-S88.

269. Walker, D.I., et al., *Pilot metabolome-wide association study of benzo(a)pyrene in serum from military personnel.* Journal of Occupational and Environmental Medicine, 2016. **Submitted; DoD Biomarkers Supplement**.

270. Wishart, D.S., et al., *HMDB 3.0--The Human Metabolome Database in 2013.* Nucleic acids research, 2013. **41**(Database issue): p. D801-7.

271. Li, S., et al., *Predicting network activity from high throughput metabolomics.* PLOS Computational Biology, 2013. **9**(7): p. e1003123.

272. Xia, J., et al., *MetaboAnalyst 3.0--making metabolomics more meaningful.* Nucleic Acids Res. , 2015. **43**(W1): p. W251-7.

273. Xia, J. and D.S. Wishart, *MSEA: a web-based tool to identify biologically meaningful patterns in quantitative metabolomic data.* Nucleic Acids Research, 2010. **38**(Web Server issue): p. W71-7.

274. Banga, A.K., *Transdermal and intradermal delivery of therapeutic agents: Application of physical technologies*. 2011, Boca Raton, FL: Taylor and Francis Group LLC. 282.

275. Junge, T., *Blood clotting mechanism.* Surgical Technologist, 2006. **38**(10): p. 12.

276. Clegg , D.O., et al., *Glucosamine, Chondroitin Sulfate, and the Two in Combination for Painful Knee Osteoarthritis.* New England Journal of Medicine, 2006. **354**(8): p. 795-808.

277. Ivy, J.L., *Muscle glycogen synthesis before and after exercise.* Sports Med, 1991. **11**(1): p. 6-19.

278. Kraeling, M.E.K., J.J. Yourick, and R.L. Bronaugh, *In vitro human skin penetration of diethanolamine.* Food and Chemical Toxicology, 2004. **42**(10): p. 1553-1561.

279. Holleran, W.M., Y. Takagi, and Y. Uchida, *Epidermal sphingolipids: Metabolism, function, and roles in skin disorders.* FEBS Letters, 2006. **580**(23): p. 5456-5466.

280. Fent, K. and P.W. Looser, *Bioaccumulation and bioavailability of tributyltin chloride: Influence of pH and humic acids.* Water Research, 1995. **29**(7): p. 1631-1637.

281. Antizar-Ladislao, B., *Environmental levels, toxicity and human exposure to tributyltin (TBT)-contaminated marine environment. A review.* Environment International, 2008. **34**(2): p. 292-308.

282. Dávalos, A., et al., *Citicoline in the treatment of acute ischaemic stroke: an international, randomised, multicentre, placebo-controlled study (ICTUS trial).* The Lancet, 2012. **380**(9839): p. 349-357.

283. Saver, J.L., *Citicoline: update on a promising and widely available agent for neuroprotection and neurorepair.* Rev Neurol Dis, 2008. **5**(4): p. 167-77.

284. Smedman, A.E., et al., *Pentadecanoic acid in serum as a marker for intake of milk fat: relations between intake of milk fat and metabolic risk factors.* Am J Clin Nutr, 1999. **69**(1): p. 22-9.

285. Jiang, Q., et al., *gamma-tocopherol, the major form of vitamin E in the US diet, deserves more attention.* Am J Clin Nutr, 2001. **74**(6): p. 714-22.

286. Lichten, E.M., et al., *The Confirmation of a Biochemical Marker for Women's Hormonal Migraine: The Depo-Estradiol Challenge Test.* Headache: The Journal of Head and Face Pain, 1996. **36**(6): p. 367-371.

287. Vangala, S. and A. Tonelli, *Biomarkers, metabonomics, and drug development: Can inborn errors of metabolism help in understanding drug toxicity?* The AAPS Journal, 2007. **9**(3): p. E284-E297.

288. Deacon, A.C. and T.J. Peters, *Identification of acute porphyria: evaluation of a commercial screening test for urinary porphobilinogen.* Ann Clin Biochem, 1998. **35 (Pt 6)**: p. 726-32.

289. Hiramatsu, K., et al., *N(1),N(12)-Diacetylspermine as a sensitive and specific novel marker for early- and late-stage colorectal and breast cancers.* Clin Cancer Res, 2005. **11**(8): p. 2986-90.

290. *Toxicology and carcinogenesis studies of triethanolamine*, U.S.D.o.H.a.H. Services, Editor. 1999: Research Triangle Park, NC.

291. Miura, Y., *The biological significance of ω-oxidation of fatty acids.* Proceedings of the Japan Academy, Series B, 2013. **89**(8): p. 370-382.

292. Neuschwander-Tetri, B.A., et al., *Farnesoid X nuclear receptor ligand obeticholic acid for non-cirrhotic, non-alcoholic steatohepatitis (FLINT): a multicentre, randomised, placebo-controlled trial.* The Lancet, 2015. **385**(9972): p. 956-965.

293. Farthing, D., et al., *An HPLC method for determination of inosine and hypoxanthine in human plasma from healthy volunteers and patients presenting with potential acute cardiac ischemia.* J Chromatogr B Analyt Technol Biomed Life Sci, 2007. **854**(1-2): p. 158-64.

294. Schwarzschild, M.A., et al., *Inosine to increase serum and cerebrospinal fluid urate in Parkinson disease: a randomized clinical trial.* JAMA Neurol, 2014. **71**(2): p. 141-50.

295. Patel, D.K., K. Patel, and V. Tahilyani, *Barbaloin: A concise report of its pharmacological and analytical aspects.* Asian Pacific Journal of Tropical Biomedicine, 2012. **2**(10): p. 835-838.

296. Jin, X.F., et al., *Circulating microRNAs: a novel class of potential biomarkers for diagnosing and prognosing central nervous system diseases.* Cell Mol Neurobiol, 2013. **33**(5): p. 601-13.

297. Klinefelter, G.R., et al., *Bromochloroacetic acid exerts qualitative effects on rat sperm: implications for a novel biomarker.* Toxicological sciences, 2002. **68**(1): p. 164-173.

298. Cornejo-García, J.A., et al., *Pharmacogenomics of prostaglandin and leukotriene receptors.* Frontiers in pharmacology, 2016. **7**.

299. Terao, M. and I. Katayama, *Local cortisol/corticosterone activation in skin physiology and pathology.* J Dermatol Sci, 2016. **84**(1): p. 11-16.